High-Resolution Direction-of-Arrival Estimation

Murdifi Bin Muhammad

Matriculation Number:

Submitted in fulfilment of the requirements for the

Degree of Doctor of Philosophy

James Watt School of Engineering

College of Science and Engineering

University of Glasgow

June 2022

Abstract

Direction of Arrival (DOA) estimation is considered one of the most crucial problems in array signal processing, with considerable research efforts for developing efficient and effective direction-finding algorithms, especially in the transportation industry, where the demand for an effective, real-time, and accurate DOA algorithm is increasing. However, challenges must be addressed before real-world deployment can be realised. Firstly, there is the requirement for fast computational time for real-time detection. Secondly, there is a demand for high-resolution and accurate DOA estimation.

In this thesis, two state-of-the-art DOA estimation algorithms are proposed and evaluated to address the challenges. Firstly, a novel covariance matrix reconstruction approach for single snapshot DOA estimation (CbSS) was proposed. CbSS was developed by exploiting the relationship between the theoretical and sample covariance matrices to reduce estimation error for a single snapshot scenario. CbSS can resolve accurate DOAs without requiring lengthy peak searching computational time by computationally changing the received sample covariance matrix. Simulation results have verified that the CbSS technique yields the highest DOA estimation accuracy by up to 25.5% compared to existing methods such as root-MUSIC and the Partial Relaxation approach. Furthermore, CbSS presents negligible bias when compared to the existing techniques in a wide range of scenarios, such as in multiple uncorrelated and coherent signal source environments.

Secondly, an adaptive diagonal-loading technique was proposed to improve DOA estimation accuracy without requiring a high computational load by integrating a modified novel and adaptive diagonal-loading method (DLT-DOA) to further improve estimation accuracy. An in-depth simulation performance analysis was conducted to address the challenges, with a comparison against existing state-of-the-art DOA estimation techniques such as EPUMA and MODEX. Simulation results verify that the DLT-DOA technique performs up to 8.5% higher DOA estimation performance in terms of estimation accuracy compared to existing methods with significantly lower computational time.

On this basis, the two novel DOA estimation techniques are recommended for usage in real-world scenarios where fast computational time and high estimation accuracy are expected. Further research is needed to identify other factors that could further optimize the algorithms to meet different demands.

Declaration

Name: Murdifi Bin Muhammad

Matriculation Number:

The author declares that this thesis does not include work forming part of a thesis presented successfully for another degree. The thesis has been produced in accordance with the University of Glasgow's Code of Good Practice in Research.

Signature: _____

Date: 29th June 2022

Acknowledgements

The author would like to acknowledge and express sincere appreciation to the Singapore Economic Development Board (EDB), Singapore, and RFNet Technologies Pte Ltd (RFNet), Singapore, for financing and providing a good environment and facilities to support the research.

I would like to thank my supervisors, Dr Minghui (David) Li, Dr Qammer H. Abbasi, Dr Cindy Goh, and Professor Muhammad Ali Imran, for providing their professional guidance, laboratories, and IT resources to make my research work possible within the stipulated timeline. It was a great experience to tag on their networks, which indirectly enhanced my research works' visibility.

I would like to express my appreciation to my RFNet Technologies Pte Ltd co-workers, Dr Tan Moh Chuan, Dr Dai Shao Wei and Mr Deric Lee. They have participated actively in the project discussion, and I thank them for their support and guidance.

Finally, a special thanks to my parents, Muhammad Bin Abdullah & Junaina Bte Amat, family, and friends for providing unconditional support that allows me to have a clear mind throughout the course.

Publications Arising from This Thesis

[Journal]

1. M. Muhammad, M. Li, Q. H. Abbasi, C. Goh and M. A. Imran, "An Adaptive Diagonal Loading Technique to Improve Direction of Arrival Estimation Accuracy for Linear Antenna Array Sensors," in *IEEE Sensors Journal*, doi: 10.1109/JSEN.2022.3168785.
2. M. Muhammad, M. Li, Q. Abbasi, C. Goh, and M. A. Imran, "A Covariance Matrix Reconstruction Approach for Single Snapshot Direction of Arrival Estimation," *Sensors,* vol. 22, no. 8, 2022, doi: 10.3390/s22083096.

[Conference]

3. M. Muhammad, M. Li, Q. H. Abbasi, C. Goh, and M. Imran, "Performance Evaluation for Direction of Arrival Estimation Using 4-Element Linear Array," in 2019 13th European Conference on Antennas and Propagation (EuCAP), 31 March-5 April 2019, pp. 1-5.
4. M. Muhammad, M. Li, Q. H. Abbasi, C. Goh, and M. Imran, "Direction of Arrival Estimation using Root-Transformation Matrix Technique," in 2019 IEEE International Symposium on Antennas and Propagation and USNC-URSI Radio Science Meeting, 7-12 July 2019, pp. 1369-1370, doi: 10.1109/APUSNCURSINRSM.2019.8889249.
5. M. Muhammad, M. Li, Q. H. Abbasi, C. Goh, and M. Imran, "Direction of Arrival Estimation Using Hybrid Spatial Cross-Cumulants and Root-MUSIC," in 2020 14th European Conference on Antennas and Propagation (EuCAP), 15-20 March 2020, pp. 1-5, doi: 10.23919/EuCAP48036.2020.9135813.
6. M. Muhammad, M. Li, Q. H. Abbasi, C. Goh, and M. Imran, "Auto-calibration of Linear Array Antenna Positioning for Single Snapshot Direction of Arrival Estimation," in 2020 IEEE International Symposium on Antennas and Propagation and North American Radio Science Meeting, 5-10 July 2020, pp. 491-492, doi: 10.1109/IEEECONF35879.2020.9330495.
7. M. Muhammad, M. Li, Q. H. Abbasi, C. Goh and M. Imran, "A Novel Subspace-Averaging Direction of Arrival Estimation Technique," 2021 IEEE 6th International

Conference on Signal and Image Processing (ICSIP), 2021, pp. 744-748, doi: 10.1109/ICSIP52628.2021.9688940.

Contents

Abstract ..... **i**

Declaration ..... **ii**

Acknowledgements ..... **iii**

Publications Arising from This Thesis ..... **iv**

List of Tables ..... **x**

List of Figures ..... **xi**

Nomenclature and Abbreviations ..... **xiii**

1 Introduction **16**

1.1 Research Motivation 17

1.2 Research Aims & Objectives 18

1.3 Key Contributions 19

1.4 Thesis Outline 21

2 An Overview of Direction of Arrival Estimation **23**

2.1 Recent Trends in DOA Estimation – A Literature Review 23

2.2 General Data Model for DOA Estimation 27

2.2.1 Received Signal Data Model Formulation 27

2.2.2 Array Covariance Matrix 28

2.3 Common DOA Estimation Methods 28

2.3.1 Root-MUSIC 29

2.3.2 Root-Weighted Subspace Fitting 29

2.3.3 Beamspace-ESPRIT Algorithm 30

2.4 Performance Analysis of Common DOA Methods 30

2.4.1 Low-Frequency Against High-Frequency Operating Performance 30

2.4.2 Closely-Sourced Signals 31

2.4.3 Computational Time Performance 34

2.4.4 Coherent Signal Source Performance 34
2.5 Performance Summary of Existing DOA Estimation Techniques 35
3 Innovative Techniques to Independently Overcome Problems with Existing DOA Estimators 37
3.1 Root-Transformation Method for DOA Estimation 38
3.1.1 Algorithm for Root-Transformation DOA Estimator 38
3.1.2 Performance Analysis for Root-T DOA Estimator 39
3.1.2.1 Low SNR Performance (SNR = -30 dB) 39
3.1.2.2 Closely-Spaced Signals (SNR = -20 dB) 40
3.1.2.3 Computational Runtime 40
3.1.3 Root-T DOA Estimator Performance Summary 41
3.2 DOA Estimation using Hybrid Higher-Order Spatial Cross-Cumulants and Root-MUSIC 41
3.2.1 Higher-Order Spatial Cross Cumulants 42
3.2.2 Cross Cumulants-MUSIC (CC-MUSIC) DOA Estimator 43
3.2.3 Performance Analysis of CC-MUSIC DOA Estimator 44
3.2.3.1 Single Source SNR-RMSE Performance 45
3.2.3.2 Multi-Source SNR-RMSE Performance 46
3.2.4 CC-MUSIC Summary 46
3.3 Subspace-Averaging DOA Estimator (SADE) 47
3.3.1 SADE Data Model 47
3.3.2 SADE Performance Analysis 49
3.3.2.1 Varying the Number of Snapshots 49
3.3.2.2 Varying the Number of Array Elements 52
3.3.3 SADE Performance Summary 53
3.4 Snapshot Sample Reduction for Lower Computational Load 53
3.4.1 Single Snapshot DOA Estimation Signal Model 54
3.4.2 Auto-calibration of Antenna Positioning & Proposed Technique 54
3.4.3 Simulation Results for SS-DOA 56

3.4.4 Auto-Calibration of Single Snapshot Estimator Performance Summary.....57

3.5 Overall Summary of Proposed Novel DOA Estimation Techniques 58

4 A Covariance Matrix Reconstruction Approach for Single Snapshot DOA Estimation 60

4.1 Covariance-based Single Snapshot DOA Estimator 61

4.1.1 Defining the Error Terms in Covariance Matrices.....61

4.1.2 Determining the Lower & Upper Bounds of the Diagonal-Loading Factor for Error Minimization 62

4.1.3 Practical Implementation for DOA Estimation Error Minimization Using Sample Covariance Matrix 63

4.2 Simulation Results and Discussion of CbSS.....66

4.2.1 DOA Estimation Accuracy for Single Signal Source and Multiple Finite Snapshots 69

4.2.2 DOA Estimation Accuracy for Multiple Uncorrelated and Coherent Signal Sources 72

4.2.2.1 DOA Estimation Accuracy for Multiple Uncorrelated Signal Sources 73

4.2.2.2 DOA Estimation Accuracy for Multiple Coherent Signal Sources.....76

4.2.3 Estimation Accuracy for Single Signal Source and Single Snapshot 79

4.2.4 Parametric Performance Impact.....81

4.3 Performance Summary for CbSS DOA Estimator 81

5 An Alternative DOA Estimation Method by Using an Adaptive Diagonal Loading Technique.....83

5.1 Diagonal Loading 83

5.2 Proposed Traced Diagonal-Loading DOA Estimation Method 85

5.3 Simulation Results & Discussion of DL-DOA 88

5.3.1 Limited Finite Snapshot Sample Performance with Single Signal Source of Interest 90

5.3.2 Limited Finite Snapshot Sample with Multiple Signal Sources of Interest...92

5.3.3 Single Snapshot Sample with a Single Signal Source of Interest 95

5.4 Performance Summary for DL-DOA 96

5.5 A Comparison between CbSS and DL-DOA 97

6 Conclusion and Future Work 98

6.1 Conclusion 98

6.2 Future Work 99

6.2.1 Hardware Implementation for Proposed DOA Algorithms 99

6.2.2 Extension of CbSS and DL-DOA Technique to Other Antenna Array Structures 99

6.2.3 Extended Performance Validation of Proposed Techniques into a Dynamic Scenario 100

6.2.4 Real-world Impact & Potential of the Proposed DOA Estimation Techniques 100

Bibliography 102

List of Tables

Table 2.1 Varying Operating Frequency Performance 31
Table 2.2: 8 Degree Signal Source Separation Performance 33
Table 2.3: 4 Degree Signal Source Separation Performance 33
Table 2.4: Computation Time Performance 34
Table 2.5: Coherent Signal Source Performance 35
Table 3.1 Algorithms Computational Runtime Comparison 41
Table 3.2 Averaged Array Sensor Coordinates 56
Table 4.1. Common Simulation Parameters 68
Table 4.2 Comparison of Varying Delta Values 81
Table 5.1 Common Simulation Parameters 89
Table 5.2 Summary of Simulation Results for Single Signal Source 92
Table 5.3 Summary of Simulation Results for Multiple Signal Sources 94
Table 5.4 Summary of Simulation Results for Single Snapshot Scenario 96
Table 5.5 Features Comparison Between CbSS and DLT-DOA 97

List of Figures

Figure 2.1 Sensor Array Model....27
Figure 2.2 Variance level of 8 degrees spacing....32
Figure 2.3 Variance level of 4 degrees spacing....33
Figure 2.4 DOA Detection in Coherent Signal Environment....35
Figure 3.1 Root-T Algorithm Flowchart....38
Figure 3.2 Low SNR Performance for Root-T DOA Estimator....39
Figure 3.3 Closely-Spaced Signal Performance for Root-T....40
Figure 3.4 CC-MUSIC DOA Estimator Algorithm Flow....43
Figure 3.5 Single-Source SNR-RMSE Performance for CC-MUSIC....45
Figure 3.6 Multi-Source SNR-RMSE Performance for CC-MUSIC....46
Figure 3.7 Proposed SADE Algorithm....49
Figure 3.8 SNR-RMSE for K Number of Snapshots = 10....50
Figure 3.9 SNR-RMSE for K Number of Snapshots = 100....51
Figure 3.10 SNR-RMSE for K Number of Snapshots = 1000....51
Figure 3.11 SNR-RMSE for Antenna Elements M = 6....52
Figure 3.12 SNR-RMSE for Antenna Elements M = 16....53
Figure 3.13 Auto-Calibrating SS-DOA Estimator Flowchart....55
Fig. 3.14 Averaged DOA Estimation Results in Normalized Polar Plot....57
Figure 4.1 CbSS Algorithm Flow....66
Figure 4.2 SNR-RMSE performance for M = 4 and M = 8 where the number of snapshots K = 100....69
Figure 4.3 Bias comparison for M = 4 and M = 8 where the number of snapshots K = 100 with varying SNR....69
Figure 4.4 Standard deviation where M = 4 and M = 8 against the number of snapshots K ranging from 1-100....70
Figure 4.5 Bias performance comparison where M = 4 and M = 8 against the number of snapshots K ranging from 1 to 100....70
Figure 4.6 SNR-RMSE estimation performance for M = 4 with a fixed number of snapshots K = 100 for uncorrelated signal source separation of 5 and 10 degrees....73
Figure 4.7 Bias performance comparison for M = 4 with a fixed number of snapshots K = 100 for uncorrelated signal source separation of 5 and 10 degrees....73

Figure 4.8 Standard deviation of DOA estimation comparison against varying snapshots for M = 4 and M = 8, fixed SNR = 0 dB with uncorrelated signal source separation of 10 degrees.....74
Figure 4.9 Bias comparison against varying snapshots for M = 4 and M = 8, SNR = 0 dB with uncorrelated signal source separation of 10 degrees.....74
Figure 4.10 SNR-RMSE estimation performance for M = 4 with a fixed number of snapshots K = 100 for coherent signal source separation of 5 and 10 degrees 76
Figure 4.11 Bias performance comparison for M = 4 with a fixed number of snapshots K = 100 for coherent signal source separation of 5 and 10 degrees.....76
Figure 4.12 Standard deviation of DOA estimation comparison against varying snapshots for M = 4 and M = 8, fixed SNR = 0 dB with coherent signal source separation of 10 degrees.....77
Figure 4.13 Bias comparison against varying snapshots for M = 4 and M = 8, SNR = 0 dB with coherent signal source separation of 10 degrees.....77
Figure 4.14 SNR-RMSE for single snapshot comparison where the number of antenna array elements M = 4 and K = 1.....80
Figure 4.15 Statistical bias performance comparison across the demonstrated techniques for a single snapshot scenario.....80
Figure 5.1 DLT-DOA Estimation Algorithm Flow 88
Figure 5.2 SNR-RMSE Performance for M = 4, N = 1, and K = 10 90
Figure 5.3 SNR-RMSE Performance for M = 8, N= 1, and K = 10 90
Figure 5.4 SNR-RMSE Performance for M = 8, N = 2, $\Delta\theta$=10°, and K = 10 92
Figure 5.5 SNR-RMSE Performance for M = 8, N = 2, $\Delta\theta$=5°, and K = 10 93
Figure 5.6 SNR-RMSE Performance for M = 4, N = 1, and K = 1 95

Nomenclature and Abbreviations

Acronyms	
3G	Third Generation
AWGN	Additive White Gaussian Noise
BS-ESPRIT	Beamspace-ESPRIT
CbSS	Covariance-based Single Snapshot
CC-MUSIC	Cross-cumulant MUSIC
CRB	Cramer-Rao Bound
DL	Diagonal Loading
DL-DOA	Diagonal Loading-Direction of Arrival
DOA	Direction of Arrival
EPUMA	Enhanced Principal Singular-Vector Utilization for Modal Analysis
ESPAR	Electronically Steerable Parasitic Array Radiator
ESPRIT	Estimation of Signal Parameters via Rotational Invariance Technique
FBSS	Forward-Backward Spatial Smoothing
FPGA	Field Programmable Gate Array
HST	High-speed Train
IG	Information Geometry
IoT	Internet of Things
ML	Machine Learning
MODE	Method of Direction Estimation
MUSIC	Multiple Signal Classification
PR	Partial Relaxation
RMSE	Root Mean Squared Error
Root-T	Root-Transformation
Root-WSF	Root-Weighted Subspace Fitting
RSSI	Received Signal Strength Indicator
SADE	Subspace-averaging Direction of Arrival Estimation
SAGE	Space-Alternating Generalized Expectation
SD	Standard Deviation

SNR	Signal-to-Noise Ratio
SNR-RMSE	Signal-to-Noise Ratio – Root Mean Squared Error
SQP	Sequential Quadratic Programming
SS-DOA	Single Snapshot-Direction of Arrival
STRING	Scaling Transform-based Information Geometry
UAV	Unmanned Aerial Vehicle
UCA	Uniformed Circular Array
ULA	Uniformed Linear Array
UMTS	Universal Mobile Telecommunication System
URA	Uniformed Rectangular Array
V2I	Vehicle to Infrastructure
V2X	Vehicle to Everything

Physical Constants

c	3 x 10^8 m/s, speed of light in free space

Symbols

M	Number of Antenna Array Elements
L	Number of Signals of Interest
λ	Wavelength
f_c	Carrier Frequency
K	Number of Snapshots
$\mathbf{A}$	Array Steering Matrix
$\mathbf{S}$	Signal Matrix
$\mathbf{N}$	Noise Matrix
$\mathbf{I}$	Identity Matrix
$\mathbf{R_{xx}}$	Theoretical Covariance Matrix
$\mathbf{X}$	Received Signal Matrix
$\mathbf{E_S}$	Signal Subspace
$\mathbf{E_N}$	Noise Subspace
$\mathbb{E}\{\cdot\}$	Expectation Operator
$(\cdot)^{\mathrm{H}}$	Hermitian Transpose
$\widehat{\mathbf{R}}_{\mathbf{xx}}$	Sample Covariance Matrix
θ	Angle of Arrival
d	Distance Between Adjacent Antenna Element
V	Variance

Q	Number of Observations
$\mathbf{R_{RR}}$	Transformation-Based Correlation Matrix
$\mathbf{R_{SS}}$	Time-averaged Signal Subspace
$\mathbf{R_{NN}}$	Time-averaged Noise Subspace
$\mathbf{R_{4X}}$	4th Order Cross-Cumulant Covariance Matrix
$\odot$	Hadamard product
$\mathbf{D}$	Zero-mean Random Matrix with Unit Variance
μ	Covariance Matrix Error Terms
ε_{DL}	Diagonal Loading Factor
$\mathrm{tr}(\cdot)$	Transpose Operator
$\emptyset$	Standard Deviation Error Identifier
δ	Recursive Tolerance Value
$\mathbf{R_{xx-DL}}$	Diagonally Loaded Covariance Matrix
F	Scalar Diagonal Loading Factor
$\widehat{\mathbf{R}}_{\mathbf{xx-DLT}}$	Traced Diagonally Loaded Sample Covariance Matrix
$\mathrm{diag}(\cdot)$	Diagonal Elements of a Matrix

1 Introduction

Smart antenna techniques are well-known in wireless communication systems for mitigating air space congestion, overcoming wireless interference, and lowering the system deployment cost. The ever-increasing requirements for providing large bandwidth and efficient and seamless data access to commuters have prompted new challenges for wireless solution providers. Furthermore, the advancement in the hybrid beamforming technique and the adoption of commercially available components into the smart antenna system has been proven to drastically reduce operational costs. This has created a clear path for the smart antenna to expand its service into commercial and industrial applications such as the transportation sector, government, public service, and industrial applications. Amongst all, the transportation sector has benefited most from the advancement of smart antenna technology simply due to the nature of the application environments where the wireless infrastructures are expected to serve uncoordinated mobile clients such as commuters, vehicle to infrastructure and vehicle-to-vehicle communication. This has cultivated the continuous interests amongst which researchers continue to improve the smart antenna systems that best suit the transportation industry.

Direction of Arrival (DOA) estimation plays a critical role in a smart antenna system and array signal processing. Estimation of DOA is especially important when coupled with an adaptive antenna array and in interference environments. However, some key challenges must be addressed before real-world implementation, mainly if it were to be used in the transportation industry. One key issue is finding the optimal tradeoff between computational time and DOA estimation accuracy. In short, due to the reliance on statistical data, computational time will linearly increase as the demand for DOA estimation accuracy increases. Furthermore, real-world environment is not considered in most past works of literature to highlight the performance of these past techniques in a best-case scenario.

This thesis focuses on the DOA estimation aspect in an innovative antenna system, particularly in improving the computational time and estimation accuracy. In general, DOA estimation methods can be described in three basic steps. First, the acquisition of the data signal matrix is followed by the generation of the instantaneous correlation matrix for each data time step. Then, temporal data averaging is conducted over time, followed by a form of data correlation analysis. Finally, the DOA is derived. The key focus is on the improvement of efficiency in terms of estimation accuracy and computational load of the DOA algorithm.

Multiple novel DOA algorithms are presented in this thesis to investigate and overcome the challenges faced by existing techniques. The results are published in 2 journal papers [1, 2] and 5 conference papers [3-7].

1.1 Research Motivation

DOA estimation is essential, especially in real-world applications such as intelligent transportation systems and wireless communication. For example, a beamforming smart antenna system requires DOA estimation to estimate the location of the signal source for efficient signal beam reproduction [8]. Furthermore, DOAs of interest tend to change rapidly; thus, the DOAs must be determined quickly and accurately. Although there have been some past works on the problem of fast computational time and high-accuracy DOA estimation, it is typically a compromise between one or the other due to the heavy statistical reliance on received sample data. In the most basic form, the lower the received sample data, the lower the estimation accuracy. Otherwise, the higher the received sample data, the higher the estimation accuracy. For example, classical subspace-based techniques such as Multiple Signal Classification (MUSIC) [9] and the Enhanced Principal Singular-vector Utilization for Modal Analysis (EPUMA) [10] have been proposed to solve for outright DOA estimation accuracy but at the expense of computational time.

In contrast, techniques such as a fully-trained machine-learning-based DOA estimation system were introduced to solve computational time but lacked estimation accuracy in a dynamic scenario [11]. Recent attempts have been made to solve these problems simultaneously [12, 13]. However, these techniques require constant back-end data training and are not feasible for mass deployment in a dynamic, real-world scenario as they can be costly and inefficient [14, 15].

Furthermore, the lack of fast and accurate DOA estimation techniques for real-time application is a critical challenge that DOA estimation development faces. It has been previously established that a few antenna sensor elements and small temporal samples often limit DOA estimation performance. A smart antenna system coupled with a fast and efficient DOA estimator for a dynamic environment is required to be solved to address the challenges faced in real-world scenarios. Furthermore, there is a lack of research in aligning the needs of a real-world scenario for DOA estimation. In existing DOA systems, DOA estimation development has always been algorithm-focused instead of application-based. In many past research works, real-world models such as different operating frequencies and low

computational time requirements have not been considered to independently highlight the algorithm's raw estimation and computational performance via a best-case scenario.

The demand for real-time implementation has motivated research to improve the statistical efficiency of subspace-based DOA algorithms such as MUSIC [9] and the Estimation of Signal Parameters via Rotational Invariance Technique (ESPRIT) [16, 17]. Many approaches to solving the DOA estimation problem have been proposed in past works of literature [10, 18, 19]. However, multiple challenges still have yet to be solved, especially in terms of computational time and DOA estimation accuracy. In general, a practical DOA algorithm must provide a real-time response solution that is computationally efficient and utilizes a minimal number of array snapshot samples. Currently, most of the suitable techniques for real-time implementation have explicitly aimed at reducing the computational load of subspace decomposition per refresh update, but not at the number of array snapshots necessary to attain a certain level of performance [10, 20, 21].

The problem here lies in the lack of development of real-time and fast DOA estimators for real-world dynamic scenarios, such as in applications in intelligent transportation systems and wireless communication networks. This thesis addresses this problem by developing single-time instant snapshot-based DOA estimation methods based on a modified subarray architecture and a modified correlation matrix computation while exploiting the spatial features of the fixed antenna array structure.

1.2 Research Aims & Objectives

The research in this thesis aims to enhance current DOA estimation techniques that are feasible for real-world applications such as transportation and wireless communication in a low-cost smart antenna system. The objective of this research is as follows:

i) To assess the importance of DOA estimation algorithms and their development path trend, focusing on identifying the computational complexity and estimation accuracy limitations.
ii) To identify the problems faced with current state-of-the-art DOA estimation algorithms.
iii) To investigate the complexity of current DOA estimation algorithms and identify trade-offs in reducing the computational time required for rapid DOA changes common in real-world scenarios.
iv) To develop a DOA estimation algorithm that can resolve multiple closely-spaced signals of interest with high-resolution and enhanced DOA estimation accuracy without

needing a significant computational time to reduce the need for expensive hardware costs and implementation.

v) To analyse the performance of the proposed DOA estimation algorithms developed in this thesis and what could be done as part of future work.

1.3 Key Contributions

To address the unique challenge of DOA estimation in terms of computational time and estimation accuracy, efficient and accurate algorithms to calculate the DOAs are proposed in this thesis. A two-pronged strategy was adopted to address these challenges:

1. Firstly, it is to reduce estimation time while maintaining DOA estimation accuracy that is equivalent to existing DOA estimation techniques
2. Secondly, it is to improve DOA estimation efficiency, which will lead to developing a fast and high estimation accuracy DOA estimator.

Based on these concepts, various novel DOA algorithms are proposed in this thesis:

- Root-Transformation (Root-T) DOA estimation algorithm [3] utilizes polynomial rooting to solve and determine the estimated DOAs with reduced computational time. It has been shown that the root-T technique reduced the computational time by 49.5% against existing DOA techniques. Root-T is investigated and proposed in Section 3.1.
- Cross-Cumulants MUSIC (CC-MUSIC) DOA estimator [6] that utilizes a unique hybrid higher-order statistical data coupled with polynomial rooting to improve DOA estimation accuracy by up to 83.3%. CC-MUSIC was proposed and presented in Section 3.2.
- A Subspace-Averaging DOA Estimator (SADE) [7] was proposed as a hybrid system to improve DOA estimation accuracy with a Root-Mean Squared Error (RMSE) of 9.5% against the true DOAs of interest by using both signal and noise subspaces. The SADE technique is detailed and presented in Section 3.3.
- Snapshot sample reduction in a perturbed array configuration for DOA estimators (SS-DOA) [5] to reduce computational time and improve DOA estimation accuracy. The proposed SS-DOA technique garnered a DOA estimation performance gain of up to 75.2% compared to a non-calibrated set-up. SS-DOA is investigated and presented in detail in Section 3.4.

- A covariance-based single snapshot (CbSS) DOA estimator aims to reduce computational load while maintaining high estimation accuracy in both single and multiple signal source environments with a single snapshot sample [1]. This work is presented in Chapter 4.
- A hybrid diagonal-loading DOA estimation technique further enhances DOA estimation accuracy for antenna array sensors without needing a large computational load [2]. This work is presented in Chapter 5.

The contribution of this thesis can be summarised in the following three points.

- Firstly, the necessity for a fast and accurate DOA algorithm is identified by analyzing existing DOA estimation in scenarios such as in a transportation environment.
- Secondly, a set of four novel DOA estimators is proposed to individually solve the computational time and estimation accuracy challenges faced in existing techniques in a real-world scenario. These techniques have been published as conference papers in [3-7].
- Thirdly, two novel DOA estimators are proposed based on the set of novel techniques presented in past conference papers. The main results of the two algorithms have been published in journal papers [1, 2].

1.4 Thesis Outline

The rest of the thesis is organized as follows:

Chapter 2 covers an overview of DOA estimation. Firstly, a literature review on various DOA estimation techniques of interest is presented. Next, the fundamental general data model for DOA estimation is derived, including the received signal data model and array covariance matrix. The evaluation criterion for DOA estimation is also defined, which will be used as the different environmental parameters and scenarios to compare the other developed techniques. Existing DOA estimators' performance evaluation and analysis are also presented as an initial benchmark for subsequent algorithm development and problem identification.

Chapter 3 covers multiple novel and preliminary DOA techniques to overcome problems faced with existing DOA estimators that have been highlighted in Chapter 2. Multiple novel DOA estimators are presented here. Firstly, the Root-Transformation matrix DOA estimator is shown to reduce computational load. Next, a higher-order DOA estimation technique called the CC-MUSIC is introduced to attempt an enhanced DOA estimation performance of multiple closely-spaced signal sources. Then, SADE is introduced to reduce computational load without sacrificing DOA estimation accuracy. Lastly, a single snapshot DOA estimation is explored. Due to the sensitivity and lack of statistical information of single snapshot estimators, an auto-calibration technique was proposed to sustain good DOA estimation performance.

Chapter 4 covers an in-depth analysis of a proposed recursive covariance matrix reconstruction approach for single snapshot DOA estimation based on the information gained from Chapter 3. The CbSS technique leverages the analytical information gained from the research on existing and proposed preliminary methods. A data model and problem formulation are presented, including defining the error terms in covariance matrices that are commonly overlooked in past DOA estimators. Then, a lower and upper bound is defined to determine accurate DOA estimation. The CbSS technique is then studied and analyzed in the simulation and discussion section with recommendations for further improvements.

Chapter 5 then presents an adaptive diagonal loading technique to improve DOA estimation based on the recommendation for further improvements of the CbSS technique that has been demonstrated in Chapter 4. The diagonal loading technique is first introduced. Then, the data model of the proposed method is defined in detail. Simulation results are presented and discussed based on different scenarios, such as limited snapshot samples with

single and multiple signal sources. In addition, the single snapshot performance with a single signal source is also presented and analyzed.

Chapter 6 concludes the thesis, including the future work section that proposes potential future research, such as hardware implementation and the real-world impact the proposed DOA estimation techniques have in different applications.

2 An Overview of Direction of Arrival Estimation

2.1 Recent Trends in DOA Estimation – A Literature Review

Over recent years, DOA estimation has been considered a crucial field in signal processing with applications such as mobile communication, marine communication, space communication & localization, radar surveillance, vehicle auto-navigation & avoidance, and medical diagnosis [20, 22-24]. Coupled with an antenna array and beamforming technology to form a smart antenna, these systems have gained a positive reputation due to their ability to have adaptive radiation patterns and high directivity gain compared to a conventional omnidirectional antenna and multipath signal attenuation [25].

With Wi-Fi systems in the IEEE 802.11 protocol enabling smart cities and infrastructures, there is a need to develop simplified smart antennas to cater to the exponential growth of wireless usage by improving wireless transmission efficiency, as discussed in [26] and [27]. Some wireless infrastructure examples are wireless hotspots in crowded areas such as in shopping malls and in public transportation networks such as trains and buses. To that end, a robust and accurate DOA technique must be employed to cater to the high usage of a wireless network to reduce wireless traffic congestion and improve efficiency without sacrificing the data bandwidth as much as possible.

There has been an increase in demand for research for a DOA-enabled smart antenna system – typically in transportation and vehicular application [28-30]. One example would be in [31], where a measurement campaign was carried out in a high-speed train (HST) environment where the downlink (Access Point to Client) signals were deployed along an HST railway. The DOA was estimated based on the Space-Alternating Generalized Expectation-maximization (SAGE) principle by constructing a virtual antenna array based on the train speed knowledge by exploiting the Doppler frequency characteristics trajectory and least-square method. [31] only carried out the test in the third generation (3G) Universal Mobile Telecommunications System (UMTS) frequency band of 2-3 GHz Results

This chapter is partially reproduced from paper #3 in the publication list on page iv, where the thesis author is the main author in the paper.

demonstrated reasonable estimation using the SAGE principle. However, this technique is deemed complex as it requires the parallel computation of geometrical parameters of the train, the formation of a virtual antenna array, and DOA algorithm application [32, 33].

Another example would be in [34], which employs a 12-element Electronically Steerable Parasitic Array Radiator (ESPAR) antenna designed for DOA estimation as part of a railway control system. The DOA techniques used were the cross-correlation and MUSIC algorithm [34-36]. It was discovered in [34] that the method employed in combination with ESPAR is susceptible to residual in-band interference, resulting in a broad and less precise DOA estimation.

Alternatively, newer techniques such as implementing Machine-Learning (ML) [37-39] and Information Geometry (IG) [40-42] have recently been in active research for DOA estimation. In [11], an ML-based DOA estimator was proposed for vehicular applications, yielding excellent estimation accuracy. In [41], the implementation of IG with DOA estimation was conducted by exploiting the relationship between probability density and the differential geometry structure of the received data and geodesic distance. This IG technique, known as Scaling Transform-based Information Geometry (STRING), resulted in higher accuracy and DOA estimation resolution.

However, these existing techniques have some significant drawbacks. First, these techniques yield high computational complexities and are impractical for real-world applications that differ in various environments [43].

For example, a sensor array can be developed based on a 5500 MHz operating frequency band but loses signal and estimation performance when operating in other frequency bands [44]. In addition, ML-based techniques require elaborate and comprehensive offline data training for optimization and operational efficiency [45]. Moreover, although the IG-based approach presents good DOA estimation accuracy but has significant statistical bias and results in poor robustness, especially at a high Signal-to-Noise Ratio (SNR) [46].

In recent years, numerous state-of-the-art DOA estimation techniques have been proposed with increased accuracy and robustness. In [10], the EPUMA DOA estimation approach was proposed. The EPUMA technique provides reliable performance when the number of snapshot samples is small, even when the number of samples is lower than the number of impinging signals. The simulation results in [10] indicate that the EPUMA approach outperforms many other subspace-based DOA estimators, especially for small sample scenarios [47]. In [48], an Eigenvalue-based DOA estimator named the Partial-Relaxation (PR) approach was proposed. The PR approach is based on the deterministic maximum

likelihood, weighted subspace fitting, and covariance fitting methods. Using an iterative rooting scheme based on the rational function approximation, the DOA is determined by first relaxing the manifold structure of the remaining interfering signals, resulting in a closed form estimation. Then, DOA is approximated by using a simplified peak spectral search. The simulation results of [48] shows that, irrespective of any structure of the sensor array, the performance of the PR approach is superior to the conventional methods in low SNR and snapshots while maintaining comparable computational costs to MUSIC [49].

A simple technique to reduce complexities is by reducing the number of snapshots required for DOA estimation [50-53]. An algorithm requires little data processing to determine the covariance matrix if the number of snapshot sample data is reduced. There have been many attempts in past works of literature to use a single snapshot for DOA estimation, particularly in reducing the DOA estimation error in an exhausted statistical sample size [54-56]. In [57], a low complex single snapshot DOA estimation was proposed. This technique was conducted by first obtaining rough initial DOA estimates and searching for accurate estimates within a very small region. The proposed approach offered high accuracy with low complexity but required many antenna array elements for the best performance. Alternatively, [58] presented a novel method for recursively estimating the DOAs as measurements based on worst-case gain minimization to reduce estimation error with a single snapshot. The simulations in [58] presented good DOA estimation results but required significantly high SNR levels of up to 35 dB, which is impractical in real-world scenarios.

In more recent years, Diagonal Loading (DL) of the sample covariance matrix has been a popular technique to improve DOA estimation efficacy and beamforming capabilities while reducing computational costs in a limited sample situation [59, 60]. The DL algorithms can be considered an auxiliary subsystem into the primary DOA technique by correcting all the sample eigenvalues with the same parametric value to increase the resolution for improved beamforming and signal direction selection [61]. More precisely, the DL method addresses the problem of optimally selecting suitable loading values along the diagonals of a covariance matrix to maximize the SNR in the presence of steering vector errors [62]. In [21], a DOA estimation method was proposed by integrating a modified orthogonal propagator technique with spline interpolation, a form of DL. This was done by restoring the noise-free diagonal elements through an interpolation procedure while the propagator can be directly extracted from the denoised sample covariance matrix. The proposed method offers a unique approach to reducing the noise impact and DOA mismatch. However, this method is solely based on the pseudo-spectrum DOA estimation technique, which is still considered computationally expensive with an inherently slow DOA estimation detection. The complexity of their

proposed approach increases exponentially as the number of signal sources increases. It only presents good estimation in a significantly high SNR environment and weak estimation performance in low SNR of < 0 dB. In addition, operating frequency mismatch was not taken into consideration in the development of their proposed technique.

In another example, [63] presented a similar DL-based approach – a robust quadratically constrained beamformer against DOA mismatch. A DL method was used to force magnitude responses at the arrival angles between two steering vectors that exceed unity in the pseudo-spectrum. This method causes the gains at a desired range of angles to exceed a constant level while suppressing the interferences and noise with numerical results that have excellent estimation performance. However, the critical drawback of the proposed technique in [63] is that the complexity depends on the number of iterations wholly dependent on the SNR. The higher the SNR, the higher the iteration, which leads to higher computational costs.

Furthermore, there is an additional iteration that was not mentioned. The condition presented in [63] is based on granular angle values (i.e., $0°, 30°, 80°$). The computational complexity increases exponentially when a high-resolution estimation is required.

In this chapter, the general data model for DOA estimation is derived, which will be the basis of the formulation of all subsequent algorithm development, such as the received signal data model and the crucial array covariance matrix. Then, some existing DOA estimation techniques are highlighted, such as root-MUSIC, root-Weighted Subspace Fitting (root-WSF), and the beamspace-ESPRIT algorithm. Then, a standard evaluation criterion, such as varying operating frequency, signal source separation, identification capability, and coherent signal sources, is presented, which will be used to compare and analyze the existing and proposed DOA estimation techniques. Lastly, a performance analysis is conducted to show and highlight the usage of the evaluation criterion for the various DOA estimation techniques, which allows for the identification of some problems and research gaps such as a lack of estimation accuracy and computational time that needs to be solved and rectified which will be presented in subsequent chapters.

2.2 General Data Model for DOA Estimation

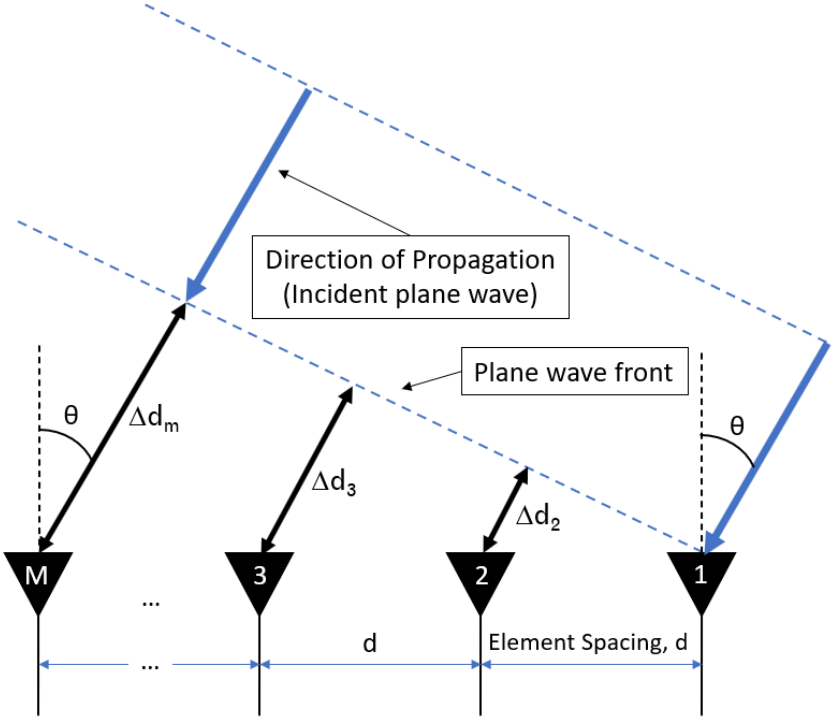

Figure 2.1 Sensor Array Model

2.2.1 Received Signal Data Model Formulation

With reference to Figure 2.1, consider an array of M sensors receiving the signals emitted by L narrowband far-field sources with unknown DOAs $\{\theta_1, \ \dots, \ \theta_L\}$ with inter-element spacing d being no greater than $\lambda/2$. The number of L incident signals is assumed to be available where the wavelength of incident signals, $\lambda = c/f_c$, where f_c is the signal carrier frequency and c is the speed of light in a vacuum. The k^{th} array snapshot of the received signal is expressed as [20, 22]

$$\mathbf{x}(k) = \mathbf{A}\mathbf{s}(k) + \mathbf{n}(k), \tag{2.1}$$

where $\mathbf{A} = [\mathbf{a}(\theta_1), \mathbf{a}(\theta_2), \cdots, \mathbf{a}(\theta_L)]$ is the steering matrix of size $M \times L$, $\mathbf{s}(k) = [s_1(k) \ \dots \ s_L(k)]^{\mathrm{T}}$ is the source signal vector with $(\cdot)^{\mathrm{T}}$ being the transpose, K is the total number of snapshots, and $\mathbf{a}(\theta_L)$ is the steering vector of the L^{th} signal source, which can be expressed as

$$\mathbf{a}(\theta_L) = \left[1 \quad e^{j\frac{2\pi}{\lambda}\sin d_2(\theta_L)} \quad \dots \quad e^{j\frac{2\pi}{\lambda}\sin d_M(\theta_L)}\right]^{\mathrm{T}} \tag{2.2}$$

where $f_m(\theta)$ is a known operating frequency function with respect to θ for given coordinates of the mth sensor and j is a complex number, and $-90 \geq \theta < 90$ with half-wavelength Uniformed Linear Array (ULA) with inter-element spacing, where $f_m(\theta) = \pi(m-1)\sin\,\theta$.

2.2.2 Array Covariance Matrix

In (2.1), $\mathbf{s}(k) = [s_1(k), s_2(k) \ldots, s_L(k)]^T$ and $\mathbf{n}(k) = [n_1(k), n_2(k), \cdots, n_M(k)]^T$ denote the signal and noise vectors, respectively which are assumed to be uncorrelated. The noise parameter $\mathbf{n}(k)$ is considered to be zero-mean with variance $\sigma^2\mathbf{I_M}$ white Gaussian noise vector independent of $\mathbf{s}(k)$ while $\mathbf{I_M}$ is an $M \times M$ identity matrix. Then, the theoretical array is defined as a covariance matrix as [9, 64]

$$\mathbf{R_{xx}} = \mathbb{E}\{\mathbf{X}\mathbf{X}^{\mathrm{H}}\} = \mathbf{A}\mathbf{E}_{\mathrm{s}}\mathbf{A}^{\mathrm{H}} + \mathbf{E}_{\mathrm{N}}, \tag{2.3}$$

where $\mathbf{R_{xx}}$ is the theoretical covariance matrix of size $M \times M$ while $\mathbb{E}\{\cdot\}$ and $(\cdot)^{\mathrm{H}}$ represents the mathematical expectation and Hermitian transpose, respectively while $\mathbf{E}_{\mathrm{s}} = \mathbb{E}\{\mathbf{s}(k)\mathbf{s}^{\mathrm{H}}(k)\}$ is the signal subspace, and $\mathbf{E}_{\mathrm{N}} = \mathbb{E}\{\mathbf{n}(k)\mathbf{n}^{\mathrm{H}}(k)\}$ is the noise subspace.

In practice, however, the exact covariance matrix of $\mathbf{R_{xx}}$ is challenging to obtain due to the limited number of data sets received and processed by a sensor array system. Thus, an estimation is made using limited, finite snapshot samples in an instantaneous time to overcome this limitation. Assuming that all underlying random noise processes are ergodic, the statistical expectation in (2.3) can be replaced by a time average. An estimate of the data covariance matrix $\mathbf{R_{xx}}$ can be presented as a sample covariance matrix, which is expressed as

$$\mathbf{R_{xx}} \approx \widehat{\mathbf{R}}_{\mathbf{xx}} = \frac{1}{K}\sum_{k=1}^{K}\mathbf{x}(\mathrm{k})\mathbf{x}^{\mathrm{H}}(\mathrm{k}) = \frac{1}{K}\mathbf{X}\mathbf{X}^{\mathrm{H}}, \tag{2.4}$$

where $\widehat{\mathbf{R}}_{\mathbf{xx}}$ is the sample covariance matrix, $\mathbf{X}$ is the input data matrix of size $M \times K$, and K is the number of snapshot samples.

2.3 Common DOA Estimation Methods

The primary objective of the DOA algorithms is to collect the incoming signal source data received from the antenna array and estimate the direction of the signal source relative to the array's location. Many state-state-of-the-art DOA estimation methods are rooted in time series analysis, spectrum analysis, periodograms, eigenstructure, parametric, linear prediction, beamforming, array processing, and adaptive array methods [65]. This section

discusses and evaluates some of the existing DOA estimation methods commonly used as a benchmark and the basis for further development.

2.3.1 Root-MUSIC

The Root-MUSIC technique is a modification to the MUSIC algorithm proposed by Schmidt [66] and is based on polynomial rooting from the noise subspace, which provides higher angular resolution. However, it only applies to a uniform linear array [67]. The expression of the Root-MUSIC technique, as shown in [20], can be presented as,

$$P_{rootmusic}(\theta) = \frac{1}{|a(\theta)^H \boldsymbol{C} a(\theta)|} \tag{2.5}$$

where $a(\theta)$ is the steering vector, and **C** is a Hermitian matrix given as,

$$\boldsymbol{C} = \mathbf{E}_{\mathrm{N}} \mathbf{E}_{\mathrm{N}}{}^{\mathrm{H}} \tag{2.6}$$

The poles of the MUSIC pseudo-spectrum are the corresponding polynomial roots that lie closest to the unit circle.

With reference to [20], DOA is calculated by:

$$\theta_i = \sin^{-1}\left(\frac{Im(logz_i)}{kd}\right) \tag{2.7}$$

Where, $z_i = e^{j\frac{2\pi}{\lambda}d\sin\theta}$ and $k = \frac{2\pi}{\lambda}$.

2.3.2 Root-Weighted Subspace Fitting

Another technique employed for DOA estimation is the Root-WSF algorithm [68]. With the capability to detect coherent signals, such as in a multipath environment, this is one of the most sought out techniques, especially in a Wi-Fi environment where the multipath environment is common. However, it is essential to note that this technique is iterative to obtain its accuracy and differentiate coherent signal sources. Therefore, it is demanding in terms of computational complexity leading to a longer computational time. Additional analytical details of the Root-WSF algorithm can be found in [69, 70]. This technique has been chosen for this chapter as past works of literature have proven that it provides good angular resolution and multipath attenuation. As analyzed by [71], it has been shown that the root-WSF technique provides good resolution performance according to the simulation results.

2.3.3 Beamspace-ESPRIT Algorithm

The beamspace-ESPRIT algorithm presents reduced computational complexity, which derives from the ESPRIT algorithm [72]. This approach solves a subspace DOA estimation problem with reduced dimensions in beamspace.

The main drawback of this technique is that it always requires a priori knowledge of the sector where the signals are located to position the center of the output beam fan [73-76]. More details regarding the Beamspace-ESPRIT algorithm can be found in [77]. This technique was chosen for the analysis as it has been shown in past works of literature, such as [72] presenting significant computational savings and performance.

2.4 Performance Analysis of Common DOA Methods

To evaluate the performance of the DOA algorithms, the following standard model is assumed, which is based on [78]:

- Number of elements: 4
- Element spacing: 27.25mm
- Number of samples: 1024
- Noise Power: -20dBW/0.01W

For the number of the signal source, it is assumed that this value is known a priori (number of clients does not change per detection). As for the array element spacing, it is considered fixed in real-world applications and can perform across multiple Wi-Fi channels. In this case, the element-spacing half wavelength of 5500 MHz operating frequency. Noise is assumed to be an Additive White Gaussian Noise (AWGN) at 0.01W/-20dBW power, considering propagation and cable loss. All simulations ran for 500 times and tabulated as mean values across all iterations unless otherwise stated. The simulation for this section was performed using MATLAB R2018b.

2.4.1 Low-Frequency Against High-Frequency Operating Performance

Typically, in a 5 GHz Wi-Fi scenario, a list of channels can be selected per the 802.11ac wave 2 protocol. The different channels will have different performance levels. For example, one channel may be noisier and/or congested than another. The frequency of a signal directly influences the DOA performance. At low frequency, it was proven that good

coherence and well-correlated signals are achievable while having poor coherence and uncorrelated signals at high frequency.

This section presents an evaluation of DOA algorithms with varying operating frequencies. For the simulation, the 5 GHz Wi-Fi band regulated in Singapore is used, ranging from 5160 MHz to 5845 MHz. The results of the simulation can be found in Table 2.1. The 3 DOAs of interest were tested at -45°, 10°, and 45°.

Table 2.1 Varying Operating Frequency Performance

	Root-MUSIC			**Root-WSF**			**Beamspace-ESPRIT**		
True DOA (degree)	-45	10	45	-45	10	45	-45	10	45
5160 MHz	-45.01	10.01	45.141	-45.01	10.01	45.138	-45.1	9.98	45.115
5500 MHz	-45.01	10.01	45.115	-45.001	10.01	45.112	-45.06	9.997	45.103
5845 MHz	-45.001	10.007	45.09	-45.0004	10.02	45.09	-45.04	9.991	45.0942

Based on the simulation results in Table 2.1, all three techniques can estimate the actual direction of arrival. The Root-MUSIC and Root-WSF algorithms perform similarly at the lowest operating frequency. Both algorithms perform much better than the Beamspace-ESPRIT technique in terms of their resolution accuracy.

However, at higher operating frequency, the results deviate slightly between Root-MUSIC and Root-WSF. The Root-WSF technique performs much better at high frequency than Root-MUSIC and BS-ESPRIT.

2.4.2 Closely-Sourced Signals

In a real-world wireless communication environment, sources can be close to each other. For example, a user may be connected via Wi-Fi with their phone and laptop at the same time within a short distance away from each other. If a DOA estimator cannot resolve the signal source, it will cause erratic signal behaviour in a practical scenario [79, 80]. Therefore, this evaluation criterion is necessary to determine the DOA algorithm with high precision and accuracy. For this part, the variance of each sample is taken, which is expressed as,

$$V = \frac{1}{Q-1}\sum_{i=1}^{Q}|B_i - \mu|^2 \tag{2.8}$$

where V is the variance value, Q is the number of observation samples, B is the estimated DOA data, and μ is the mean of A, which is expressed as:

$$\mu = \frac{1}{Q}\sum_{i=1}^{Q} A_i \tag{2.9}$$

Consider a scenario where the signal sources are closely spaced with one another. For this section, the same standard model parameters are assumed. The operating frequency is fixed at 5500 MHz. In addition, the array receives two signal sources at the same time. The two sources are spaced and simulated at 8° and 4° apart.

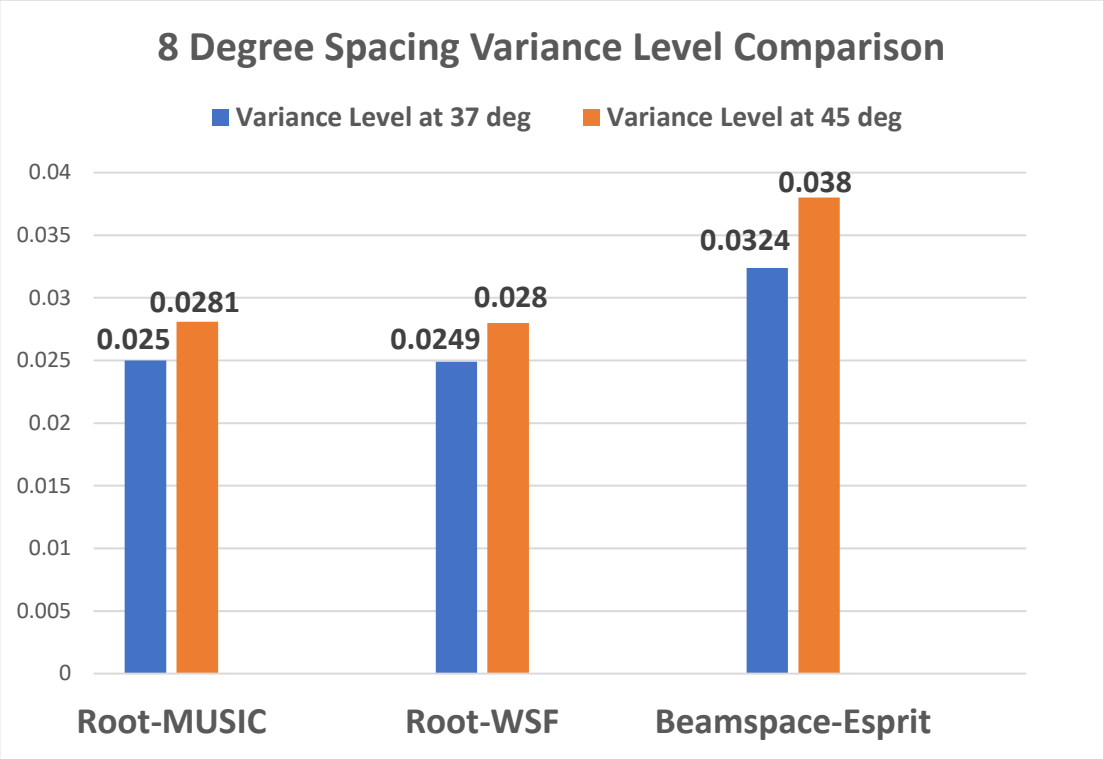

Figure 2.2 Variance level of 8 degrees spacing

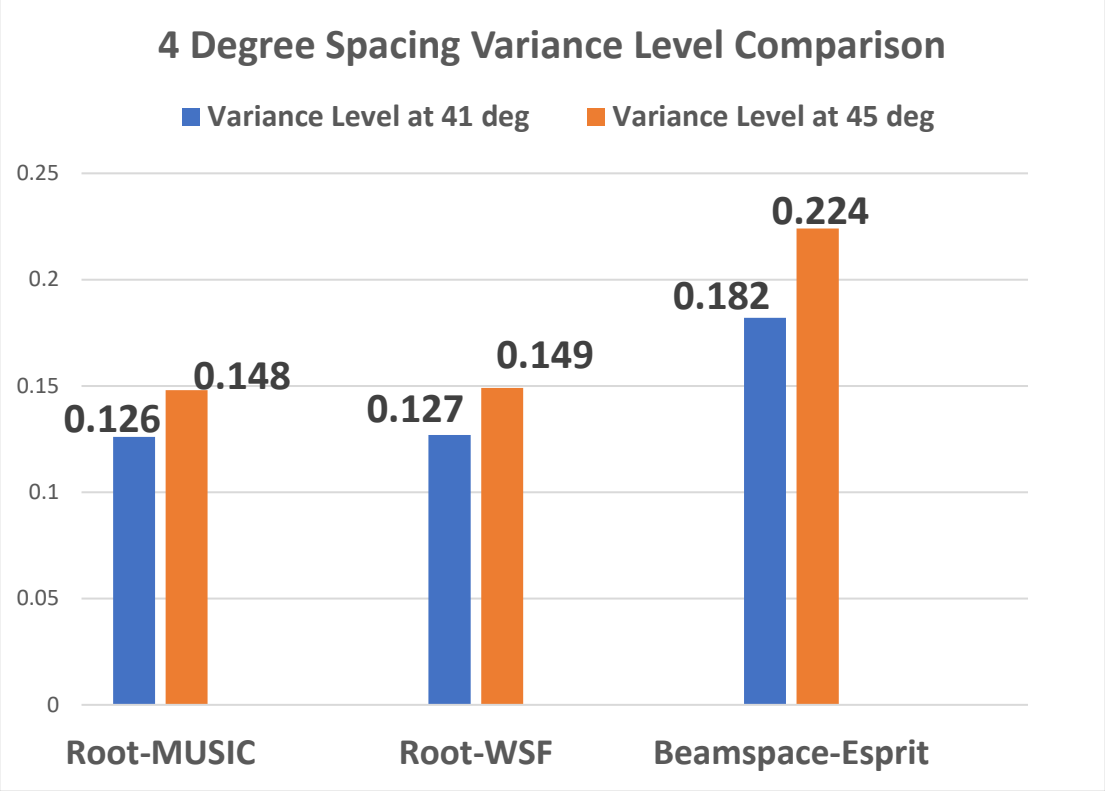

Figure 2.3 Variance level of 4 degrees spacing

Table 2.2: 8 Degree Signal Source Separation Performance

	Root-MUSIC		Root-WSF		Beamspace-Esprit	
True DOA (Degrees)	37	45	37	45	37	45
Spaced 8 degrees	37.349	44.934	37.342	44.942	37.279	44.879
Variance	0.025	0.0281	0.0249	0.028	0.0324	0.038

Table 2.3: 4 Degree Signal Source Separation Performance

	Root-MUSIC		Root-WSF		Beamspace-Esprit	
True DOA (Degree)	41	45	41	45	41	45
Spaced 4 degrees	41.912	45.016	41.875	45.051	41.772	44.872
Variance	0.126	0.148	0.127	0.149	0.182	0.224

Based on the simulation results, it is observed that all techniques can estimate sources that are closely spaced apart. Based on the variance results, the Root-WSF method performs slightly better at 8 degrees spacing, while the Root-MUSIC technique performs better at 4-degree spacing at a small margin. The BS-ESPRIT technique performs worst in both cases compared to Root-MUSIC and Root-WSF.

2.4.3 Computational Time Performance

Computational time taken is crucial, especially in real-world wireless communication scenarios, especially when fast-tracking of the signal source is required. Theoretically, faster computational time is preferred without sacrificing angular resolution accuracy. However, in practice, this may not be the case as most of the time, DOA techniques are either accurate or fast – hardly at the same time. This criterion will allow us to observe which method is the quickest and correlate the results to accuracy to select the best one for real-world application.

This section evaluates the computational time performance across the 3 DOA techniques. This scenario assumes the same standard model with an operating frequency of 5500 MHz. In addition, the array is only receiving one signal source.

Table 2.4: Computation Time Performance

	Root-MUSIC	**Root-WSF**	**Beamspace-Esprit**
Computational Time (ms)	22.5	36.7	29.4

Based on the simulation results tabulated in Table 2.4, Root-MUSIC is the fastest in terms of computational time, followed by the BS-ESPRIT and the Root-WSF technique. This is in line with the theory that accuracy comes at the expense of computational time. The Root-WSF method is iterative in obtaining the DOA and, therefore, the most computationally complex. However, in almost all cases, the Root-WSF technique provides the best overall performance in terms of accuracy.

2.4.4 Coherent Signal Source Performance

Suppose several sources are coherent such as in terms of a multipath scenario. In that case, the spatial covariance matrix will become rank deficient and cause the subspace-based DOA estimation technique to fail [81-83]. To ensure robustness, DOA techniques must be able to perform in a coherent environment to maintain estimation robustness in a wide variety of scenarios.

In this coherent signal source scenario, there are two signal sources with a true DOA of 20° and 45°. The same standard model is applied as before with an operating frequency of 5500 MHz. To simulate a multipath environment, one of the two signals is the first source's multipath reflection with a magnitude of ¼ of that first source.

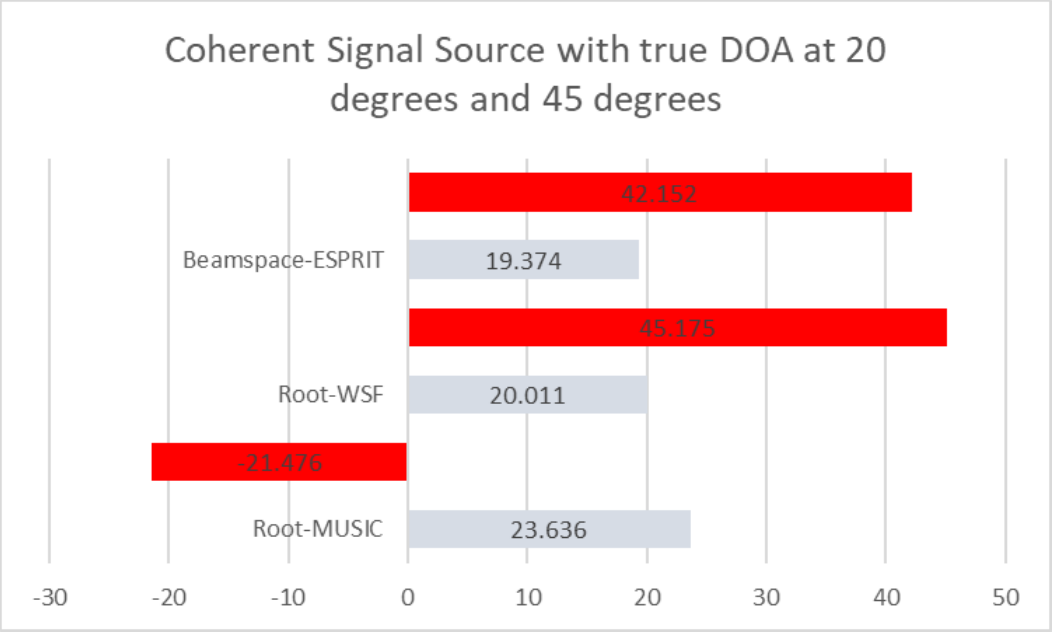

Figure 2.4 DOA Detection in Coherent Signal Environment

Table 2.5: Coherent Signal Source Performance

	Root-MUSIC		**Root-WSF**		**Beamspace-ESPRIT**	
True DOA (degree)	20	45	20	45	20	45
Coherent Signal Source	23.636	-21.476	20.011	45.175	19.374	42.152

With reference to Figure 2.4 and Table 2.5, the results show that the Root-WSF algorithm performs the best compared to the Root-MUSIC and BS-ESPRIT techniques, with a mean accuracy of 99.78% compared to 64.77% and 95.27%, respectively. It can be observed that in the context of correlated signals, Root-MUSIC will fail. This is because, for the Root-MUSIC and all the derivatives of the MUSIC algorithm, it can only estimate if sources are uncorrelated, which is true in accordance with literature studies.

2.5 Performance Summary of Existing DOA Estimation Techniques

The main objective of this chapter is to identify the problems faced by existing DOA estimators and formulate standard performance criterion metrics. According to the performance analysis and evaluation, it can conclude that the best overall performing DOA estimation algorithm would be the Root-WSF algorithm with respect to the performance

criterion. It can detect signals accurately in a multipath environment, perform optimally across a range of frequency bands, and perform well in a close-source signal environment.

Although the computational time is longer as compared to the Root-MUSIC and BS-ESPRIT algorithms, the benefit outweighs the disadvantage of having a slightly longer computational time. This can be resolved by adaptively changing the iteration with just enough cycles to obtain the most accurate DOA estimation.

Clearly, there is room for improvements based on existing techniques' DOA estimation performance results and the computational load. The next chapter introduces multiple novel DOA estimation techniques to solve the identified problems.

3 Innovative Techniques to Independently Overcome Problems with Existing DOA Estimators

Sub-space techniques such as the classical MUSIC [66] and ESPRIT [17] have been some of the most sought-after DOA estimation methods in many past works of literature due to their consistent estimation performance, reliability and ease of understanding for implementation. Although these subspace methods like MUSIC are old techniques that were proposed decades ago, these techniques are still being improved on or used as a platform to further develop state-of-the-art DOA methods such as the integration of MUSIC with machine-learning [25, 37] and many other techniques that can trace their roots back to the MUSIC and many other subspace-based DOA estimation techniques [84, 85].

Past literature has presented modifications to the MUSIC DOA algorithm called improved-MUSIC to improve performance in a coherent signal environment with high resolution compared to the classical MUSIC algorithm [22, 86, 87]. The problem with improved-MUSIC and many existing DOA estimation techniques is computationally intensive. It requires a scan of all possible angles to obtain pseudo-spectrum peaks to determine the signal's DOAs. Based on the literature review, there is clear evidence that fast computational time with high DOA estimation accuracy is yet to be met.

In this chapter, various proposed designs of DOA estimators are presented to solve the problems of computational time and estimation accuracy faced by existing estimators individually. First, the Root-T technique is introduced to reduce the computational load while conserving DOA estimation accuracy [3]. Next, higher-order DOA estimators called the CC-MUSIC [6] are introduced to improve the DOA estimation accuracy in a closely-spaced signal source scenario. Then, the SADE is introduced further to enhance the DOA estimation performance [7]. Lastly, single snapshot DOA estimation is investigated with a novel technique to ensure high estimation accuracy using auto-calibration of sensor data [5].

This chapter is reproduced from paper #4 - #7 in the publication list on page iv, where the thesis author is the main author in the paper.

3.1 Root-Transformation Method for DOA Estimation

A simple technique is presented here by introducing a polynomial-solving algorithm called the Root-T technique by obtaining the roots of the improved MUSIC algorithm to obtain the DOAs, a similar technique employed for root-MUSIC [5] for a ULA antenna structure. This conserves the performance of the improved-MUSIC technique while reducing computational complexity. Its performance in low SNR, closely-spaced signals and computational efficiency will be observed. In theory, this enables localization applications such as low-cost beamforming smart antennas and Internet-of-Things (IoT) devices. Although [6] presented a comprehensive study on various state-of-the-art DOA techniques based on a similar 4-ULA structure as presented in this section, it can be too complex for lightweight implementation.

3.1.1 Algorithm for Root-Transformation DOA Estimator

Figure 3.1 presents the algorithm flowchart for the root-T technique.

Algorithm 1 DOA Estimation using Root-T Algorithm

Require: Incoming SNR Data Matrix from Sensor Array, $\mathbf{X}$

procedure ROOT-T(θ)

Evaluate Transformation Correlation Matrix $\mathbf{R_{RR}} = \mathbf{A R_{SS} A^H} + \mathbf{I A R_{SS} A^H I^H} + \mathbf{2 R_{NN}}$

Decompose Signal and Noise Subspace $\mathbf{R_{RR}} = \mathbf{E_s \Omega_s {E_s}^H} + \mathbf{E_n \Omega_n {E_n}^H}$

Evaluate $\mathbf{C} = \mathbf{E_N} * \mathbf{E_N^H}$

Conduct Polynomial Rooting $\theta_{i(p)} = (\frac{\lambda}{2\pi d} arg(z_{i(p)}))$

end procedure

Figure 3.1 Root-T Algorithm Flowchart

In stage 1, the transformation-based correlation matrix, $\mathbf{R_{RR}}$ as derived in [22, 86, 87], is obtained, where **A** denotes the array steering matrix, **I** is the transformation diagonal identity matrix, $\mathbf{R_{SS}}$ is the signal correlation matrix, and $\mathbf{R_{NN}}$ is the noise correlation matrix as derived in [86]. $\mathbf{R_{RR}}$ here is different from the correlation matrix used for root-MUSIC as it allows the detection of signals in a coherent environment [87]. Assuming an ergodic estimation process, $\mathbf{R_{SS}}$ and $\mathbf{R_{NN}}$ can be approximated by using time-averaged correlation as derived in [87]. Stages 2 and 3 perform the eigendecomposition of $\mathbf{R_{RR}}$ to obtain the noise subspace and subsequently multiply it by its Hermitian to obtain **C**. The algorithm is modified from stage 4 onwards by employing a polynomial solving technique, unlike the improved-MUSIC process, which uses a pseudo-spectrum scan method. Stage 4 evaluates the sum across the diagonal of **C** and obtain the polynomial roots with length (-M+1) to (M-1), where M is the number of ULA antenna elements which significantly reduces computational costs.

Roots closest to the unit circle corresponds to the DOAs of interest. Thus, stage 5 processes the estimated roots and converts it into DOAs as in [88].

3.1.2 Performance Analysis for Root-T DOA Estimator

For the simulation, there are two narrowband signals impinging on a 4-element ULA of 10° and 10° at an operating carrier frequency of 5500 MHz. the antenna element spacing was set to half-wavelength, and the number of K samples is 1024. Noise is assumed to be of an ideal AWGN. For simplicity, only DOA in the azimuth plane and assumed elevation is 0° is obtained. 500 independent simulations with different noise processes are used to obtain the mean and RMSE values. For all simulation study, all poles and thus, potential DOA solutions, will be shown in the plotted graphs. There are a total of (X+1) roots, where X represents the total number of potential DOA solutions where (X+1) = (-M+1):(M-1). Therefore, in the case of M = 4, then X = 6, where a total of 6 DOA solutions are expected. However, as the DOA range of interest falls from -30 to 30 degrees, any roots that fall outside of this range is omitted.

3.1.2.1 Low SNR Performance (SNR = -30 dB)

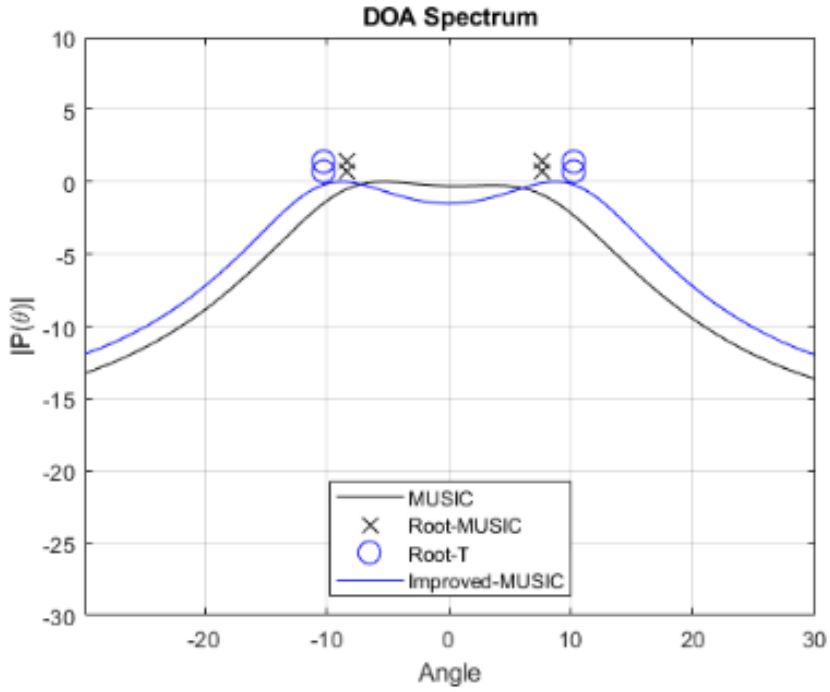

Figure 3.2 Low SNR Performance for Root-T DOA Estimator

Figure 3.2 presents mean performance in low SNR. At -30 dB, it can be observed that root-T achieves closer to the true DOA at -10.27° and 10.27°, whereas root-MUSIC achieves -8.34° and 7.61°, respectively. This presents an RMSE of 0.27 and 2.025 for

root-T and root-MUSIC, respectively. This shows an 86.7% performance increase over the root-MUSIC technique.

3.1.2.2 Closely-Spaced Signals (SNR = -20 dB)

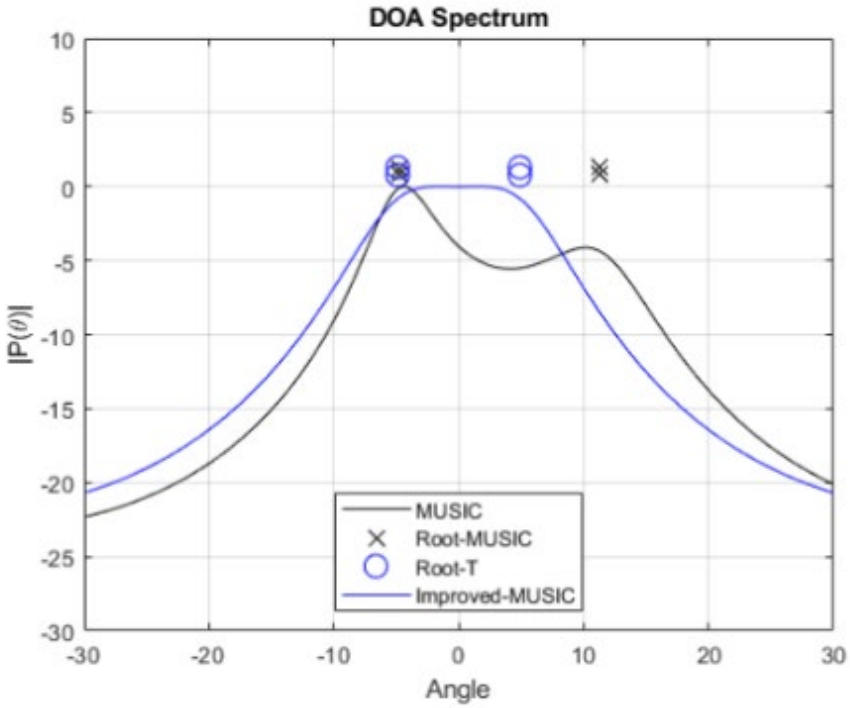

Figure 3.3 Closely-Spaced Signal Performance for Root-T

Figure 3.3 presents the mean performance of closely-spaced signals at -5° and 5°. It can be observed that the root-T performs better with a DOA estimation of -4.89° and 4.9°, whereas root-MUSIC estimated the DOA at -4.73° and 11.29°, respectively. This presents an RMSE of 0.105 and 3.28 for root-T and root-MUSIC, respectively, which is a 96.8% performance increase for root-T. It can also observe an asymmetrical detection for MUSIC because as signals converge towards each other, it leads to a coherency of signals. When signals are coherent, $\mathbf{R_{RR}}$ becomes singular as the rows are linear combinations of each other. Unlike an uncorrelated environment where $\mathbf{R_{RR}}$ is a diagonal matrix, its off-diagonal elements do not correlate. A singular $\mathbf{R_{RR}}$ causes a significant error and degradation in statistical estimation [88]. Thus, [22, 86, 87] solves this problem by introducing the **I** matrix to decorrelate the incoming signals.

3.1.2.3 Computational Runtime

Both MUSIC and improved-MUSIC employ a spectral scan of all possible angles. For example, if the sweeping scan is from -90° to 90° with a resolution of 1° in the

azimuth plane, there is a need to compute 181 iterations to determine the peaks in the pseudo-spectrum. At the same time, the root-MUSIC and Root-T techniques solve for polynomial roots along the diagonal with a maximum iteration of range -M+1:M-1 of the **C** matrix.

The mean computational time is also observed for the various DOA techniques. With reference to Table 3.1 for a 1° resolution step, it is observed that root-T is 49.5% faster than improved-MUSIC due to significantly lower computational iterations. Although root-T is 0.2 ms slower over root-MUSIC, it is a trade-off to obtain better performance in low SNR and coherent signal situations.

Table 3.1 Algorithms Computational Runtime Comparison

Technique	MUSIC	Improved-MUSIC	Root-MUSIC	Root-T
Mean Runtime (milliseconds)	2.69	3.03	1.29	1.5

3.1.3 Root-T DOA Estimator Performance Summary

From the simulation results and comparison, root-T maintains improved-MUSIC performance with lower computational complexity by 49.5% while superseding the estimation performance of root-MUSIC. However, one of the critical drawbacks of root-T is the lacklustre DOA estimation accuracy in a low SNR scenario. In the following sub-section, a hybrid system combining higher-order spatial cross cumulants and root-MUSIC improves DOA estimation performance in low SNR scenarios.

3.2 DOA Estimation using Hybrid Higher-Order Spatial Cross-Cumulants and Root-MUSIC

The fourth-order covariance matrix contains more information, such as the phase difference at the reference element, than that of the second-order covariance matrix [89]. This is calculated via the Kronecker product of the received data and its conjugate value. In other words, by introducing a phase difference to the reference antenna array element, a virtual array element is introduced by extending the antenna array element by $(M + 1)$ [89]. This method would theoretically allow efficient noise suppression and higher resolution accuracy, especially in a multi-signal source scenario. It has also been demonstrated that by using higher-order statistics applied to the classical MUSIC algorithm, as in [90], the effectiveness

of the cumulant-based MUSIC can restrain efficiently in the effect of coloured noise when compared to the equivalent second-order covariance-based version with higher resolution probability and in low SNR scenario for DOA estimation.

While the classical MUSIC has been deemed a high-resolution DOA estimator, as demonstrated in [47, 48], the computational load of executing a spectral scan of all possible angles is still needed to determine the DOAs. One such technique to solve for the high computational load was the introduction of the root-MUSIC [88] technique which encompasses the polynomial solving method to solve for the DOAs. Regarding computational time, root-MUSIC reduces the computational time by half compared to the classical MUSIC technique [87]. In addition, as the fourth-order cross cumulant has the same matrix size as the second-order covariance matrix, implementation and realization for real-world applications are relatively simple. To that end, it is desirable to develop an algorithm that has the benefits of using a fourth-order cumulant-based covariance matrix on its excellent performance in low SNR scenarios as well as root-MUSIC's computational efficiency.

This technique improves a DOA estimator's resolution and accuracy, particularly in a low SNR scenario. A hybrid fourth-order cross cumulant-based technique is proposed to determine a higher-order sample covariance matrix coupled with the root-MUSIC algorithm and solve the polynomial roots to assess the respective DOAs. The root-MUSIC estimator is also chosen as the base algorithm. It retains high-resolution accuracy and is relatively easy to implement in real-world scenarios, as demonstrated in [91, 92].

3.2.1 Higher-Order Spatial Cross Cumulants

It has also been demonstrated that cross cumulants-based covariance matrix has higher resolution probability, especially in low SNR scenarios for DOA estimation [90, 93]. The second-order complex-valued cross cumulant for two generic variables X and Y is the cross-power spectrum which is expressed as [89]:

$$C_2(X, Y^*) = \mathbb{E}[XY^*] - \mathbb{E}[X]E[Y^*] \tag{3.1}$$

A fourth-order complex-valued cross cumulant for two generic zero-mean processes X and Y can be extended from (3.1) and is expressed as [89]:

$$C_4(X, X, Y^*, Y^*) = \mathbb{E}[X^2Y^{*2}] - \mathbb{E}[X^2]\mathbb{E}^*[Y^2] - 2\mathbb{E}[XY^*]^2 \tag{3.2}$$

To that end, it should be noted that there are many variants of cross cumulants techniques for complex-valued random processes. Generally, for a complex-valued cross cumulant of order N, there are 2^N ways to configure the complex conjugate on the parameters to C_N which results in different definitions.

The fourth-order covariance matrix $\mathbf{R_{4X}}$ based on the received signal data matrix can be extended with reference from (3.2) and is expressed as follows:

$$\begin{aligned}\mathbf{R_{4X}} = \mathbb{E}\{(\mathbf{X} \otimes \mathbf{X}^*)(\mathbf{X} \otimes \mathbf{X}^*)^{\mathrm{H}}\} \\ -\mathbb{E}\{\mathbf{X} \otimes \mathbf{X}^*\}\mathbb{E}\{\mathbf{X} \otimes \mathbf{X}^*\}^{\mathrm{H}} \\ -\mathbb{E}\{\mathbf{X}\mathbf{X}^{\mathrm{H}}\} \otimes \mathbb{E}\{(\mathbf{X}\mathbf{X}^{\mathrm{H}})^*\}\end{aligned} \quad (3.3)$$

Where $(\cdot)^*$ denotes the complex conjugate, $\mathbb{E}\{\cdot\}$ denotes the Expectation operator and $\otimes$ denotes the Kronecker product.

3.2.2 Cross Cumulants-MUSIC (CC-MUSIC) DOA Estimator

Instead of using the second-order sample covariance matrix to determine the noise subspace and the polynomial roots to obtain the DOAs, a modified fourth-order cross cumulant matrix is proposed, derived from the incoming received signal data. It has been shown in past literature, such as in [90], that using cross cumulants can resolve multiple closely spaced sources in a noisy environment. The proposed method consists of 10 stages, illustrated in Figure 3.4.

Algorithm 1 DOA Estimation using CC-MUSIC Algorithm

Require: Incoming SNR Data Matrix from Sensor Array, $\mathbf{X_{raw}}$

procedure CC-MUSIC(θ)

Detrend received signal matrix $\mathbf{X} = \mathbf{X_{raw}} - mean(\mathbf{X_{raw}})$

Evaluate fourth-order moments $\mathbf{Z} = \mathbf{X} \odot \mathbf{X}\mathbf{X}^*$

Evaluate $\mathbf{C_{4M}} = \frac{1}{K}\mathbf{Z^H}\mathbf{X}^*$

while $\mathbf{C_{4M}}$ is evaluated, **do**

Determine $\mathbf{R_{corr}} = \frac{1}{K}\mathbf{X^H}\mathbf{X}$

Determine $\mathbf{R_{mom}} = \frac{1}{K}\mathbf{X^H}\mathbf{X}^*$

end while

Evaluate $\mathbf{R_{4X}} = \mathbf{C_{4M}} - 2diag(diag(\mathbf{R_{corr}}))\mathbf{R_{corr}} - diag((diag(\mathbf{R^*_{mom}}))\mathbf{R_{mom}}$

Decompose Signal and Noise Subspace $\mathbf{R_{Decomp-CCMUSIC}} = \mathbf{R_s}\mathbf{\Omega_s}\mathbf{R_s}^{\mathrm{H}} + \mathbf{R_n}\mathbf{\Omega_n}\mathbf{R_n}^{\mathrm{H}}$

Conduct Polynomial Rooting $\theta_{i(p)} = (\frac{\lambda}{2\pi d}arg(z_{i(p)}))$

end procedure

Figure 3.4 CC-MUSIC DOA Estimator Algorithm Flow

Stage 1 is to obtain the received signal data matrix of size K-by-N. Stage 2 is to detrend $\boldsymbol{X_{raw}}$ by removing the mean values of the data. By removing the mean values of the data, an analysis is performed based on the fluctuation in the data. Stage 3 is to determine the fourth-order moment, which is expressed as [92]:

$$\mathbf{Z} = \mathbf{X} \odot \mathbf{X}(\mathbf{X}^*) \quad (3.4)$$

Where $\odot$ denotes the element-wise multiplication or Hadamard product. Stage 4 evaluates the fourth-order cross moments, which are expressed as [92]:

$$\mathbf{C_{4M}} = \frac{1}{\mathrm{K}}\sum_{\mathrm{k=1}}^{\mathrm{K}}(\mathbf{Z}^{\mathrm{H}}\mathbf{X}(\mathrm{k}))^{*} \tag{3.5}$$

Then, stage 5 & 6 evaluates the correlation and moment matrix, respectively, which is presented as:

$$\mathbf{R_{corr}} = \frac{1}{\mathrm{K}}\sum_{\mathrm{k=1}}^{\mathrm{K}}(\mathbf{X}^{\mathrm{H}}\mathbf{X}(\mathrm{k}))^{*} \tag{3.6}$$

$$\mathbf{R_{mom}} = \frac{1}{\mathrm{K}}\sum_{\mathrm{k=1}}^{\mathrm{K}}\mathbf{X}^{\mathrm{H}}(\mathrm{k})\mathbf{X}^{*}(\mathrm{k}) \tag{3.7}$$

Next, stage 7 evaluates the cross-cumulant matrix, which is expressed as [92]:

$$\begin{aligned}\mathbf{R_{4X}} = \mathbf{C_{4M}} - 2\mathrm{diag}\big(\mathrm{diag}(\mathbf{R_{corr}})\big)\mathbf{R_{corr}} \\ -\mathrm{diag}\big((\mathrm{diag}(\mathbf{R_{mom}}^{*})\big)\mathbf{R_{mom}}\end{aligned} \tag{3.8}$$

Where $\mathrm{diag}(\cdot)$ represents the diagonal elements of the matrix. Finally, stages 8-10 evaluate the polynomial roots to determine the respective DOAs.

3.2.3 Performance Analysis of CC-MUSIC DOA Estimator

The proposed technique for DOA estimation, CC-MUSIC, is evaluated, and the performance is compared to the root-MUSIC and ESPRIT algorithms. This is mainly to present the benefits of using fourth-order cross cumulants for the sample covariance matrix compared to the one utilizing the second-order sample covariance matrix technique, such as those typically employed for root-MUSIC and ESPRIT. The root-MUSIC and ESPRIT are chosen as the comparison because it all uses the same polynomial approach to determine the DOAs [16].

To evaluate the performance of the DOA algorithms, a simple single-user Wi-Fi antenna configuration is modelled that is employed typically between vehicular clients and access points for wireless communication [44, 78]:

- Carrier Frequency: 5500MHz
- Number of elements: 4
- Element spacing: $\lambda/2$

There are many algorithms and statistical techniques that can predict the number of signal sources, such as the Akaike Information Criterion (AIC) and Minimum Description Length (MDL), such as in [94, 95]. However, this prediction of the number of signal sources is beyond the scope of this research, and the number of narrowband signal sources is assumed to be known a priori for simplicity.

3.2.3.1 Single Source SNR-RMSE Performance

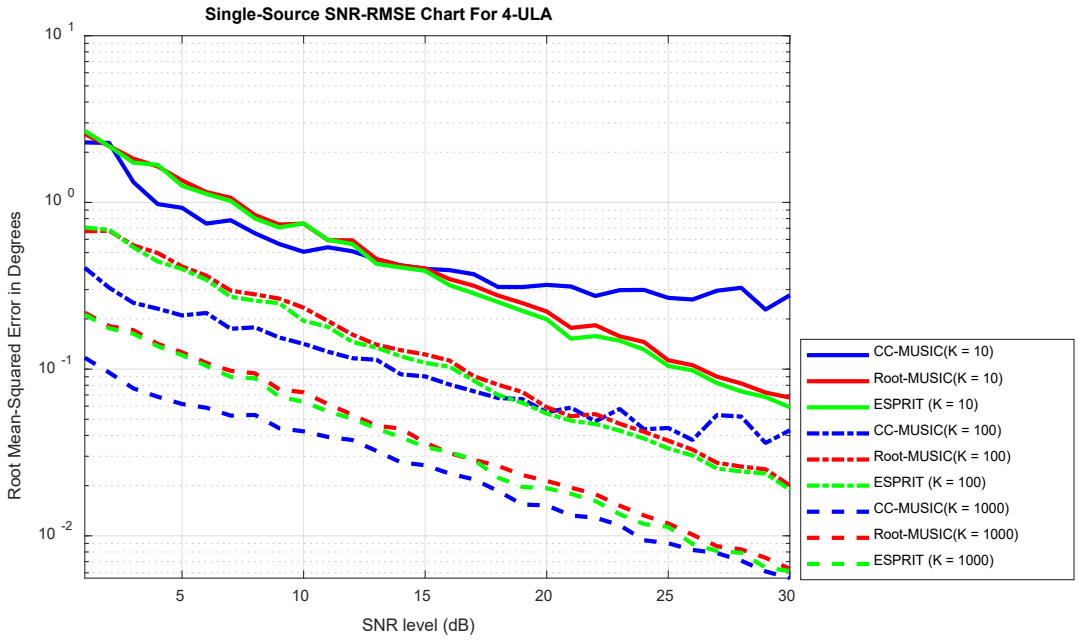

Figure 3.5 Single-Source SNR-RMSE Performance for CC-MUSIC

With reference to Figure 3.5, at low SNR (<15dB), CC-MUSIC outperforms root-MUSIC and ESPRIT by a minimum average of 10.99%, 39.64%, and 46.33% in terms of RMSE for K = 10, 100 and 1000 respectively. It was also observed that at higher SNR (>15dB) for low K snapshot values, root-MUSIC and ESPRIT outperform CC-MUSIC. At high K values, CC-MUSIC performs similarly compared to root-MUSIC and ESPRIT, with an average RMSE difference of 10%. One of the reasons as to why high SNR affects the performance of CC-MUSIC is due to the fluctuations and over-saturation of phase information in the moment matrix, $\boldsymbol{R}_{\boldsymbol{mom}}$. However, as it is unlikely that in a real-world application that, SNR will be as high as >15dB, it can be considered as a compromise – especially if there is a need to perform statistically well in low SNR scenarios.

3.2.3.2 Multi-Source SNR-RMSE Performance

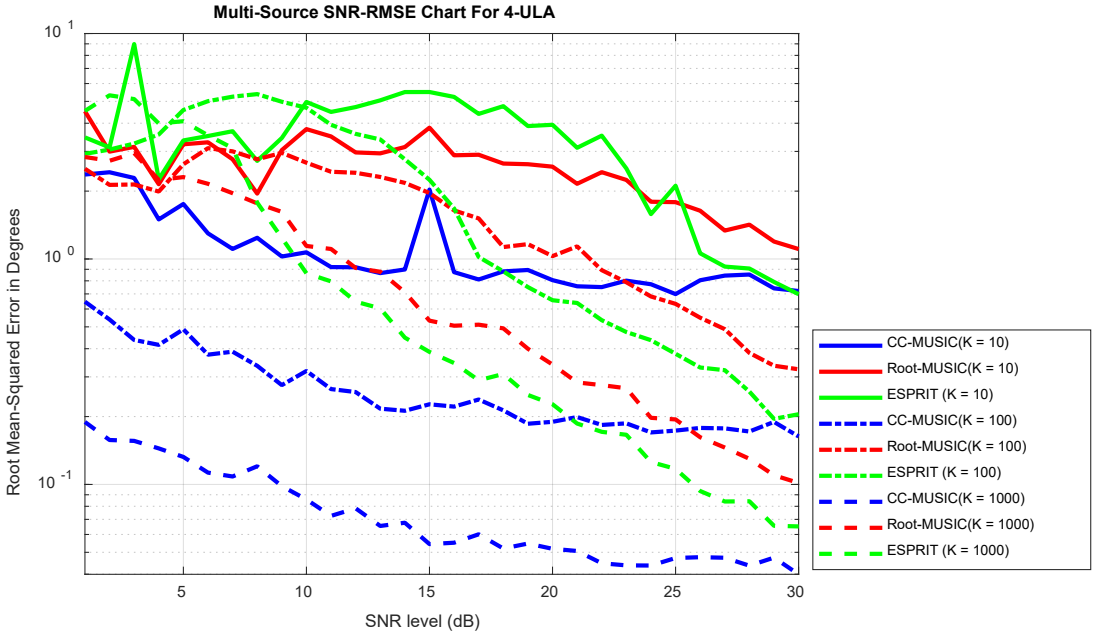

Figure 3.6 Multi-Source SNR-RMSE Performance for CC-MUSIC

Figure 3.6 presents the SNR-RMSE performance for a multi-signal source scenario. In this scenario, two narrowband signals are impinging onto the array set 5° apart at 40° and 45°. The simulation results confirm that in a multi-source scenario, the use of the cross cumulants in CC-MUSIC outperforms the classical second-order covariance-based DOA estimators across the SNR range and in varying snapshot values. On average, across the whole range of SNR values, CC-MUSIC outperforms root-MUSIC and ESPRIT by 48.1%, 20.37%, and 4.5% for K = 10, 100, and 1000 respectively. However, one thing to note is that CC-MUSIC significantly outperforms root-MUSIC and ESPRIT at lower SNR values. If the range from 1dB to 15dB is observed, it is determined that the average SNR-RMSE for CC-MUSIC compared against root-MUSIC and ESPRIT is 39.1%, 79.1%, and 83.8% for K = 10,100 and 1000 respectively. To that end, the introduction of an extended virtual array element allows improved resolution accuracy and noise suppression which has been demonstrated in this simulation scenario.

3.2.4 CC-MUSIC Summary

The proposed novel DOA estimation technique, CC-MUSIC, used fourth-order cross-cumulant statistics to significantly improve the estimator's performance, particularly in low SNR scenarios, without the expense of computational cost based on the RMSE

performance. It is best to determine the DOAs using second order-based sample covariance techniques at high SNR scenarios for a single signal source based on the simulation results. However, in a multi-signal source scenario, it is best to use higher-order statistics to resolve multiple signals, mainly if the sources are closely related, as demonstrated from the simulation results.

One way to overcome this is by implementing a detect and switch algorithm that allows automatic switching of the sample covariance matrix from fourth-order to second-order based on either the SNR threshold if the noise power is known or the Received Signal Strength Indicator (RSSI) values if noise power from the emitter is unknown. To achieve this, a correlation between known RSSI and noise values can be determined by mapping the two variables together. This would allow a threshold to be set and determine when the switching can occur upon reaching a specific level of RSSI which can be estimated. However, using this switching technique may result in higher computational complexity. In terms of computational costs, CC-MUSIC has the same complexity as compared to ESPRIT and root-MUSIC. In the next section, another DOA estimation technique is introduced by using multiple subspace information to determine the DOAs of interest with the purpose of reducing the computational load while preserving the DOA estimation accuracy.

3.3 Subspace-Averaging DOA Estimator (SADE)

This section aims at a preliminary attempt to develop a novel DOA estimation method for narrowband and short-range signal source environments called SADE. This is carried out by utilizing and averaging both the noise and signal subspaces concurrently to form a new covariance matrix which is a crucial data point for DOA estimation. The proposed DOA technique estimates exact DOA points at a range of SNR values (> 10 dB) while maintaining low computational complexity. The receiver is configured to process multiple DOA information impinging from different DOA positions in space. The simulation results verify the proposed method and supersede existing DOA estimation techniques as an asymptotically unbiased estimator under static AWGN conditions.

3.3.1 SADE Data Model

The proposed method identifies and modifies the signal and noise subspaces within the received data. Then, the DOA is estimated using a polynomial solving technique to reduce computational complexity.

Firstly, the modified received data signal, **Y** is defined as:

$$\mathbf{Y} = \mathbf{I}_{\mathrm{M}}\mathbf{X}^{*} \tag{3.9}$$

Where $\mathbf{X}^{*}$ is defined as the complex conjugate of the received data signal $\mathbf{X}$ and $\mathbf{I}_{\mathrm{M}}$ is an anti-diagonal identity matrix of size $\mathrm{M} \times \mathrm{M}$ represented as:

$$\mathbf{I_M} = \begin{bmatrix} 0 & \dots & 1 \\ \vdots & \ddots & \vdots \\ 1_{(\mathrm{MxM})} & \cdots & 0 \end{bmatrix} \tag{3.10}$$

Next, the reformulated secondary sample covariance matrix $\widehat{\mathbf{R}}_{\mathbf{yy}}$ is expressed as:

$$\widehat{\mathbf{R}}_{\mathbf{yy}} = \frac{1}{\mathrm{K}}\sum_{i=1}^{\mathrm{K}} \mathbf{Y}\mathbf{Y}^{\mathrm{H}} \tag{3.11}$$

To that end, the resultant sample covariance matrix $\mathbf{R}$ is obtained as follows:

$$\mathbf{R} = \frac{\left(\widehat{\mathbf{R}}_{\mathbf{xx}} + \widehat{\mathbf{R}}_{\mathbf{yy}}\right)}{2} \tag{3.12}$$

From the equation, it can be observed that the noise components of both covariance matrices have equal values. This can be proven using the Expectation Value formula represented as [96]:

$$\mathbf{R}_{\mathrm{yy}} = \mathrm{E}[\mathbf{Y}\mathbf{Y}^{\mathrm{H}}] \tag{3.13}$$

$$\mathbf{R}_{\mathrm{yy}} = \mathbf{I}_{\mathrm{M}}\mathbf{A}^{*}\mathbf{R_s}^{*}(\mathbf{A}^{*})^{\mathrm{H}}\mathbf{I}_{\mathrm{M}} + \mathbf{R_n} \tag{3.14}$$

$$\mathbf{R}_{\mathrm{yy}} = \mathbf{I}_{\mathrm{M}}\mathbf{R_s}^{*}\mathbf{I}_{\mathrm{M}} \tag{3.15}$$

Thus, both the noise and signal subspaces are utilized to determine the DOA. Lastly, a simple root polynomial technique is employed to determine the DOAs with the purpose and benefit of lower computational complexity. This essentially means that scanning the entire span of possible DOA angles is not required – significantly reducing the costs. The poles of the pseudo-spectrum are the corresponding roots that lie closest to the unit circle. For example, an M-element ULA covariance matrix is of dimension $\mathrm{M} \times \mathrm{M}$ and will have $2(\mathrm{M}-1)$ diagonals. Thus, each root can be written as [4]:

$$z_i = |z_i| e^{j\arg(z_i)} \quad i = 1,2,\dots,2(\mathrm{M}-1) \tag{3.16}$$

where $z = e^{j\frac{2\pi}{\lambda}d\sin\theta_i}$ and $\arg(z_i)$ is the phase angle of z_i.

By comparing $e^{j\arg(z_i)}$ and $e^{j\frac{2\pi}{\lambda}d\sin\theta_i}$ The p^{th} roots closest to the unit circle are mapped and converted into the estimated DOAs of interest by:

$$\theta_{i(p)} = sin^{-1}\left(\frac{\lambda}{2\pi d}\arg\left(z_{i(p)}\right)\right) \tag{3.17}$$

where $\theta_{i(p)}$ are the estimated DOAs of interest.

Note that the range of i values depends on the number of signal sources. For example, if there are two signal sources, then the two roots closest to the unit circle are the estimated DOAs of interest and so forth. It is assumed that the number of signal sources is known. In summary, the proposed SADE algorithm is summed up in Figure 3.7.

Algorithm 1 DOA Estimation using SADE Algorithm

Require: Incoming SNR Data Matrix from Sensor Array, $\mathbf{X}$

procedure SADE(θ)

Determine $\hat{\mathbf{R}}_{xx} = \frac{1}{K}\mathbf{X}\mathbf{X}^{\mathbf{H}}$

while $\hat{\mathbf{R}}_{\mathbf{xx}}$ is being determined **do**

Construct $\mathbf{Y} = \mathbf{I}_{\mathbf{M}}\mathbf{X}^{*}$

Determine $\hat{\mathbf{R}}_{yy} = \frac{1}{K}\mathbf{Y}\mathbf{Y}^{\mathbf{H}}$

end while

Reformulate $\mathbf{R} = \frac{\hat{\mathbf{R}}_{xx}+\hat{\mathbf{R}}_{yy}}{2}$

Decompose Signal and Noise Subspace $\mathbf{R}_{\mathbf{Decomp-SADE}} = \mathbf{R_s}\boldsymbol{\Omega}_{\mathbf{s}}\mathbf{R_s}^{\mathbf{H}} + \mathbf{R_n}\boldsymbol{\Omega}_{\mathbf{n}}\mathbf{R_n}^{\mathbf{H}}$

Conduct Polynomial Rooting $\theta_{i(p)} = (\frac{\lambda}{2\pi d} arg(z_{i(p)}))$

end procedure

Figure 3.7 Proposed SADE Algorithm

3.3.2 SADE Performance Analysis

The proposed SADE technique was implemented using MATLAB R2020b. It is assumed that the signal source is uncorrelated, and only AWGN was considered for simplicity. The SADE algorithm is compared to ESPRIT and Root-MUSIC – a relatively similar but simple subspace DOA estimation technique for demonstrating comparison and presenting the key benefits of using a subspace-averaging-based technique as the sample covariance matrix by leveraging on both the signal and noise subspaces instead of just the latter. The element spacing is half the operating frequency's wavelength. In this section, some key factors will be observed and discussed.

To evaluate the performance of the proposed technique, a simple scenario is modelled where only a single far-field signal source is impinging onto the antenna array at $50°$ for ease of comparison. This study focuses on the performance of varying antenna array elements and snapshot values across SNR values.

3.3.2.1 Varying the Number of Snapshots

This section observes the proposed SADE technique under varying snapshots against Root-MUSIC and ESPRIT. In this scenario, the number of the antenna array element is assumed to be $M = 4$. The Cramer-Rao Bound (CRB) is also provided as an indicator of the statistical performance of the estimators. With reference from Figure 3.8 to Figure 3.10,

there is a clear indication and consistency across any snapshot value. At a low SNR value (< 15dB), the RMSE for SADE is approximately 23.01% higher than that of Root-MUSIC and ESPRIT, respectively. However, as the SNR value approached >15dB, SADE presents a significantly lower RMSE when compared to the latter. At 30 dB SNR, SADE can attain closer to the CRB with an RMSE of approximately 99.84% accuracy compared to Root-MUSIC and ESPRIT against the CRB value. Since the number of elements in this performance study is relatively small, the noise and signal subspace eigenvalues are inherently significant at high SNR. Furthermore, as SADE utilizes both the noise and subspace subspaces, the eigenvalues from both subspace components allow higher estimation resolution. As discussed in the next section, this effect has an inversely proportional impact when the number of elements increases.

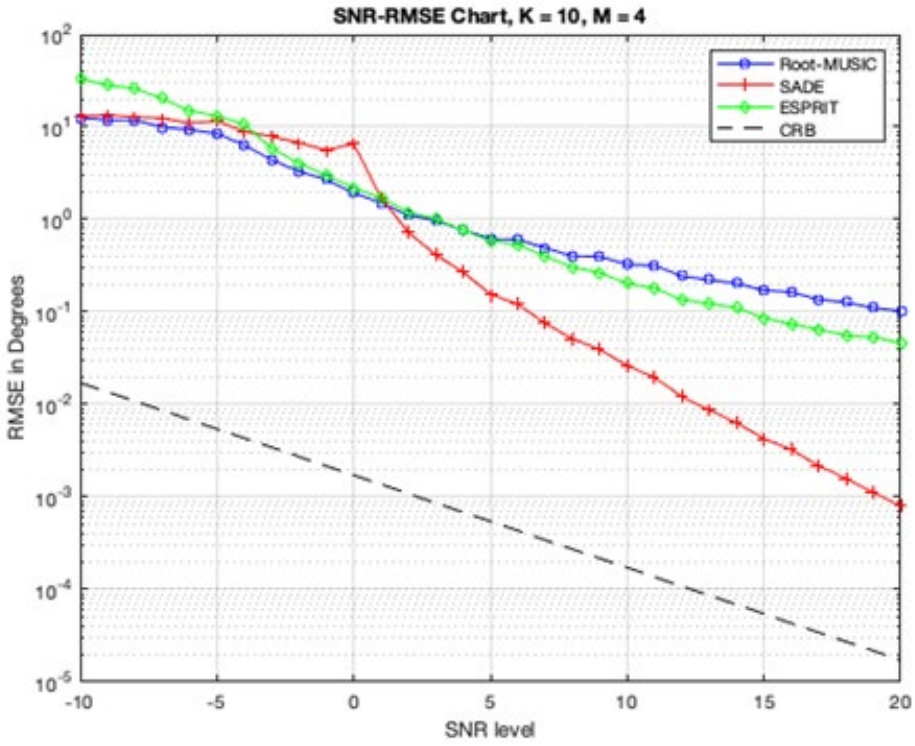

Figure 3.8 SNR-RMSE for K Number of Snapshots = 10

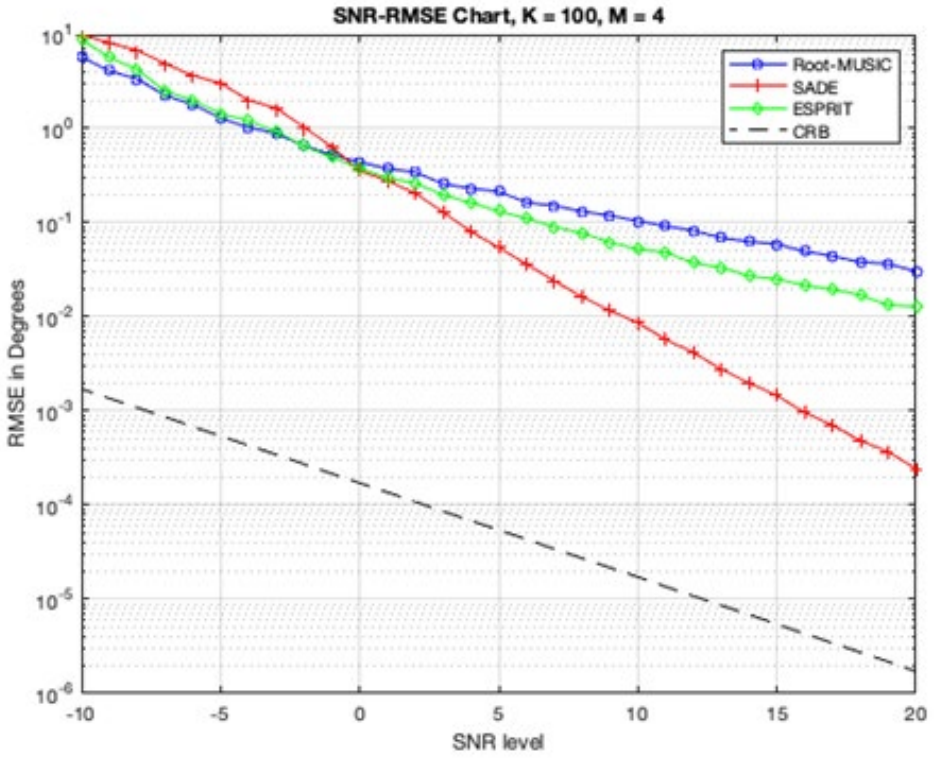

Figure 3.9 SNR-RMSE for K Number of Snapshots = 100

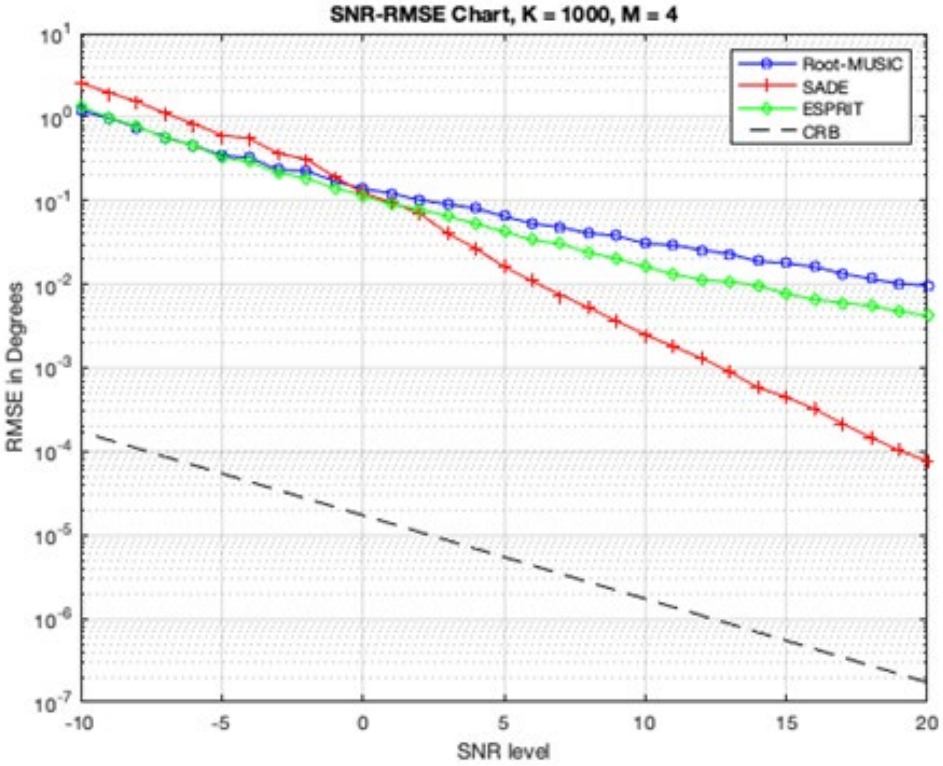

Figure 3.10 SNR-RMSE for K Number of Snapshots = 1000

3.3.2.2 Varying the Number of Array Elements

This section observes the DOA estimation performance of the SADE algorithm under varying antenna array elements. For simplicity, the CRB is omitted and observed closely and precisely on the SNR-RMSE performance among the three estimators. A fixed snapshot value is fixed at $K = 1000$ for consistent comparison. In the case where $M = 4$ is demonstrated in Figure 3.10, SADE's RMSE is significantly lower than the other DOA techniques across the wide range of SNR values. Figure 3.10 shows that RMSE for SADE obtains lower RMSE compared to root-MUSIC and ESPRIT as the SNR increases. However, as the number of elements increases, SADE's performance decays compared to root-MUSIC. This is because the signal subspace E_s as the number of antenna arrays increases, the noise subspace, E_n are significantly higher in value when compared to the signal subspace ($\mathbf{E_n} \gg \mathbf{E_s}$). Therefore, the averaging technique loses estimation performance as the eigenvalues in the signal subspace approach nominal values. Thus, conducting a subspace-averaging method would result in poorer performance. This trend is observed in Figure 3.11 and Figure 3.12, where SADE performs slightly worse than Root-MUSIC but has higher accuracy when compared to ESPRIT. When the number of elements is less than 8, the SADE has an average RMSE of 9.5% when compared to root-MUSIC and ESPRIT at 15.6% and 16.7%, respectively, when compared to the actual signal source DOA.

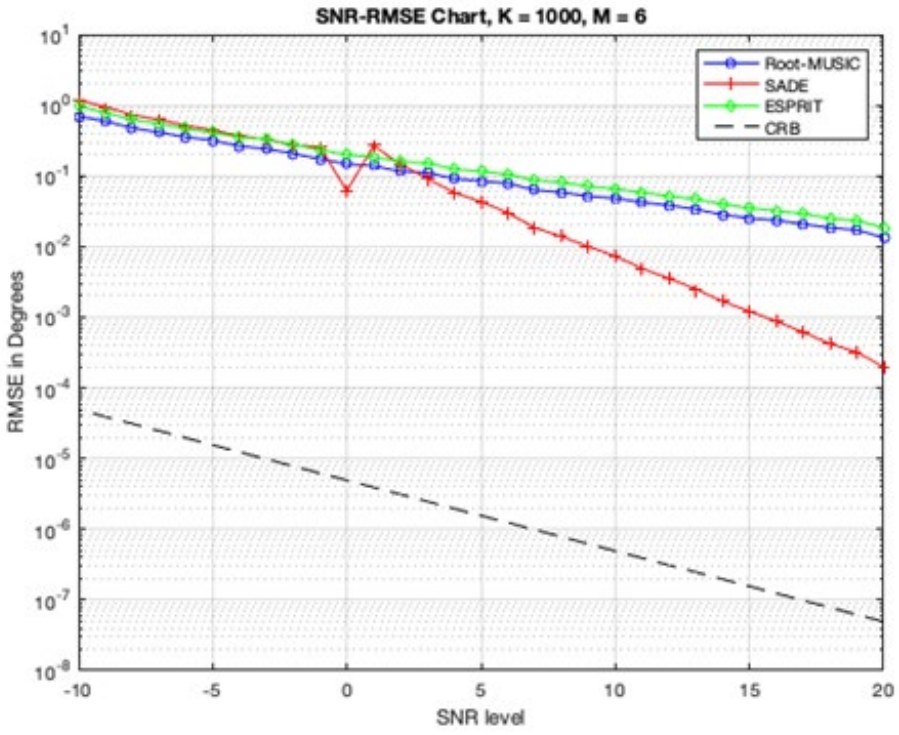

Figure 3.11 SNR-RMSE for Antenna Elements M = 6

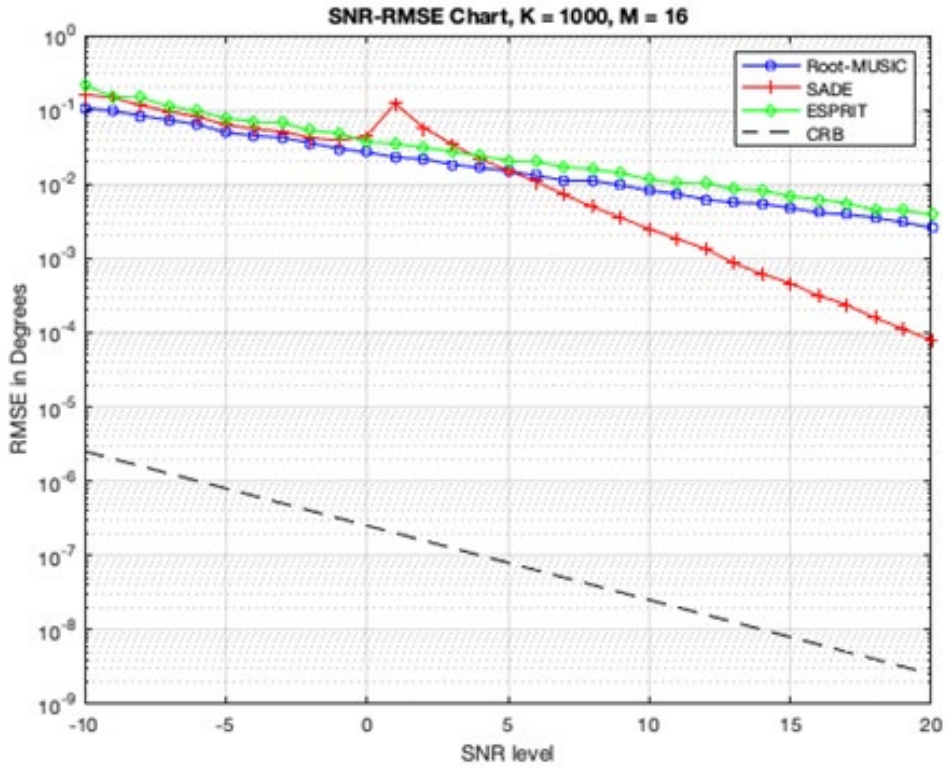

Figure 3.12 SNR-RMSE for Antenna Elements M = 16

3.3.3 SADE Performance Summary

The proposed subspace-averaging DOA estimation technique, SADE, was presented to significantly improve the performance of an estimator without the expense of computational costs and improve estimation accuracy based on the RMSE results. From the simulation results of varying snapshot values and under AWGN, the SADE technique manages to attain 99.84% of the CRB at >15dB SNR. In addition, from the simulation of varying antenna array elements, when the number of elements is less than 8, the SADE technique performs with an RMSE of 9.5% of the actual direction compared to 15.6% and 16.7% of the root-MUSIC and ESPRIT techniques. In addition, there is also room for improvement for DOA estimation with a lower RMSE that is closer to the CRB. Furthermore, as the number of snapshots reduces, the estimation performance will also diminish. In the following sub-section, an alternative approach is proposed to reduce the computational load via the number of snapshots without impacting the DOA estimation accuracy.

3.4 Snapshot Sample Reduction for Lower Computational Load

This section proposes and studies a snapshot sample reduction for DOA estimation. Many methods have been proposed in [97] for a single snapshot scenario by exploiting the

spatial properties of a ULA to estimate its covariance matrix with potential application in automotive radar where the snapshot sampling frequency is low [98] or in any low-cost situation where hardware performance is limited without compromising accuracy. The main drawback in [98] is that because it depends on the spatial properties of the ULA, precision is required when it comes to the position of the array elements. Any measurement uncertainties or miscalibration can lead to a degradation of estimation performance for the DOA estimator in [98]. [99] presented a self-calibration technique by iterating between direction estimation and gain/phase estimation via minimizing a cost function until convergence. However, this technique still requires a high number of snapshots to obtain reasonable convergence to its cost function.

To that end, this method aims to enable a single snapshot technique by introducing a Sequential Quadratic Programming (SQP) optimization technique enabling auto-calibration of the antenna array positioning that allows a higher accuracy when deriving the covariance matrix.

3.4.1 Single Snapshot DOA Estimation Signal Model

To reiterate, a typical approach for estimating the covariance matrix is denoted as $\widehat{\mathbf{R}}_{\mathbf{xx}}$ is by using K temporal snapshots $x(k), k = 1, \dots, K$ as follows [98, 100]:

$$\widehat{\mathbf{R}}_{\mathbf{xx}} = \frac{1}{\mathrm{K}}\sum_{\mathrm{k}=1}^{\mathrm{K}} \mathbf{x}(\mathrm{k})\mathbf{x}^{\mathbf{H}}(\mathrm{k}) = \frac{1}{K}\mathbf{X}\mathbf{X}^{\mathbf{H}} \tag{3.18}$$

where $\mathbf{X}$ is composed of K temporal snapshots.

Alternatively, a single spatial snapshot approach can be realized by exploiting the spatial properties of the ULA. Thus, if only one spatial snapshot of a received signal vector-matrix x is used, the covariance matrix can be estimated as [98]:

$$\widehat{\mathbf{R}}_{\mathbf{xx(ss)}} = \frac{1}{\mathrm{M}}\mathbf{X}_{\mathbf{toep}}{}^{\mathbf{H}}\mathbf{X}_{\mathbf{toep}} \tag{3.19}$$

where $\mathbf{X}_{\mathbf{toep}}$ contains a single signal vector $\mathbf{x} = [x_1 \quad x_2 \quad \dots \quad x_M]^T$ in a sparse Toeplitz geometry.

Thus, a finite data record of length M array elements is used to estimate the covariance matrix when compared to (3.18), where only one temporal data is acquired.

3.4.2 Auto-calibration of Antenna Positioning & Proposed Technique

A cost function is proposed to measure the estimation error and the best-case relationship between (3.19) and the signal source. (3.20), which is dependent on the

covariance matrix $\widehat{\boldsymbol{R}}_{\boldsymbol{x(ss)}}$, the initial element position, d_{init} and estimates of the source locations, θ_{init} as an initialization criterion which is defined as follows:

$$\mathrm{x_{cf}} = \mathrm{f}\left(\widehat{\mathbf{R}}_{\mathbf{xx(ss)}}, \mathrm{d_{init}}, \theta_{\mathrm{init}}\right) = \log_{10}\left\|\mathrm{diag}\left(\mathbf{A^H E_N E_N}^{\mathbf{H}}\mathbf{A}\right)\right\| \qquad (3.20)$$

where $\boldsymbol{A}$ and $\boldsymbol{E_N}$ denotes the estimated array steering vector and Eigen-decomposed noise subspace, respectively, from $\widehat{\boldsymbol{R}}_{\boldsymbol{xx(single)}}$ which are dependent on the array positions.

Observing the auto-calibration as a constrained optimization problem, a state-of-the-art constraint optimizer SQP is employed coupled with an SS-DOA estimation cost function. The SQP algorithm can be referred to in [101]. Figure 3.13 presents an algorithmic flowchart of the proposed technique. The cost function in (3.20) alongside an SQP optimizer is used. The iteration ends when the step size goes below the step, angle, and location tolerance which are the convergence properties. The cost function in (3.20) is minimized when (3.19) corresponds to its smallest eigenvalue. The auto-calibration will iterate between estimating the source position and updating the calibration parameters within the user-defined tolerance.

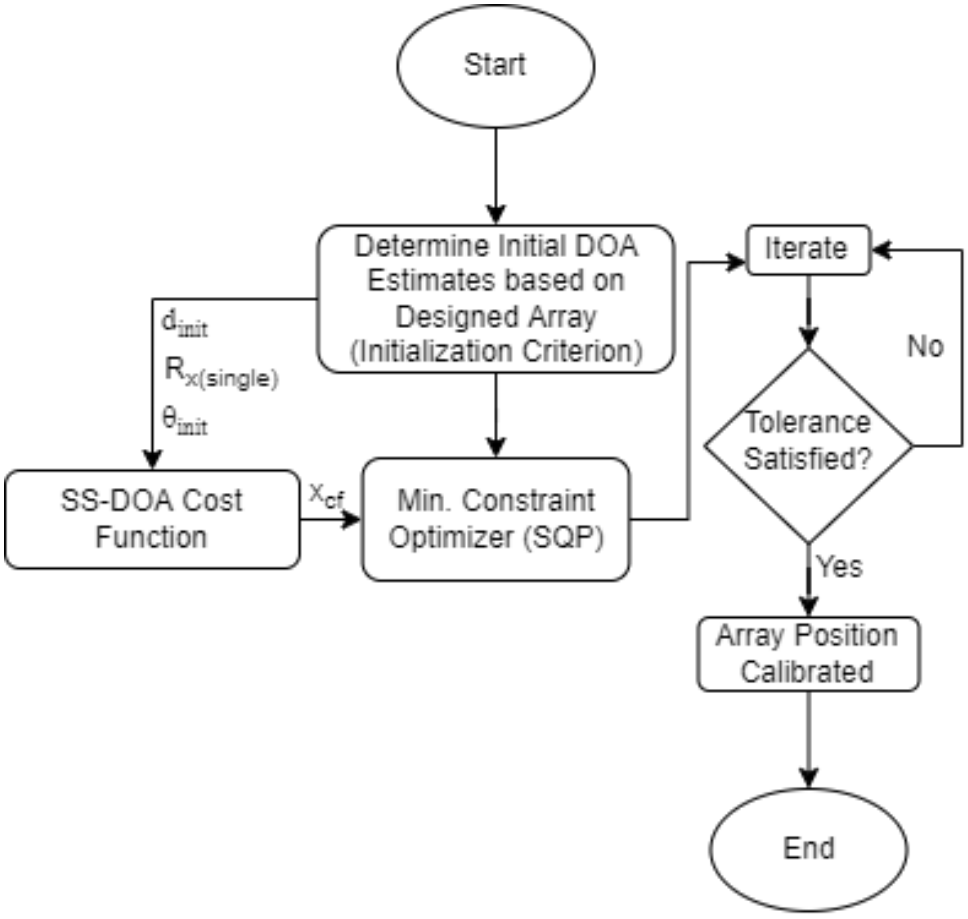

Figure 3.13 Auto-Calibrating SS-DOA Estimator Flowchart

3.4.3 Simulation Results for SS-DOA

Consider a 4-element ULA operating at 5500 MHz center frequency spaced at half-wavelength. Next, assume the perturbed first reference sensor and the direction to the second sensor are known with two narrowband signal sources impinging on the array at 10° and 35° with a Signal-to-Noise Ratio of -30dB. 300 independent simulations were run to obtain the RMSE. In this simulation, a non-calibrated SS-DOA derived in (3.19) was compared against the proposed auto-calibrating SS-DOA technique to demonstrate a single snapshot performance. Table 3.2 presents the array coordinates measured from the geometric center for the designed, perturbed, and calibrated positions and the difference between perturbed and calibrated positions. From Δd, it can see that the calibrated array closely resembles the perturbed array after auto-calibration with an average standard deviation of 21mm. The calibrated positions will have an estimation impact, as demonstrated via the results in Table 3.2.

Table 3.2 Averaged Array Sensor Coordinates

Array Position:	1 (reference)	2	3	4
Designed/Perfect (mm):	-40.9	-13.6	13.6	40.9
Perturbed (mm):	-40.9	-12.8	12.3	41.2
Calibrated (mm +/- 5%):	-40.9	-3.6	21.0	30.9
Δd of Perturbed & Calibrated (mm +/- 5%):	0	-9.2	8.7	10.3

Fig. 3.14 presents a normalized polar plot of the auto-calibrating and non-calibrated SS-DOA, respectively, where each result's magnitude has been normalized to unity for comparison. It can be observed that the calibrated estimator achieves a closer estimate to the actual directions when compared to the non-calibrated results. The calibrated and non-calibrated DOA estimators presented an average RMSE of 2.915° and 11.767°, respectively. This is a 75.22% average DOA estimation performance gain for the auto-calibrating SS-DOA. As the steering vector and Eigen-decomposed subspaces are dependent variables of the array positions, a calibrated ULA would provide an accurate estimation as opposed to a

non-calibrated SS-DOA. In addition, the proposed technique has RMSE DOA estimation performance that is similarly comparable when compared to [99] without the need for high snapshot values.

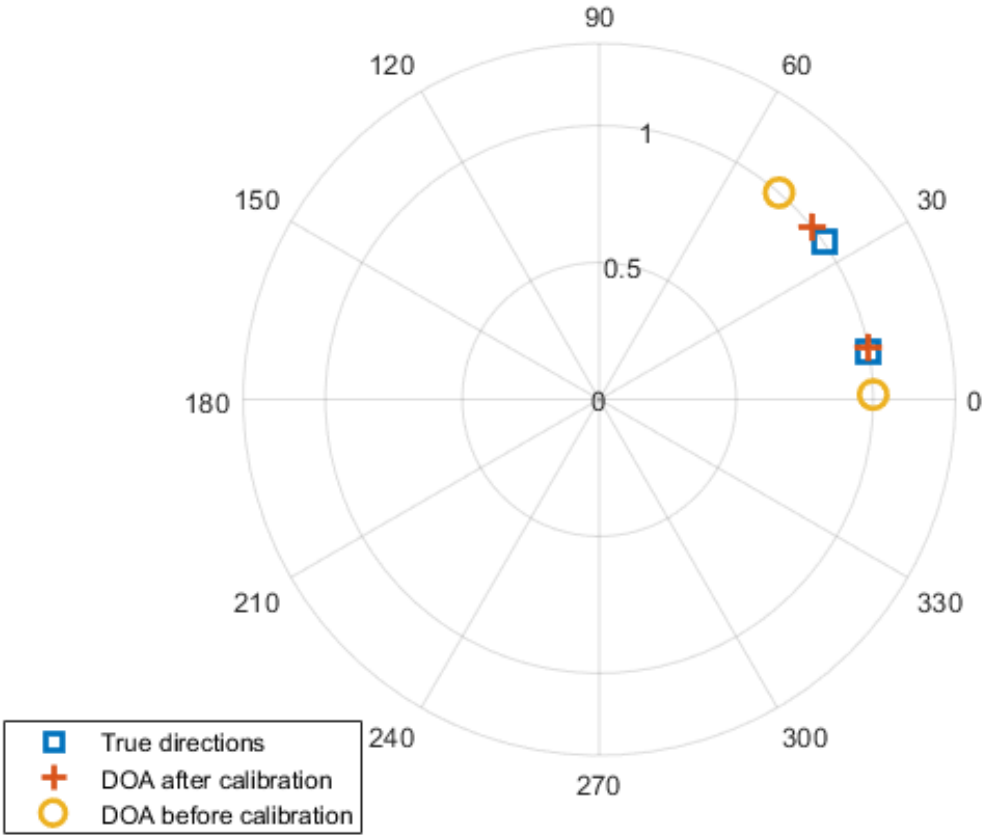

Fig. 3.14 Averaged DOA Estimation Results in Normalized Polar Plot

3.4.4 Auto-Calibration of Single Snapshot Estimator Performance Summary

The simulation results show that the proposed auto-calibration SS-DOA technique has a DOA estimation performance gain of 75.22% and a calibrated array position standard deviation of 21mm against non-calibrated algorithms. Compared to other state-of-the-art methods, similar averaged DOA estimation performance was obtained without requiring high snapshot values. This work verifies single snapshot DOA estimation when the correct cost function for the iterative-based solution is selected. Clearly, there is potential to utilize single snapshot DOA estimation without sacrificing estimation accuracy.

3.5 Overall Summary of Proposed Novel DOA Estimation Techniques

Multiple preliminary DOA estimation techniques were proposed to reduce computational time and increase estimation accuracy in mind. Firstly, the root-T DOA estimation technique was introduced with the primary objective of conserving good estimation performance compared to root-MUSIC and improved-MUSIC while reducing the computational time. The key advantages of root-T are the improved DOA estimation performance of up to 96% while reducing the computational time by 49.5%. However, compared to existing state-of-the-art techniques, the root-T method does not perform relatively well in estimation accuracy.

The CC-MUSIC DOA estimation technique was proposed to improve the DOA estimation performance compared to root-T by jointly utilizing higher-order cumulant statistics and root-MUSIC to perform high-resolution DOA estimation in low SNR scenarios. It has been demonstrated that CC-MUSIC outperforms techniques such as the standard root-MUSIC and ESPRIT methods by up to 46%, where the SNR is < 15 dB for a single signal source and up to 83% in a multi-signal source scenario. However, CC-MUSIC has significantly high computational complexity, leading to a longer computational time. The long computational time is clearly undesirable in real-world scenarios where the DOAs are rapidly changing.

The SADE DOA estimator was introduced to improve the DOA estimation accuracy further while lowering the computational time for efficient tracking. The SADE technique was proposed by exploiting the common noise subspace properties with a modified covariance matrix. Then, to further reduce the computational time, a simple polynomial root-solving technique was employed to determine the DOA as compared to the costly pseudo-spectrum search methods. Simulation results have shown that the SADE technique manages to attain up to 99% of the CRB where the SNR is > 15dB. Furthermore, the estimation accuracy of SADE is 9.5% closer to the true DOA than root-MUSIC and ESPRIT, coming in at 15.6% and 16.7%, respectively. However, the SADE technique has the drawback of insufficient DOA estimation accuracy compared to CC-MUSIC, although it has lower computational time with similar performance to that of root-T.

Lastly, single snapshot DOA estimation was explored and analysed with the primary objective of reducing computational time. This work was carried out by first considering the antenna array positioning that may not be perfect in real-world scenarios, leading to

estimation performance degradation – mainly when the number of snapshots is minimal. Then, by combining the auto-calibration of array position for accurate covariance matrix derivation and a single snapshot DOA estimation method, the proposed joint technique presented an estimation gain of up to 75% compared to a non-calibrated estimator. It has also been shown that the proposed approach gave similar average DOA estimation performance compared to existing methods without requiring high snapshot values.

To summarise, in terms of DOA estimation accuracy, CC-MUSIC outperforms root-T, SADE, and the single snapshot DOA estimator by a significant margin. Alternatively, in terms of computational time, root-T and the single snapshot methods presented the best results as compared to CC-MUSIC and SADE. Furthermore, single snapshot-based DOA estimators present promising results with low computational time without lengthy computational time, which has the potential for real-world applications that require fast and accurate estimation. Clearly, there is a potential to develop a DOA estimation method that can provide good DOA estimation performance without the expense of computational time.

In the next chapter, a covariance matrix reconstruction approach for single snapshot DOA estimation is presented that combines the effectiveness of single snapshot methods while maintaining relatively high DOA estimation accuracy that outperforms existing and state-of-the-art techniques such as root-MUSIC and the Partial Relaxation (PR) approach.

4 A Covariance Matrix Reconstruction Approach for Single Snapshot DOA Estimation

This chapter aims to develop a computationally efficient and accurate 1-D DOA estimation algorithm with a ULA antenna array geometry by exploiting the steering vector feedback and covariance matrix structure in the estimation and assuming the relationship between the number of sensors M and signal source, L is $L < M$. The fundamental characteristic of the proposed technique enables DOA estimation in many applications with cost, size, and hardware limitations, such as but not limited to the field of transportation and vehicular signal localization and high-bandwidth connectivity, especially in the current uprising of wireless communication [44] and the demand for accurate DOA estimation with fast computational time. A simple approach is proposed consisting of a pre-processing covariance matrix reconstruction to determine a comparative steering vector by manipulating the structural information of the covariance matrix to improve DOA estimation performance. The proposed algorithm achieves computational efficiency using a single snapshot instead of multiple snapshots to reduce data collection time while improving DOA estimation accuracy in a full range of SNR environments. Efficiency is achieved by using a predetermined DOA estimation stage using a root-MUSIC-like algorithm [3]. The derived DOA from the first stage is then used to determine the DOA initial estimates. This value is then used as feedback to determine the new steering vector. Finally, the final DOA estimation is computationally retrieved via the reformulated covariance matrix. With a focus on lightweight design philosophy, the proposed method presents key features that compacts a single snapshot and high DOA estimation accuracy with low computational complexity in a wide SNR range. To that end, the critical advantage of the proposed method presents efficient covariance matrix data collection with a single snapshot coupled with good DOA estimation performance.

This chapter is reproduced from paper #1 in the publication list on page iv, where the thesis author is the main author in the paper.

The key issues that need to be solved are the overall computational load time and the DOA estimation accuracy, which are yet to be addressed clearly, particularly in varying SNR environments [64]. The problem faced in a low SNR environment is challenging to distinguish the different subspaces and signal information. This proposed technique addresses this issue, especially when faced with an array size limitation without sacrificing DOA estimation accuracy. In addition, the single snapshot limitations of DOA estimation will be addressed by introducing a robust, high-resolution DOA estimator called the CbSS technique. The CbSS estimator is an all-encompassing DOA estimation algorithm robust in performance across a wide range of SNR with good functionality in estimation performance and computational time.

4.1 Covariance-based Single Snapshot DOA Estimator

This section introduces the Cb DOA estimator. First, a detailed theoretical estimation model based on the theoretical covariance matrix to identify the root cause of estimation error. Then, the determination of the lower and upper bound of an optimum diagonal-loading factor value is presented for error minimization. Lastly, error minimization and noise suppression are shown for a practical single snapshot DOA estimation implementation based on the theoretical model estimation.

4.1.1 Defining the Error Terms in Covariance Matrices

Firstly, it is worth highlighting an apparent disparity in data information between the theoretical covariance matrix in (2.3) and the sample covariance matrix in (2.4) that eventually leads to DOA estimation performance degradation. As the number of snapshot samples is limited, the sample covariance matrix in (2.4) has inherent errors. Thus, (2.3) and (2.4) have a simple additive error mathematical relationship that can be written as

$$\widehat{\mathbf{R}}_{\mathbf{xx}} = \mathbf{R}_{\mathbf{xx}} + \mu\mathbf{D} \tag{4.1}$$

where $\mathbf{R}_{\mathbf{xx}}$ is the theoretical covariance matrix in (2.3), $\mathbf{D}$, is a zero-mean random matrix with unit variance, and μ is a constant that indicates the estimation error of the estimated covariance matrix.

In (4.1), the term $\mu\mathbf{D}$ represents the additive inherent error by the sample covariance matrix. The errors are the numerical differences between the theoretical and sample covariance matrices. Evidently, the larger the estimation error, the worst the DOA estimation performance will be as $\widehat{\mathbf{R}}_{\mathbf{xx}}$ is numerically further away from the theoretical covariance matrix, $\mathbf{R}_{\mathbf{xx}}$. Clearly, $\mu\mathbf{D}$ is the leading cause of estimation performance degradation in the sample covariance matrix relative to the theoretical covariance matrix.

In past research studies, the diagonal loading method is a simple and efficient method for improving the robustness of an estimator that conducts matrix decomposition [102]. Thus, a data-dependent approach is introduced to determine an optimal diagonal loading factor. From (4.1), the sample covariance matrix is combined with a diagonal loading value and the estimation error. Therefore, the diagonal loading parameter is included in the sample covariance matrix in (4.1), which is defined as

$$\mathbf{R_{DL}} = \mathbf{R_{xx}} + \mu\mathbf{D} + \varepsilon_{DL}\mathbf{I} \tag{4.2}$$

where ε_{DL} is the additive diagonal loading factor of interest to improve the DOA estimation accuracy.

4.1.2 Determining the Lower & Upper Bounds of the Diagonal-Loading Factor for Error Minimization

Assuming that, at sufficiently high SNR values or a high number of snapshot samples, the theoretical covariance matrix and diagonal loading term combined are much larger than the inherent error, $\|\mathbf{R_{xx}} + \varepsilon_{DL}\mathbf{I}\| \gg \mu\|\mathbf{D}\|$. Then, the orthogonal properties of (2.4) and (4.2) can be exploited to identify the cause of error by taking the inverse of the diagonally loaded covariance matrix in (4.6). Considering the inverse matrix approximation properties, the inverse of (4.2) can be expressed as

$$\begin{aligned}\mathbf{R_{DL}}^{-1} &= (\mathbf{R_{xx}} + \varepsilon_{DL}\mathbf{I})^{-1}[\mathbf{I} + \mu\mathbf{D}(\mathbf{R_{xx}} + \varepsilon_{DL}\mathbf{I})^{-1}]^{-1} \\ &\approx (\mathbf{R_{xx}} + \varepsilon_{DL}\mathbf{I})^{-1}[\mathbf{I} + \mu\mathbf{D}(\mathbf{R_{xx}} + \varepsilon_{DL}\mathbf{I})^{-1}] \\ &= (\mathbf{R_{xx}} + \varepsilon_{DL}\mathbf{I})^{-1}\left\{\mathbf{I} - \frac{\mu}{\varepsilon_{DL} + \sigma_n^2}\mathbf{D}\left[\mathbf{I} - \mathbf{A}\left[\mathbf{A}^{\mathrm{H}}\mathbf{A} + (\mathbf{R_{xx}} + \varepsilon_{DL}\mathbf{I})\mathbf{E_s}^{-1}\right]^{-1}\mathbf{A}^{\mathrm{H}}\right]\right\}.\end{aligned} \tag{4.3}$$

The sample and theoretical covariance matrix are equal in a perfect scenario. However, due to the existing error terms in real-world scenarios where the sample covariance matrix is used, it is impractical to achieve zero error. Thus, the diagonal-loading factor is introduced to minimize error and noise terms. However, it is crucial to determine the lower and upper boundary values to not statistically skew the covariance matrix estimation, which is directly linked to the estimation of the DOAs of interest. If the diagonal loading factor lies beyond the boundary, it will result in poor estimation results, which is undesirable.

Therefore, based on the hypothesis, from (4.3), the terms inside the first brackets should ideally be a close non-zero value to the theoretical covariance matrix, which can be given as $\mathbf{R_{xx}} + \varepsilon_{DL}\mathbf{I} \cong \mathbf{R_{xx}}$. If $\varepsilon_{DL}\mathbf{I}$ is set to zero, then no diagonal loading factor is used, particularly inside the curly brackets, and would result in the exact error-prone covariance

matrix estimation. Due to the existing $\varepsilon_{DL}\mathbf{I}$ and other error terms in the curly brackets, only a relative value would be achievable for either a sufficiently high SNR or snapshots samples. Therefore, the diagonal loading value should be much smaller than the diagonal element value of the theoretical covariance matrix. This ideal assumption and a diagonal loading factor upper bound can be expressed as

$$\varepsilon_{DL} \ll \mathbf{R_{xx}}(i,i), \varepsilon_{DL} \neq 0. \tag{4.4}$$

where i represents values from 1 to M.

Next, the lower bound must be determined to decide the optimal diagonal loading factor. It can be observed that the leading cause of performance degradation by the second term is in the curly brackets in (4.3). Optimal performance is achieved if the second term equates to zero, minimising the estimation error in an ideal scenario. Therefore, to achieve minimal error, it is ideal to have the following hypothetical constraint,

$$\frac{\mu}{\varepsilon_{DL} + \sigma_n^2} \ll 1. \tag{4.5}$$

Then, the parameters of (4.9) are rearranged, which should then result in the following inequality,

$$\varepsilon_{DL} + \sigma_n^2 \gg \mu, \tag{4.6}$$

where (4.6) effectively limits the sample covariance matrix to within the theoretical covariance matrix by minimizing the error terms while effectively reducing the dependency on snapshot values and noise level variability.

4.1.3 Practical Implementation for DOA Estimation Error Minimization Using Sample Covariance Matrix

The diagonal element values of the theoretical covariance matrix can be estimated by the average of the estimated covariance matrix diagonal elements denoted as $\widetilde{\mathbf{R}}_{\mathbf{xx}}(i,i)$ and is defined as

$$\widetilde{\mathbf{R}}_{\mathbf{xx}}(i,i) = \frac{\mathrm{tr}\left(\widehat{\mathbf{R}}_{\mathbf{xx}}\right)}{M}, \tag{4.7}$$

where $\mathrm{tr}(\widehat{\mathbf{R}}_{\mathbf{xx}})$ denotes the trace of the sample covariance matrix, $\widehat{\mathbf{R}}_{\mathbf{xx}}$.

Note that the trace of the matrix $\widehat{\mathbf{R}}_{\mathbf{xx}}$ is the sum of its complex eigenvalues, and it is invariant to a change of basis. Note that, unlike standard diagonal-loading utilization, where the factor is always generalized and static, the proposed method in (4.7) is adaptive to its

application needs and environmental scenarios, such as the SNR, the number of snapshots used, and antenna array geometry.

Using the same observation, the standard deviation of the diagonal elements can also indicate the covariance matrix estimation error. The standard deviation method to approximate the estimation error has been used in many past covariance matrix reformulations, such as in [103, 104]. In an error-induced scenario, the higher the standard deviation, the higher the variability along the matrix diagonal within that estimated sample, leading to a higher DOA estimation error. Therefore, this assumption can be expressed as

$$\emptyset = \mathrm{SD}\left(\mathrm{diag}\left(\widehat{\mathbf{R}}_{\mathbf{xx}}\right)\right), \tag{4.8}$$

where $\mathrm{SD}(\cdot)$ means the standard deviation and $\mathrm{diag}(\cdot)$ is the diagonal element of the matrix.

Therefore, the error term, μ, which is an unknown value, is replaced with the standard deviation error identifier $\emptyset$. From (4.8), an ideal and optimal diagonal loading value to improve DOA estimation via the modified sample covariance matrix should satisfy the following constraint

$$\emptyset \geq \varepsilon_{DL} \ll \widetilde{\mathbf{R}}_{\mathbf{xx}}(i,i), \tag{4.9}$$

where $\varepsilon_{DL} = \emptyset$ is set as an initialization value.

Finally, the constraints in (4.9) are combined onto the sample covariance matrix equation in (4.6), considering the assumption in (4.7), which is presented as

$$\widehat{\mathbf{R}}_{\mathbf{DL}} = \widehat{\mathbf{R}}_{\mathbf{xx}} + \varepsilon_{DL}\mathbf{I}. \tag{4.10}$$

To that end, as the steering vector, $\hat{\mathbf{a}}(\theta)$ is embedded into the received signal matrix, there is a need to extrapolate $\hat{\mathbf{a}}(\theta)$ before applying (4.10). Therefore, a broad initial DOA estimate is necessary to estimate obtain $\hat{\mathbf{a}}(\theta)$. This can be done by initiating a rough estimation of the DOA using well-known subspace-based techniques such as root-MUSIC [88]. Then, the first steering matrix, $\hat{\mathbf{a}}(\theta)$, is estimated as the initial bound estimates. A benefit of extrapolating the steering vector is enabling sufficient system robustness from undesired noise, assuming that the DOA does not deviate and remain static at an instantaneous snapshot that amplifies the steering vector parameter [105]. Furthermore, in a real-world application, the only prior information required to perform good DOA estimation is the knowledge of the antenna array geometry and the angular sector in which the actual steering vector lies [105]. If the incident angle of the signal remains static, then the last $(\mathrm{M} - \mathrm{L})$ eigenvalues and their corresponding eigenvectors of the new covariance matrix are invariant. Given the hypothesis,

(4.10) is expanded further with the inclusion of the steering vector estimates, which can be represented as

$$\widehat{\mathbf{R}}_{\mathbf{DL}} = \left(\widehat{\mathbf{R}}_{\mathbf{xx}} + \varepsilon_{DL}\mathbf{I}\right) + \boldsymbol{a}(\theta)\boldsymbol{a}(\theta)^{\mathrm{H}}. \quad (4.11)$$

Next, a set tolerance value, δ, is defined, where the expected DOA does not deviate between +/- 5 degrees. However, this can be scenario-dependent based on the application and the effective beamwidth of the antenna used. For example, a wide-beamwidth antenna may have a high tolerance for DOA estimation, whereas a narrow-beamwidth-based antenna requires a small tolerance for practical DOA estimation. Then, a mathematical constraint is set between the initial DOA, θ_{init} and estimated DOA, θ_{est} with the tolerance value, δ, which can be interpreted as

$$\|\theta_{est} - \theta_{init}\| < \delta. \quad (4.12)$$

Figure 4.1 presents a flowchart summary of the proposed algorithm, the CbSS DOA estimation technique. The signal, **X**, as in (2.1), is obtained in matrix form. Next, the initial sample-based covariance matrix is formed as in (2.4). Then, the root-MUSIC is the initial DOA estimation method for the steering vector to be used in (4.11). In parallel, a predetermined tolerance range that does not overflow the angular expectation of the expected DOA is defined with reference to the initial estimates determined in the previous stage.

Moreover, the tolerance factor plays a crucial role in the final DOA output because it determines the initial and estimated DOAs. The tolerance factor is vital as it governs the final DOA estimates. For example, the delta has a linear relationship between estimation accuracy and computational time. When delta is low, it leads to higher estimation accuracy but the computational time expense of determining the final DOA. Alternatively, when the delta value is high, it leads to a significantly faster computational time while sacrificing the DOA estimation accuracy. This will be studied further in the simulation section. Depending on the use case of the proposed algorithm, the end-user can set the appropriate delta values that suit the environment and criticality of the different factors. The DOA estimation, as presented in [21], is conducted to determine the estimated steering vector. DOA estimation is then calculated using a modified polynomial root-solving technique that is efficient and with high estimation accuracy. A preliminary analysis of this technique has been demonstrated in [21] for reference. In addition, the CbSS technique allows the flexibility of both multiple and single snapshot scenarios by adapting and manipulating the snapshot variable, K. The following section will present the estimation performance of varying the snapshots and SNR.

Algorithm 1 Compute DOA using CbSS Algorithm

Require: Incoming Data Matrix, $\mathbf{X}$, δ

procedure CBSS(θ)
  Determine $\hat{\mathbf{R}}_{xx} = \frac{1}{K}\mathbf{X}\mathbf{X}^{\mathbf{H}}$ from $\mathbf{X}$
  Obtain Initial DOA Estimate, θ_{init} from $\hat{\mathbf{R}}_{xx}$
  while θ_{est} is being determined **do**
    Estimate $\hat{a}(\theta)$ from θ_{init}
    Calculate $\tilde{\mathbf{R}}_{xx} = tr(\hat{\mathbf{R}}_{xx}))/M$
    Calculate $\phi = Std(diag(\tilde{\mathbf{R}}_{xx}))$
    Set Initial DL value, $\epsilon_{DL} = \phi$
    Calculate Modified Covariance Matrix, $\hat{\mathbf{R}}_{DL} = (\hat{\mathbf{R}}_{xx} + \epsilon_{DL}) + \hat{a}(\theta)\hat{a}(\theta)^H$
    Obtain Estimated DOA θ_{est} from $\hat{\mathbf{R}}_{DL}$
  end while
  if θ_{est} - $\theta_{init} < \delta$ **then**
    end procedure
  else
    loop
      Find $\phi \leq \epsilon_{DL} < \tilde{\mathbf{R}}_{xx}$
      Update Steering Vector Estimate, $\hat{a}(\theta)$
      repeat
        $\|\theta_{est}$ - $\theta_{init}\|$
      until $\|\theta_{est}$ - $\theta_{init}\| < \delta$
    end loop
  end if
end procedure

Figure 4.1 CbSS Algorithm Flow

4.2 Simulation Results and Discussion of CbSS

In this section, numerical examples are provided to substantiate the effectiveness of the proposed method. The comparisons are carried out in different performance metrics, such as estimation accuracy, computational efficiency, and adaptability to various scenarios. As highlighted before, a compacted-size antenna array is needed to ease real-world implementation [44]. Thus, a small-scale ULA with half-wavelength inter-element spacing is considered [44], and the number of antenna array element sensors is $M = 4$ unless otherwise stated. A narrowband signal is assumed to be impinging onto the array from a far-field source. In addition, for simplicity, the signal source is considered static in space. It does not change with time for all simulation scenarios, with only an AWGN interference in the simulation environment within line of sight. The simulation environment is based on a downlink, Line-of-Sight (LOS) channel model between the receiver and transmitter. The noise data was formed using a normally distributed random number generator in MATLAB that complies with the AWGN model. In the signal model, the signal matrix, **S** is assumed to be a normalized random power, while **N** is modelled as an AWGN interference. In summary, only the received data **X** is known, whereas the individual

parameters **A**, **S**, and **N** are unknown to the DOA estimator because it is randomized in the simulation. Without loss of generality and simplicity, the impinging signal source has a plane-wave characteristic.

The SNR which is used in the simulation is defined as

$$\text{SNR} = \frac{1}{M}\sum_{m=1}^{M}\frac{p}{q_m}, \tag{4.13}$$

where p and q_m represent the signal and noise power at the m^{th} array element, respectively.

The SNR equation in (4.13) corresponds to all sensors' averaged SNRs and generalizes the definition for uniformed noise levels upon reception at the linear antenna array system. To further examine the performance of the proposed estimator, the standard deviation performance is observed against a range of SNR values and the CRB [100]. The CRB is a useful statistical comparison tool for the accuracy of parametric methods as it provides a lower bound on the accuracy of any unbiased estimator.

Lastly, all the covariance matrices were simulated using MATLAB 2020b on a Windows 10 PC with a quad-core i7 CPU with 16GB RAM. A total of 1000 randomized Monte-Carlo simulation trials were used to determine the simulation results. In addition, as it is beyond the scope of this research work, it is assumed that the number of signals is known a priori. For consistency, the proposed CbSS estimator will be evaluated against root-MUSIC [89] and the state-of-the-art PR [48] approach in all simulation scenarios. Table 4.1 provides a summary of the crucial parameters used in the simulation. In addition, all Root Mean Square Error (RMSE) is calculated up to 2 significant figures per simulation cycle to highlight the high-resolution performance across all demonstrated techniques. The RMSE equation is defined as:

$$\text{Root Mean Square Error (RMSE)} = \sqrt{\frac{1}{Q}\sum_{i=1}^{Q}\left[\frac{\left(\theta_{i_1}-\hat{\theta}_{i_1}\right)^2+\cdots+\left(\theta_{i_L}-\hat{\theta}_{i_L}\right)^2}{L}\right]}, \tag{4.14}$$

where L is the number of signal sources as before, Q is the number of simulation data points, θ_i is the actual DOA, and $\hat{\theta}_i$ is the estimated DOA.

Table 4.1. Common Simulation Parameters

Carrier Frequency, $\boldsymbol{f_c}$	5500 MHz
Antenna Geometry	Uniformed Linear Array
Array Inter-Element Spacing	$\lambda/2$, where λ is the wavelength of f_c in meters
No. of Array Elements, M	4, 8
Simulation Sample	1000
Angle of Interest	35 Degrees (Single Signal Source) 35 ± 10 Degrees (Double Signal Source)
SNR Range	-20 dB to 10 dB
Tolerance, $\boldsymbol{\delta}$	+/- 0.01

4.2.1 DOA Estimation Accuracy for Single Signal Source and Multiple Finite Snapshots

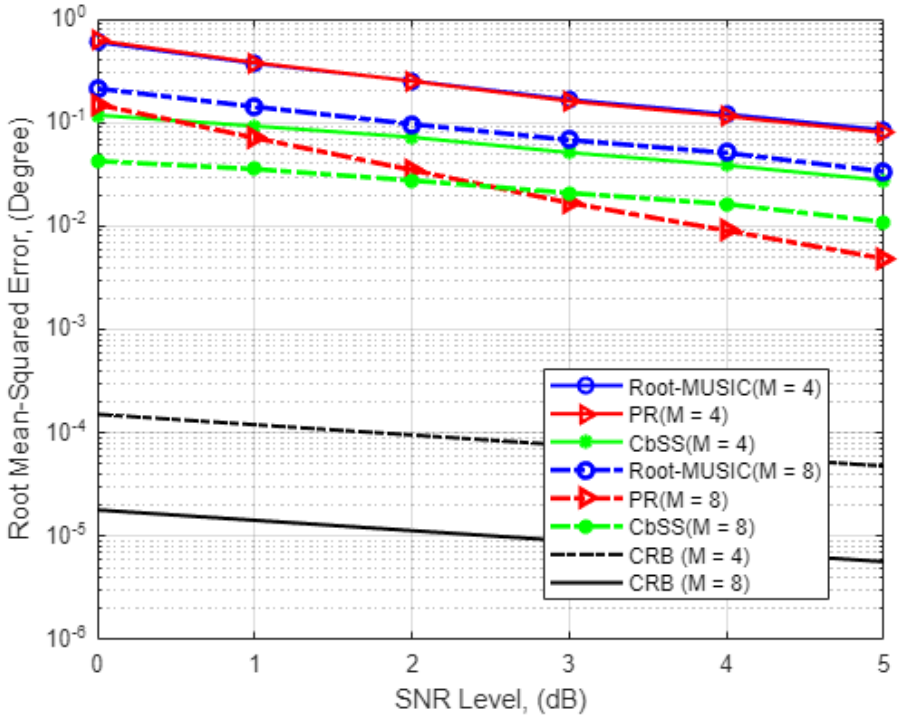

Figure 4.2 SNR-RMSE performance for M = 4 and M = 8 where the number of snapshots K = 100

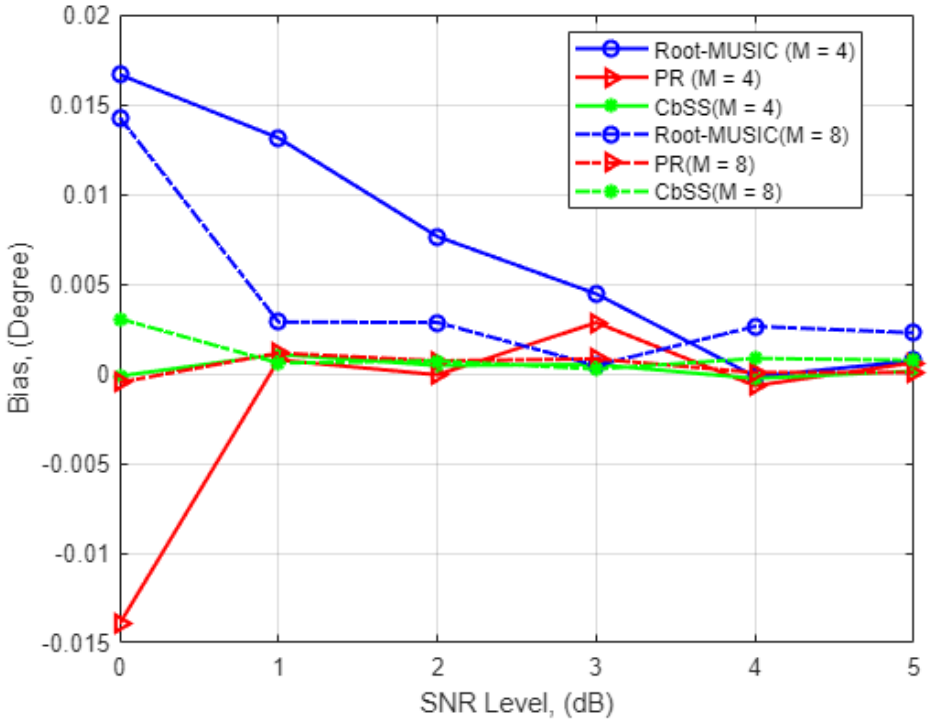

Figure 4.3 Bias comparison for M = 4 and M = 8 where the number of snapshots K = 100 with varying SNR

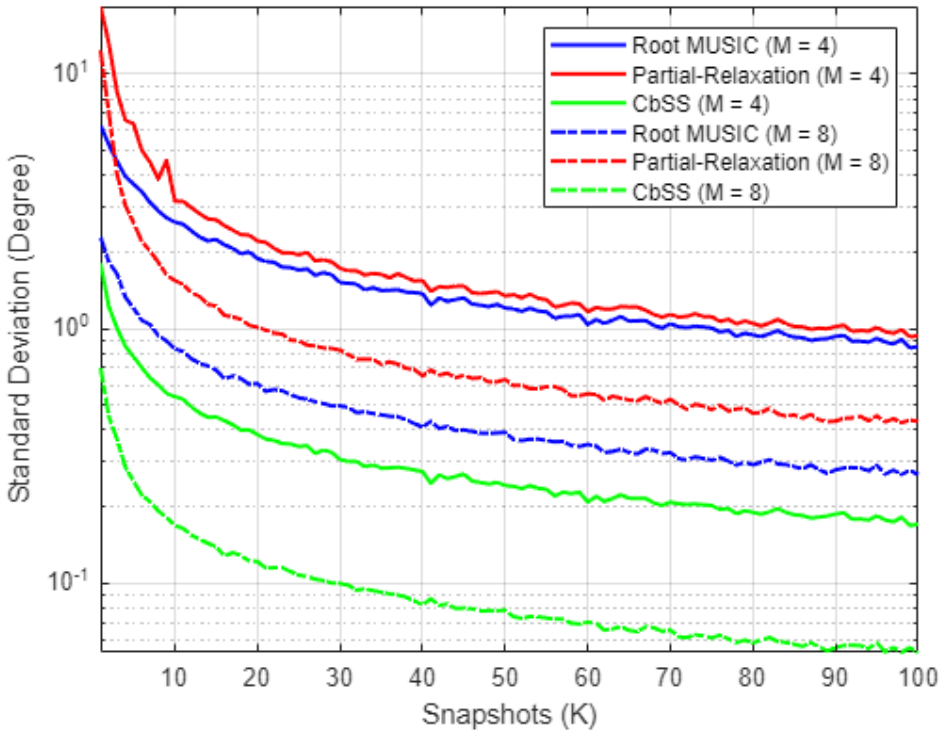

Figure 4.4 Standard deviation where M = 4 and M = 8 against the number of snapshots K ranging from 1-100

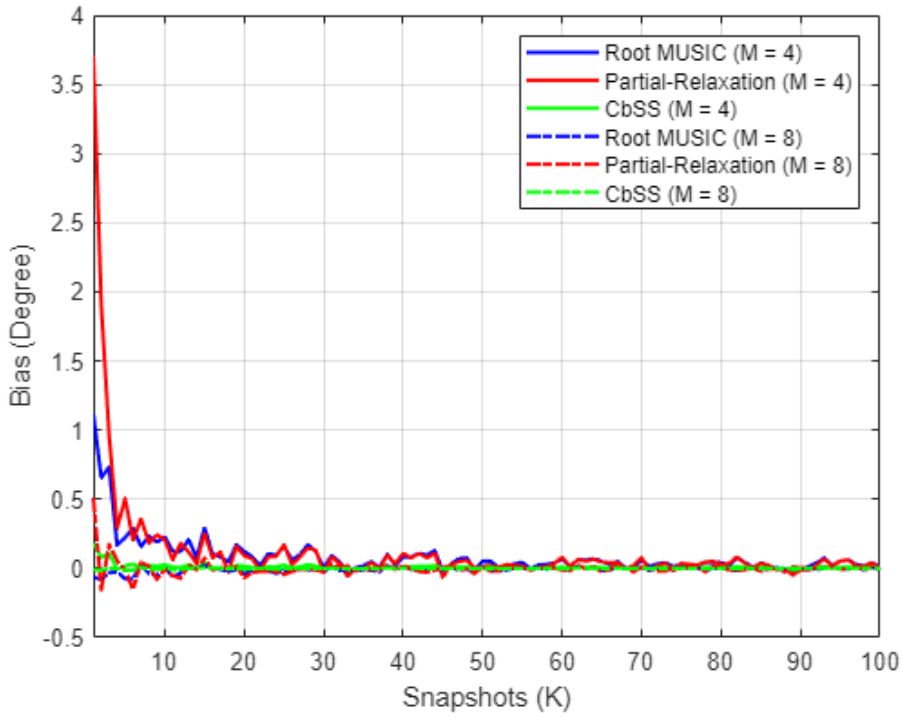

Figure 4.5 Bias performance comparison where M = 4 and M = 8 against the number of snapshots K ranging from 1 to 100

Figure 4.2 presents the RMSE of the DOA estimation against varying SNR ranging from 0 to 5 dB for root-MUSIC, PR, and the proposed CbSS technique where the number

of snapshot samples, $K = 100$, and the number of sensor array elements $M = 4$ and $M = 8$. It is worth highlighting that the proposed technique is chosen to be compared against root-MUSIC due to the likeliness of algorithm steps with improved estimation performance and the PR approach with its excellent and fast estimation performance.

As depicted in Figure 4.2, the proposed CbSS technique exhibits superior performance than root-MUSIC and PR, particularly in lower SNR threshold due to the noise and error suppressing factor in (4.11) and the array steering vector's optimal accuracy defined in (4.12).

To discuss the finding of the current state-of-the-art performance of the PR approach, at higher SNR (>2 dB), PR outperforms root-MUSIC, albeit slightly insignificant, with a small performance margin difference. Focusing on $M = 4$, when SNR = 5 dB, the root-MUSIC, PR and CbSS presented an absolute RMSE of 0.084°, 0.079° and 0.028° respectively. This yields a relative estimation performance gain of the proposed CbSS technique of 66.7% and 64.6% compared to root-MUSIC and PR, respectively. At the lowest SNR (0 dB), the three techniques present an RMSE DOA estimation of 0.59°, 0.62°, and 0.12°. These results yield a 79.7% and 80.6% relative estimation performance difference compared to root-MUSIC and PR.

Next, the performance when the number of antenna array elements, $M = 8$, is observed. When SNR = 0 dB, the root-MUSIC, PR, and CbSS have an RMSE performance of 0.21°, 0.15°, and 0.042°, respectively. This yields a relative estimation performance percentage difference of 80% and 72% when compared between CbSS and root-MUSIC and PR. When SNR = 5 dB, the RMSE difference presents 0.034°, 0.048°, and 0.011° for the three techniques. These results also yield a relative estimation performance difference of 67.6% and 77.1% between CbSS and root-MUSIC and PR.

To supplement Figure 4.2, Figure 4.3 presents the statistical bias performance of the three DOA estimation techniques with the same simulation parameters to investigate the underlying quantitative parameter. Focusing on $M = 4$, it can be observed that CbSS has a minor variation of bias across the SNR range while approaching minimal bias at a lower SNR of 1.8 dB compared to root-MUSIC and PR. In a worst-case scenario, when SNR = 0 dB, root-MUSIC, PR, and CbSS present 0.017°, −0.014°, and −0.00014°, respectively. Note that when SNR = 5 dB, the bias approaches negligible levels. Looking at the comparison when $M = 8$, when SNR = 0 dB, root-MUSIC, PR, and CbSS presents a bias of 0.014°, −0.0049°, and 0.0031°, respectively. Root-MUSIC shows a significantly lower bias when the number of sensor array elements doubles. The PR approach still has a considerably higher bias when the number of array elements is smaller. In addition, as

the PR approach only prioritizes the signal of interest and does not consider the sensor array number and noise environment [22], the PR performance in a low SNR environment is sub-optimal at best but performs significantly better at higher SNR. As the SNR increases, the noise and signal subspace separation is significant and easily differentiated for each method. In addition, as the number of sampling snapshot values increases, the bias starts to be negligible regardless of the methods. Overall, CbSS outperforms the other techniques in terms of statistical bias, proving that the estimation results are stable and predictable.

Figure 4.4 and Figure 4.5 present the DOA estimation performance among the three techniques in terms of its standard deviation against varying snapshots and its statistical bias performance, respectively. The simulation parameters are identical; however, the SNR value remains fixed at 0 dB to observe the DOA estimation performance variation in different snapshot values. Overall, CbSS outperforms root-MUSIC and PR in the case of varying snapshots with similar performance. In the scenario depicted in Figure 4.4 and Figure 4.5, it is evident that the higher the number of snapshots, the lower the standard deviation and statistical bias.

4.2.2 DOA Estimation Accuracy for Multiple Uncorrelated and Coherent Signal Sources

The second experiment observes CbSS performance when multiple signal sources are impinging onto the antenna array to demonstrate high-resolution DOA estimation. This will explain the robustness of signal source separation and estimation accuracy. The presented technique has averaged RMSE and bias between the two signal sources, and the numerical results are presented. In addition, varying snapshot against standard deviation is also presented against a variable number of antenna elements. The first subsection presents an uncorrelated signal source scenario where the difference in performance for varying signal source separation and the number of antenna elements is observed. Likewise, in the second subsection, the same simulation scenario as demonstrated in the uncorrelated signal environment is presented but with coherent signal sources.

4.2.2.1 DOA Estimation Accuracy for Multiple Uncorrelated Signal Sources

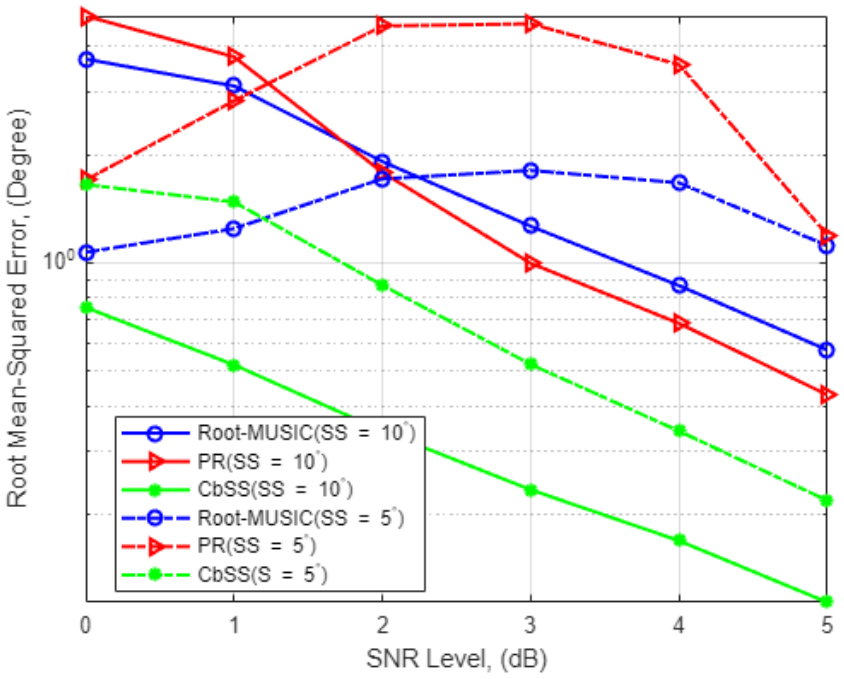

Figure 4.6 SNR-RMSE estimation performance for M = 4 with a fixed number of snapshots K = 100 for uncorrelated signal source separation of 5 and 10 degrees

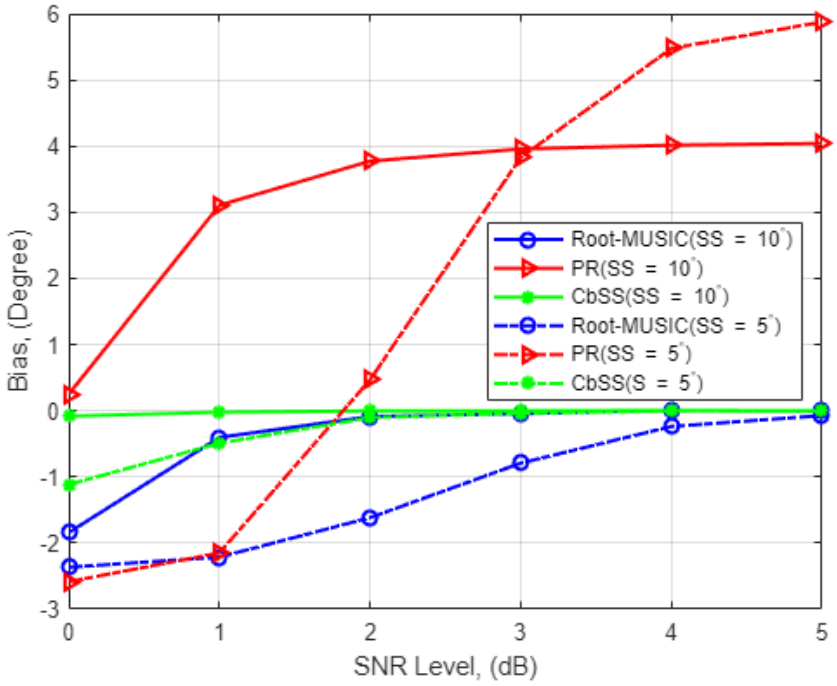

Figure 4.7 Bias performance comparison for M = 4 with a fixed number of snapshots K = 100 for uncorrelated signal source separation of 5 and 10 degrees

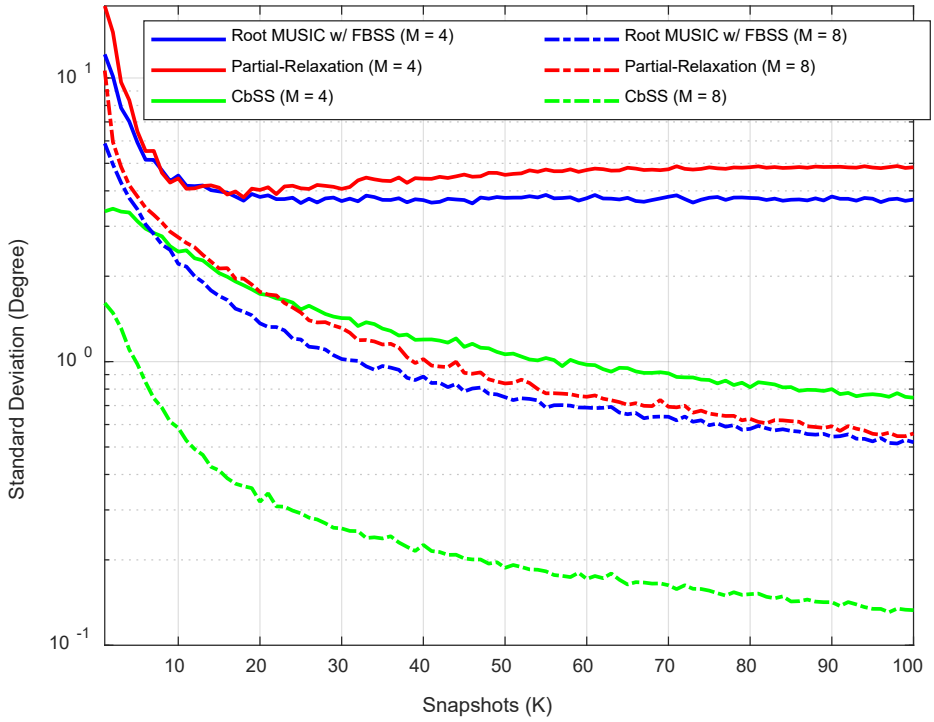

Figure 4.8 Standard deviation of DOA estimation comparison against varying snapshots for M = 4 and M = 8, fixed SNR = 0 dB with uncorrelated signal source separation of 10 degrees

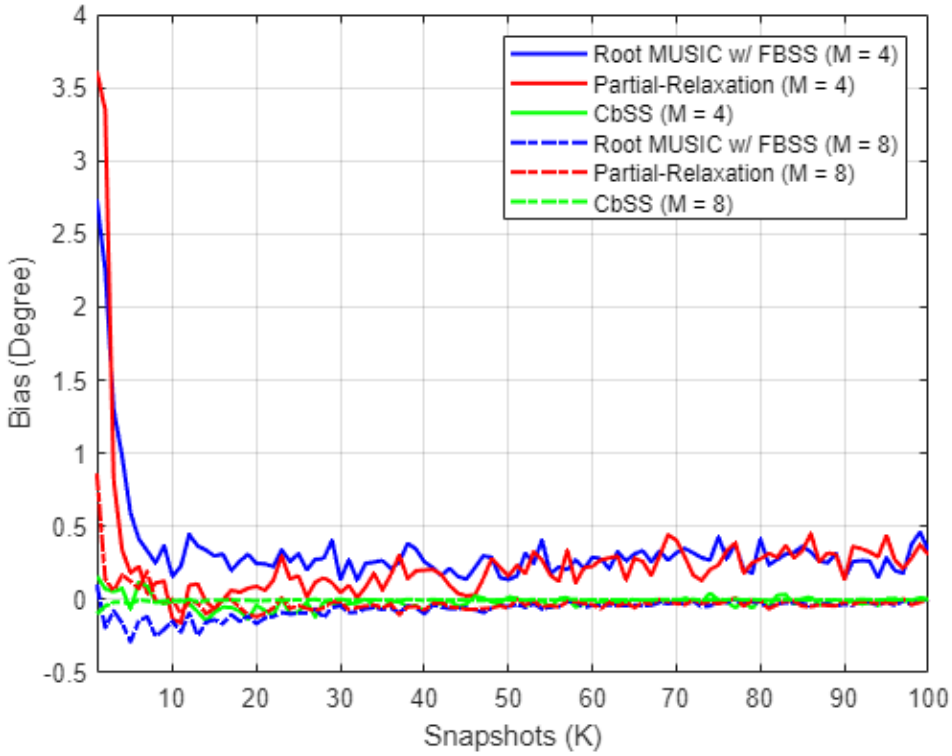

Figure 4.9 Bias comparison against varying snapshots for M = 4 and M = 8, SNR = 0 dB with uncorrelated signal source separation of 10 degrees

Figure 4.6 and Figure 4.7 present the numerical results with multiple degrees of uncorrelated signal source separation and the statistical bias where the array elements M = 4, respectively. The proposed CbSS estimation technique is consistent in performance compared to a single-source environment in a multiple signal source environment. An estimation performance decrease of cubic two degrees between a single source and multiple signal source scenarios is observed. It is consistent across all the techniques when the signal source separation is $>10^{\circ}$. It is important to note that while the estimation accuracy is high, the algorithm still needs to abide by the $M > L$ constraint. It is worth highlighting that in Figure 4.6, both root-MUSIC and PR has a significantly higher RMSE when the signal source separation is at $5°$ compared to $10°$, even though the SNR is approaching higher values. This is mainly due to these methods' minimal spatial signal source separation limitation. The covariance matrix used by both PR and root-MUSIC cannot resolve the two signals due to the two signals' inherent correlation, which results in very poor RMSE. Thus, root-MUSIC and PR have poor high-resolution DOA estimation ability due to the correlated covariance matrix.

It is noteworthy that the proposed CbSS technique still performs consistently with $10°$ signal source separation. However, there is a performance degradation of 25.5% when comparing $5°$ and $10°$ signal source separation, respectively. The inconsistent erratic DOA estimation performance is due to the correlation matrix binding with correlated matrix cell inputs. Erratic performance suppression presents the critical advantage of the proposed technique as it can differentiate and solve the two separate signal sources as they approach each other.

Figure 4.8 and Figure 4.9 present the numerical standard deviation against a varying number of snapshots. In this scenario, the SNR remains fixed at 0 dB, and the uncorrelated signal source separation was set at 10°. Figure 4.8 shows that the higher the number of snapshots, the lower the standard deviation. From the results, CbSS presented the lowest standard deviation compared to root-MUSIC and PR, regardless of the number of antenna elements.

4.2.2.2 DOA Estimation Accuracy for Multiple Coherent Signal Sources

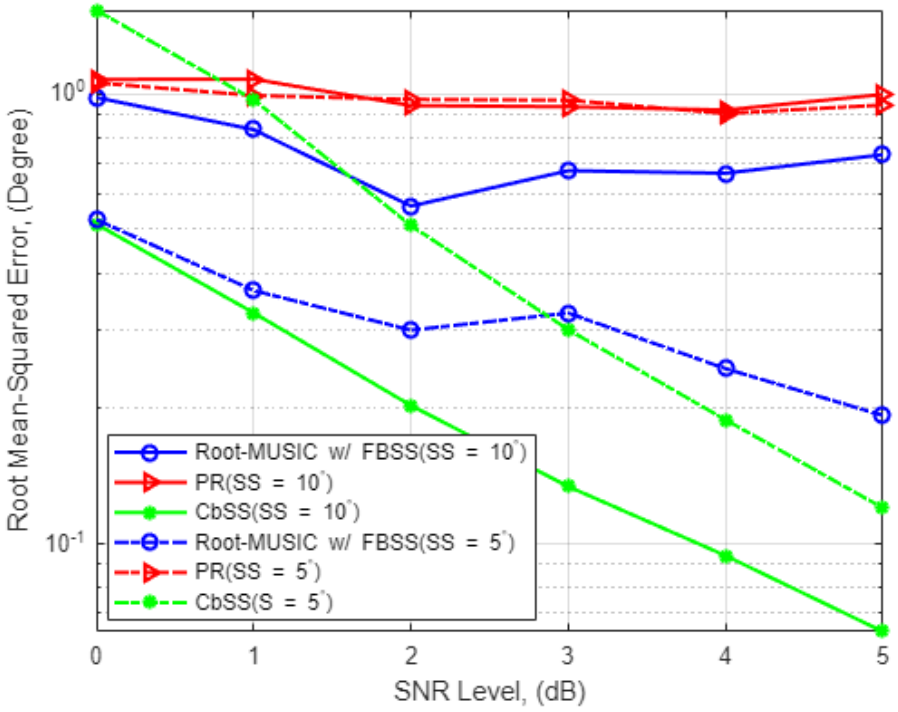

Figure 4.10 SNR-RMSE estimation performance for M = 4 with a fixed number of snapshots K = 100 for coherent signal source separation of 5 and 10 degrees

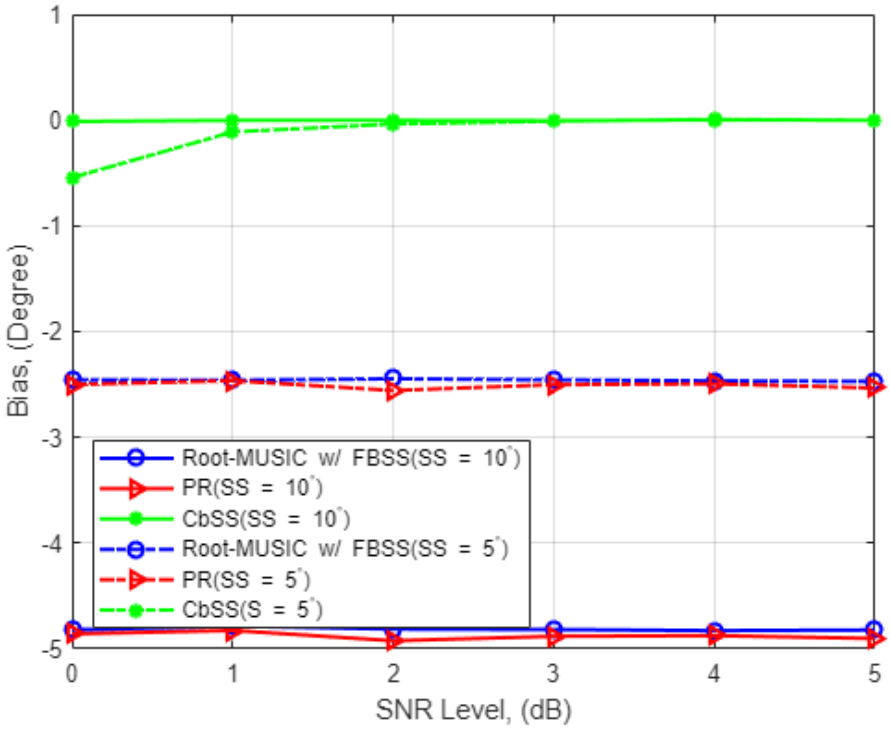

Figure 4.11 Bias performance comparison for M = 4 with a fixed number of snapshots K = 100 for coherent signal source separation of 5 and 10 degrees

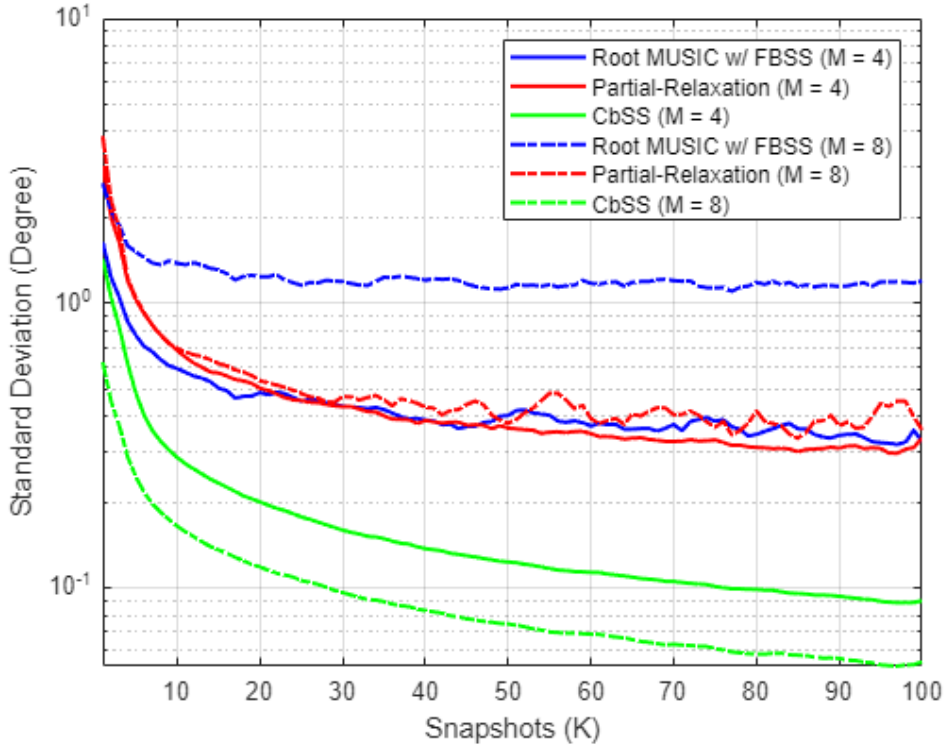

Figure 4.12 Standard deviation of DOA estimation comparison against varying snapshots for M = 4 and M = 8, fixed SNR = 0 dB with coherent signal source separation of 10 degrees

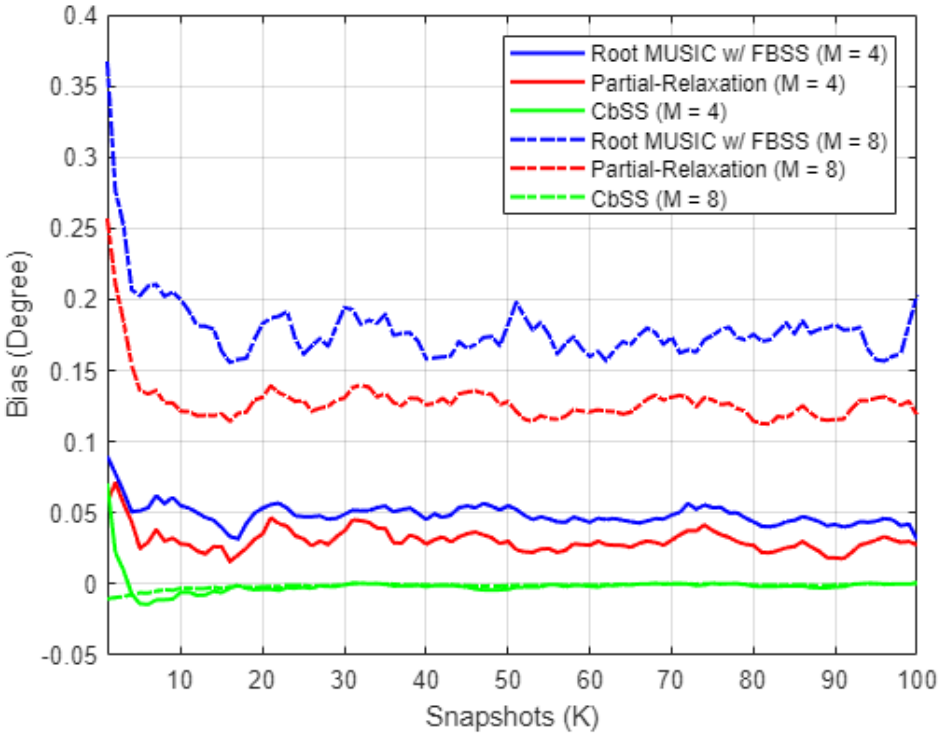

Figure 4.13 Bias comparison against varying snapshots for M = 4 and M = 8, SNR = 0 dB with coherent signal source separation of 10 degrees

The scenario where the signal sources of equal power are coherent is observed. In other words, coherent signals of interest have the same phase and frequency and a linear relationship. The same simulation environment is reenacted in the coherent signal simulation scenario as presented in 0. In addition, the Forward-backward Spatial Smoothing (FBSS) is employed for the root-MUSIC technique as this technique is well known for identifying coherent signals relatively well [106]. In addition, the FBSS application onto root-MUSIC does not make a difference in performance when applied to a coherent signal environment.

Figure 4.10 presents the SNR-RMSE DOA estimation performance for $M = 4$ with a fixed number of snapshots $K = 100$ for coherent signal source separation of 5 and 10 degrees. CbSS has the lowest RMSE compared to root-MUSIC and PR, with similar estimation performance compared to an uncorrelated scenario. However, all techniques have an estimation performance degradation of approximately 10% while sustaining a higher RMSE at higher SNR when compared to an uncorrelated signal scenario. This is expected due to the difficulty of accurately isolating and decomposing the signal and noise subspace. Figure 4.11 presents the statistical bias with the same simulation parameters as presented in Figure 4.10. The proposed CbSS technique has an almost negligible bias DOA estimation performance compared to root-MUSIC with FBSS and PR techniques. The bias results support past literature that the root-MUSIC and PR technique, although accurate in terms of RMSE, is susceptible to high bias.

Figure 4.12 presents the standard deviation of DOA estimation comparison against varying snapshots for $M = 4$ and $M = 8$, with a fixed SNR value of 0 dB and a coherent signal source separation of 10 degrees. Like Figure 4.9, it is evident that the higher the number of snapshots, the more accurate the DOA estimation is. Nevertheless, the proposed CbSS technique has the lowest standard deviation compared to root-MUSIC and PR, regardless of the number of elements. Figure 4.13 presents the statistical bias comparison for the same simulation environment, as demonstrated in Figure 4.8. Clearly, there are many bias jitters across the three techniques due to the coherent signal environment. Based on the results, CbSS presents almost negligible bias again than root-MUSIC and PR. However, compared to an uncorrelated scenario, as shown in Figure 4.4, it converges towards 0 at a much higher SNR level. At the same time, the root-MUSIC and PR techniques maintain undesirably high bias values.

In summary, the PR method performs the worst in a coherent signal environment. This is because for the PR approach, instead of enforcing the entire structure on the steering vector when formulating the DOA estimation problem, only the construction of one source of interest is preserved while other additional sources are relaxed. In a situation where there are multiple

sources, PR can only be effective when the sources are uncorrelated [48]. This is evident from Figure 4.5, where PR performs the worst compared to CbSS and root-MUSIC across the wide range of SNR.

Secondly, the root-MUSIC with FBSS performs relatively well in terms of bias performance due to spatial averaging. The difference between the estimated and actual DOA is much smaller in a coherent signal environment when FBSS is employed for root-MUSIC. The proposed CbSS technique outperforms the spatially smoothed root-MUSIC approach by presenting a significantly lower bias, especially at high SNR. When the coherent signal source separation is at its worst of 5 degrees, where SNR is -20 dB, the proposed CbSS technique has a bias of -2.2 degrees. The proposed method also approaches near 0 bias when SNR is > 0 dB in both signal source separation environments. The ability to resolve coherent signal here is possible due to the highly recursive updates and diagonal loading factor applied to the steering vector, as shown in (4.9) – (4.12).

4.2.3 Estimation Accuracy for Single Signal Source and Single Snapshot

The proposed technique estimation performance is observed in the third experiment under a single snapshot scenario where $M = 4$ and $K = 1$ as worst-case scenarios. All other parameters are the same and can be referred to in Table 4.1. Like the performance of a multiple finite snapshot sample scenario, the proposed CbSS technique outperforms the root-MUSIC and PR approaches. With reference to Figure 4.14, when SNR = 0 dB, the RMSE difference relative to the CRB in a single snapshot scenario is 7.7°, 19°, and 1.4° for the root-MUSIC and PR approach, and the proposed CbSS techniques, respectively. This yielded a performance percentage difference of 81.9% and 92.6% between CbSS and compared against root-MUSIC and PR. When the SNR = 5 dB, the RMSE difference is 0.87°, 0.88°, and 0.32° for the three estimation techniques, respectively. This yields a performance percentage difference of 63.2% and 63.6%, respectively. The simulation results prove that the CbSS technique is robust even in a single snapshot scenario providing satisfactory DOA estimation accuracy with the help of the accurate array steering vector estimation and the noise and estimation error suppressing factor in (4.12).

Figure 4.15 presents the statistical and focused biased plots for the proposed CbSS technique for $K = 1$ and $M = 4$. CbSS trumps the bias difference comparison and performance in a single snapshot scenario compared to the root-MUSIC and PR approach with an absolute maximum bias estimation of 0.0018° at the lowest SNR of 0 dB. It is also worth highlighting that the proposed CbSS technique approaches an unbiased-like performance at a lower SNR of 3.5 dB under a single snapshot environment. An essential

factor to note about the PR approach is that although it has a very high bias at low SNR compared to the other techniques overall, the computational time of the PR approach is deficient, which will be addressed in the next section. In addition, since the PR approach does not fully consider the entire signal and noise subspaces at low SNR, this technique does not perform as well as CbSS and the root-MUSIC method to prioritize computational complexity and calculation time of the final DOA estimates.

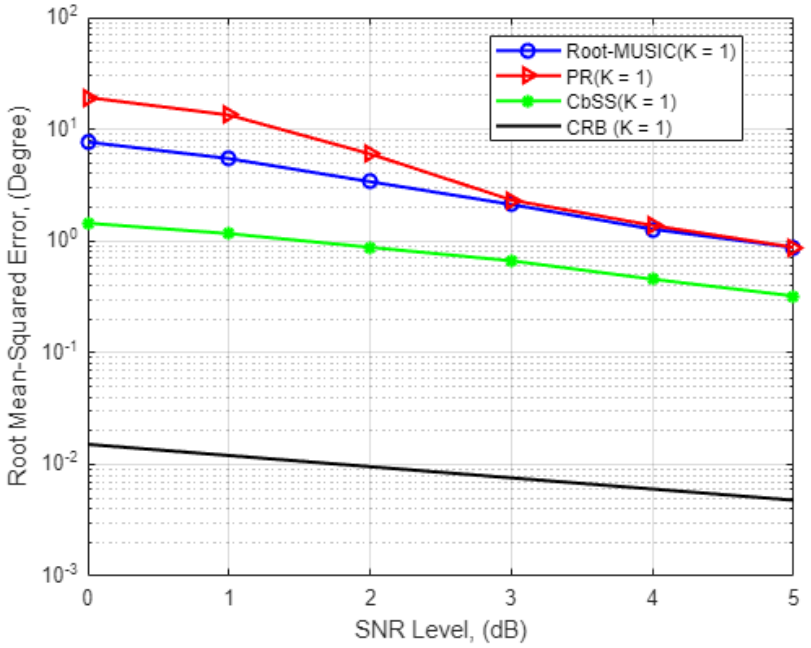

Figure 4.14 SNR-RMSE for single snapshot comparison where the number of antenna array elements M = 4 and K = 1

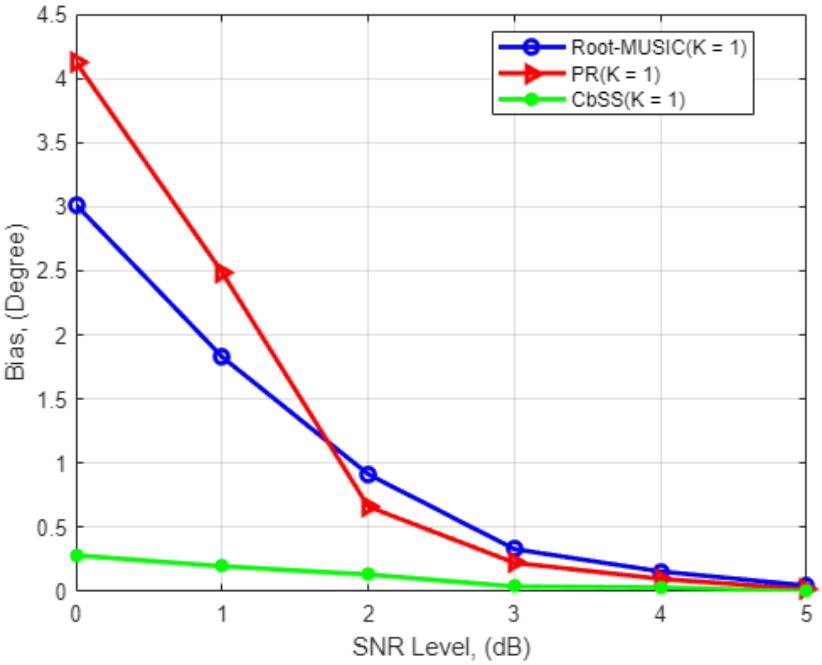

Figure 4.15 Statistical bias performance comparison across the demonstrated techniques for a single snapshot scenario

4.2.4 Parametric Performance Impact

Table 4.2 Comparison of Varying Delta Values

Delta, δ:	0.01	0.1	1	10
Peak Accuracy	98.7%	91.2%	79.2%	60.5%
Computational Time/cycle (millisecond)	0.23	0.19	0.12	0.08

Table 4.2 presents the performance comparison between peak DOA estimation accuracy and computational time for the CbSS technique. The simulation is based on a single source and single snapshot scenario with the same parameters in Table 4.1 based on the delta value in (16). As demonstrated in Table 4.2, the higher the delta value, the faster the DOA estimation sequence is completed, but this is at the expense of peak accuracy. Likewise, a lower delta value results in higher peak estimation accuracy but at the cost of computational time to completion. Depending on the application environment and priority, the end-user of CbSS has the flexibility to select the appropriate delta. For example, in a transportation application where high-speed targets are of concern, the user may choose delta values of ≥ 0.5 where there is a need for quick DOA estimation. Alternatively, in a scenario with slow speed targets, such as congested traffic, the user may select delta values of ≤ 0.1 for higher DOA estimation accuracy.

4.3 Performance Summary for CbSS DOA Estimator

This chapter investigates the problem with DOA estimators in low SNR scenarios with uniformed linear arrays in the presence of noise and the practicality of using a single snapshot to reduce computational complexity and time. The proposed algorithm's simulation results are consistent and perform well in low SNR scenarios by utilizing a well-approximated steering vector to modify the input covariance matrix. The proposed method is robust in estimation stability and can offer satisfactory DOA estimation performance. The simulation results have demonstrated that the proposed CbSS technique performs best among the three presented methods (root-MUSIC, PR, CbSS). The simulation work has been shown for multiple and single snapshot scenarios with adequate overall computational time compared to an existing state-of-the-art method like the PR approach. In addition, the proposed CbSS technique

presented good estimation performance in a multi-signal scenario even with signal separation of $< 5°$. The essential advantage of the proposed CbSS technique is efficient covariance matrix data collection coupled with accurate DOA estimation. The results present improved DOA estimation accuracy at lower SNR than the geometric-based DOA estimators with more downward statistical bias. However, at higher SNR, the geometric-based approach still shows an improved signal resolution for multiple sources compared to the subspace-based technique.

Nevertheless, the proposed method is applicable in scenarios where SNR is low and needs small-scale and lightweight antenna array localization applications and systems. One industry that urgently requires accurate DOA estimation would be the intelligent transportation system (ITS) network. As required in ITS applications, the proposed CbSS technique enables fast and precise network connectivity from stationary base stations and dynamically moving vehicular systems.

In the next chapter, the CbSS technique is further improved by introducing a novel hybrid method of implementing DL and DOA estimation to improve estimation accuracy and reduce computational load.

5 An Alternative DOA Estimation Method by Using an Adaptive Diagonal Loading Technique

This chapter aims to further develop an adaptive DL-based technique for DOA estimation applied to the sample covariance matrix to achieve high estimation accuracy for a wide range of operating frequencies and SNR without increasing computational complexity. Achieving a holistically predictable and accurate DOA estimator model complements multiple sensor applications regardless of the antenna sensor geometry and use cases. The proposed DL technique consists of a practical but straightforward adaptive DL estimator based on the steering vector's error rate of change and changes in estimation parameters such as operating frequencies for a fixed antenna array sensor position. The simulation results show that the proposed method outperforms state-of-the-art and high-performance DOA estimators such as EPUMA [10] and a modified Method of Direction Estimation (MODEX) [107]. The proposed method performs 9.5% better than the state-of-the-art EPUMA [10] technique in a finite number of snapshots and a single signal source. In a scenario where there are multiple signals of interest, the proposed method performs 2.8% better than EPUMA and up to 5% at higher SNR of > 0 dB. In a single snapshot sample with a single signal source of interest, the proposed method performs 8.5% better than EPUMA and is significantly closer to the CRB limit when compared to the other demonstrated DOA estimators.

5.1 Diagonal Loading

One of the easiest and most efficient methods to improve robustness against DOA mismatch and ensure the complete rank structure is to add constant values with the diagonal elements of the received signal correlation matrix. This is known as the fixed-diagonal loading method [59]. The diagonal loading technique is also commended for its effectiveness in

This chapter is reproduced from paper #2 in the publication list on page iv, where the thesis author is the main author in the paper.

handling various errors, including steering vector estimation and finite-sample errors. In addition, it can equalize the least significant eigenvalues of the covariance matrix or constrain the white noise gain. One of the inherent drawbacks of using DL is that it induces considerable bias [59, 102, 108]. However, this can be overcome by using bias correction [61] before parsing the final DOA. To that end, the diagonally loaded covariance matrix is defined as [10]

$$\mathbf{R}_{\mathbf{xx-DL}} = \mathbb{E}\{\mathbf{X}\mathbf{X}^{\mathrm{H}}\} + F\mathbf{I}, \tag{5.1}$$

where $\mathbf{I}$ is an identity matrix of size $M \times M$.

The scalar parameter of F denotes the amount of diagonal loading into the covariance matrix. Therefore, assuming that $F = 0$, no diagonal loading is present. In other words, it uses the standard covariance matrix, as shown in (2.4). Note that F can be positive or negative, but F must be greater than $-\sigma^2$ for the covariance matrix to be positive definite. In addition, values of F close to $-\sigma^2$ must be avoided to ensure numerical stability.

Similarly, the additive diagonal loading in (5.1) can also be demonstrated in the sample covariance matrix in (2.4), which is given as [11]

$$\widehat{\mathbf{R}}_{\mathbf{xx}} = \frac{1}{\mathrm{K}}\mathbf{X}\mathbf{X}^{\mathrm{H}} + F\mathbf{I}. \tag{5.2}$$

Before computing the weight vector, a diagonally loaded matrix is added to the sample covariance matrix in (5.2). This technique strengthens the noise components, which results in the input SNR reduction and suppression of the disturbance of small eigenvalues corresponding to the noise subspace. F should be a large enough value to reduce the input SNR. However, the interference component proportion also decreases, which reduces null depth in a pseudo-spectrum. Therefore, F should also be small enough to prevent the decline in null depth. There is always a trade-off between robustness, interference cancellation, and noise reduction. For example, for large F, the robustness against mismatch and replacement increases while interference cancellation and noise reduction capabilities decrease. Alternatively, for small F, the robustness is diminished. Therefore, the diagonal loading value should be appropriately selected to achieve performance improvement in a DOA estimation system.

A key benefit of diagonal loading is to overcome the inversion of the sample covariance matrix. When the number of snapshots is small, $\mathrm{K} < \mathrm{L}$, the inverted covariance matrix is not full rank and thus irreversible. The practical robustness can be analyzed as

follows. Let μ_l and $\mathbf{u}_l$ for $l = 1,2,\ldots,L$ be the subsequent eigenvalues and eigenvectors of $\widehat{\mathbf{R}}_{\mathbf{xx}}$, respectively. Then, with reference to (2.4), it can be further decomposed as [12]

$$\widehat{\mathbf{R}}_{\mathbf{xx}} = \sum_{l=1}^{L} \mu_l \, \mathbf{u}_l \mathbf{u}_l{}^{\mathrm{H}}, \tag{5.3}$$

which leads to the following decomposition,

$$\widehat{\mathbf{R}}_{\mathbf{xx}}{}^{-1}\mathbf{a}(\tilde{\theta}_0) = \sum_{l=1}^{L} \frac{\mathbf{u}_l{}^{H}\mathbf{a}(\tilde{\theta}_0)}{\mu_l}\mathbf{u}_l \, . \tag{5.4}$$

From (5.4), when μ_l is small, $\widehat{\mathbf{R}}_{\mathbf{xx}}{}^{-1}\mathbf{a}(\tilde{\theta}_0)$ tend towards a substantial value, leading to a high level of sidelobe errors and would result in the wrong signal direction of interest estimation. With the inclusion of diagonal loading, the decomposition becomes

$$(\widehat{\mathbf{R}}_{\mathbf{xx}} + F\mathbf{I}\,)^{-1}\mathbf{a}(\tilde{\theta}_0) = \sum_{l=1}^{L} \frac{\mathbf{u}_l{}^{\mathrm{H}}\mathbf{a}(\tilde{\theta}_0)}{\mu_l + F}\mathbf{u}_l. \tag{5.5}$$

From (5.5), adding the diagonal loading enables inversion to solve the available small sample size. Another benefit is that the sidelobes are suppressed for efficient beamforming in an intelligent antenna sensor system. Furthermore, adding the diagonal loading can reduce the influence of small eigenvalues; thereby, the weight vector norm is not amplified erratically. However, it is worth reiterating that this comes with a trade-off between the robustness and the expense of interference cancellation and noise reduction.

5.2 Proposed Traced Diagonal-Loading DOA Estimation Method

Although the diagonal-loading method, as shown in (5.5), shows promising results in a broad spectrum of SNR values, the technique still must process the entire covariance matrix, which may not even be of a Toeplitz structure, especially in a practical sample-based covariance matrix. In addition, selecting the correct loading factor remains crucial for accurate DOA estimation. Thus, the performance can vary significantly, and finding an optimal loading factor derivation remains a significant research interest.

This section shows how to further reduce and simplify the elements within the covariance matrix without sacrificing accuracy. To illustrate the proposed technique, the structure of the covariance matrix from (2.4) is observed as

$$\mathbf{R_{xx}} = \begin{bmatrix} xx_{1\times1} & \cdots & xx_{1\times m} \\ \vdots & \ddots & \vdots \\ xx_{m\times1} & \cdots & xx_{m\times m} \end{bmatrix}. \tag{5.6}$$

Then, the diagonal vector in $\mathbf{R_{xx}}$ of interest is partitioned and reformulated as a vector which can be represented as

$$\mathbf{r_{xx-diag}} = [xx_{1\times1} \quad \dots \quad xx_{m\times m}], \tag{5.7}$$

where $\mathbf{r_{xx-diag}}$ is a vector of size $M \times 1$.

From (5.7), the vector, $\mathbf{r_{xx-diag}}$, is reformed and partitioned into a Toeplitz Hermitian matrix which is represented as

$$\mathbf{R_{xx-reform}} = \begin{bmatrix} xx_{1\times1} & \dots & xx_{m\times m} \\ \vdots & \ddots & \vdots \\ xx_{m\times m} & \dots & xx_{m\times m} \end{bmatrix}, \tag{5.8}$$

where $\mathbf{R_{xx-reform}}$ is of size $M \times M$ similar to (5.6).

Note that the technique represented in (5.6) to (5.8) can be applied to the sample covariance matrix, $\widehat{\mathbf{R}}_{\mathbf{xx}}$. Comparing (5.6) and (5.8), the critical difference is that the off-diagonal elements replicate the elements along the diagonals for (5.8). One key advantage of this technique is that it reduces the computational load onto the system without calculating many different values of array elements.

Next, to determine a suitable F value for diagonal loading implementation, the following equation is defined and represented as

$$F = \frac{1}{K}\|\beta^{\mathrm{H}}\mathbf{R_{xx}}\|^2 \tag{5.9}$$

where $\beta = \mathbf{a}(\tilde{\theta}_0)/\|\mathbf{a}(\tilde{\theta}_0)\|$ is the normalized steering vector in the desired signal direction of interest.

Note that this normalization does not change the primary direction of interest, only its magnitude. This idea removes the influence of low SNR impedance in any application or scenario. The trade-off of this technique is that although it will result in consistent bias, it does not necessarily mean that there will be negligible bias. The bias discrepancy will be demonstrated later in the simulation section.

It is seen in (5.9) that the loading level depends on the signal and noise power. Finally, by combining (5.9) with (5.1) and (5.2), the following equations can be obtained,

$$\mathbf{R_{xx-DL-Mod}} = \mathbb{E}\{\mathbf{X}\mathbf{X}^{\mathrm{H}}\} + \left[\frac{1}{\mathrm{K}}\|\beta^{\mathrm{H}}\mathbf{R_{xx}}\|^{2}\right]\mathbf{I}\,, \tag{5.10}$$

$$\widehat{\mathbf{R}}_{\mathbf{xx-DL-Mod}} = \frac{1}{\mathrm{K}}\left\{\mathbf{X}\mathbf{X}^{\mathrm{H}} + \left[\|\beta^{\mathrm{H}}\mathbf{R_{xx}}\|^{2}\right]\mathbf{I}\right\}, \tag{5.11}$$

where (5.10) and (5.11) represent the theoretical and sample diagonally loaded tracing covariance matrix, respectively.

Lastly, before the decomposition to obtain the signal and noise subspace, and considering only the sampled covariance matrix, the diagonally loaded covariance matrix is modified as:

$$\widehat{\mathbf{R}}_{\mathbf{xx-DLT}} = \widehat{\mathbf{R}}_{\mathbf{xx-DL-Mod}} + \mathrm{tr}\left(\widehat{\mathbf{R}}_{\mathbf{xx-DL-Mod}}\right), \tag{5.12}$$

where $\mathrm{tr}(\cdot)$ is the trace of a matrix.

After determining the first sample covariance matrix, $\widehat{\mathbf{R}}_{\mathbf{xx}}$ as in (2.1), from the incoming received signal data matrix, the diagonal elements are extracted and reformed into a new modified covariance matrix, $\mathbf{R_{xx-reform}}$ like in (5.8). Concurrently, the diagonal loading factor, F, is calculated, which leads to the reformulation of a new diagonally loaded sample covariance matrix, $\widehat{\mathbf{R}}_{\mathbf{xx-DL-Mod}}$ as in (5.11). Finally, the traced sample covariance matrix, $\widehat{\mathbf{R}}_{\mathbf{xx-DLT}}$ is reformulated for DOA estimation as described in (5.12).
Then, the subspace decomposition of (5.12) can be presented as

$$\widehat{\mathbf{R}}_{\mathbf{xx-DLT}} = \mathbf{U}_s\mathbf{\Omega}_s\mathbf{V}_s^{\mathrm{H}} + \mathbf{U}_n\mathbf{\Omega}_n\mathbf{V}_n^{\mathrm{H}}, \tag{5.13}$$

where $\mathbf{U}_s$ and $\mathbf{V}_s$ span the column spaces of $\widehat{\mathbf{R}}_{\mathbf{xx-DLT}}$ and $\widehat{\mathbf{R}}_{\mathbf{xx-DLT}}{}^{\mathrm{H}}$ respectively, whereas $\mathbf{U}_n$ and $\mathbf{V}_n$ span their orthogonal spaces and $\mathbf{\Omega}_s$ and $\mathbf{\Omega}_n$ are the corresponding diagonal matrices with eigenvalues or singular values on the diagonal, respectively.

Figure 5.1 presents the algorithmic flowchart summary of the proposed technique for the sample covariance matrix reformulation.

Algorithm 2 Covariance Matrix Reformulation using DLT Algorithm

Require: Incoming SNR Data Matrix from Sensor Array, $\mathbf{X}$

procedure DLT-RM(θ)
  Determine $\hat{\mathbf{R}}_{xx} = \frac{1}{K}\mathbf{X}\mathbf{X}^{\mathbf{H}}$
  Extract Diagonal Elements $Diag(\hat{\mathbf{R}}_{\mathbf{xx}})$ from $\hat{\mathbf{R}}_{\mathbf{xx}}$
  Restructure $Diag(\hat{\mathbf{R}}_{\mathbf{xx}})$ into $\hat{\mathbf{R}}_{\mathbf{xx-reform}}$
  while $\hat{\mathbf{R}}_{\mathbf{xx-reform}}$ is being determined **do**
    Calculate $F = \frac{1}{K}\|\beta^{H}\hat{\mathbf{R}}_{\mathbf{xx}}\|^2$
  end while
  Reconstruct $\hat{\mathbf{R}}_{\mathbf{DL-Mod}} = \frac{1}{K}\{\|\beta^{\mathbf{H}}\hat{\mathbf{R}}_{\mathbf{xx}}\|^2\}\mathbf{I}$
  Reformulate $\hat{\mathbf{R}}_{\mathbf{DLT}} = \hat{\mathbf{R}}_{\mathbf{DL-Mod}} + trace(\hat{\mathbf{R}}_{\mathbf{DL-Mod}})$
  Decompose Signal and Noise Subspace $\hat{\mathbf{R}}_{\mathbf{Decomp-DLT}} = \mathbf{U_s}\mathbf{\Omega_s}\mathbf{V_s}^{\mathbf{H}} + \mathbf{U_n}\mathbf{\Omega_n}\mathbf{V_n}^{\mathbf{H}}$
end procedure

Figure 5.1 DLT-DOA Estimation Algorithm Flow

5.3 Simulation Results & Discussion of DL-DOA

In this section, numerical examples are provided to study the stochastic effects of the proposed method. To illustrate the simulation setup, the value of F has an impact corresponding to the input SNR and ULA with equally spaced half-wavelength geometry. The input SNR is varied to generate different $\hat{\mathbf{R}}_{\mathbf{xx-DLT}}$ with zero-mean AWGN against varying SNR ranging from -10 dB to 10 dB. To further illustrate the efficiency of the proposed method, the simulation study is presented in a different real-world-like environment that meets the challenges of estimation accuracy. Firstly, in a scenario where there is a minimal finite snapshot availability. Next, the proposed technique's estimation performance is provided, where multiple signal sources are of interest. Lastly, the performance of the proposed method is delivered where only a single snapshot is available, which can be considered a worst-case scenario.

The technique against state-of-the-art techniques is compared, such as the EPUMA [10], Method of Direction of Arrival Estimation (MODE) [109], MODEX [107], and root-MUSIC with Forward-backward Spatial Smoothing (FBSS) [88].

The simulation was conducted using MATLAB 2021a on a Windows 10 PC with a quad-core i7 CPU with 16GB RAM and 1000 randomized Monte-Carlo simulation samples to evaluate the accuracy of DOA estimation. The standard parameters for the study are presented and summarized in Table 4.1. Typical parameters are selected that are aligned with the requirements in a modern transportation market, as referenced in [44]. It is noteworthy that although the EPUMA technique is used to demonstrate the proposed method in the simulation study, any subspace-based DOA estimation algorithm can be implemented.

Table 5.1 Common Simulation Parameters

Parameters	Settings
Carrier Frequency	5500 MHz
Antenna Geometry	Uniformed Linear Array
Array Inter-Element Spacing	$\lambda/2$, where λ is the wavelength of f_c in meters
Simulation Samples	1000
Angle of Interest	30 Degrees
SNR Range	-10 dB to 10 dB

Lastly, the simulation study uses the RMSE as the primary criterion. The general RMSE equation is defined as

$$\text{RMSE} = \sqrt{\frac{1}{Q}\sum_{i=1}^{Q}\left[\frac{\left(\theta_{i_1}-\hat{\theta}_{i_1}\right)^2+\cdots+\left(\theta_{i_L}-\hat{\theta}_{i_L}\right)^2}{L}\right]} \tag{5.14}$$

where L is the number of signal sources, Q is the number of simulation data points, θ_i is the actual DOA, and $\hat{\theta}_i$ is the estimated DOA.

The CRB [9] is also included as a performance benchmark, where the CRB is computed as

$$\text{CRB} = \frac{\sigma_n^2}{2K}\text{tr}\left(\text{Re}\left(\left(\mathbf{D}^{\text{H}}(\mathbf{I}_M - \mathbf{A}\mathbf{A}^{+})\mathbf{D}\right)\odot\mathbf{R}^{\text{T}}\right)^{-1}\right), \tag{5.15}$$

with $\mathbf{D} = [\partial\boldsymbol{a}(\theta_1)/\partial\theta_1 \quad \ldots \quad \partial\boldsymbol{a}(\theta_N)/\partial\theta_N]$ and $\mathbf{R} = \text{E}[\boldsymbol{x}(t)\boldsymbol{x}^H(t)] = \mathbf{A}\mathbf{R}_\mathbf{s}\mathbf{A}^\mathbf{H} + \sigma_n^2\mathbf{I}_M$. In this case, $\mathbf{R}_\mathbf{s} = \mathbf{E}[\boldsymbol{s}(t)\boldsymbol{x}^H(t)]$ is the signal covariance matrix and $\odot$ is the Hadamard matrix product.

For root-MUSIC, the FBSS technique improves signal detection and estimation accuracy, where the number of forward-backward subarrays equals the number of desired signals.

5.3.1 Limited Finite Snapshot Sample Performance with Single Signal Source of Interest

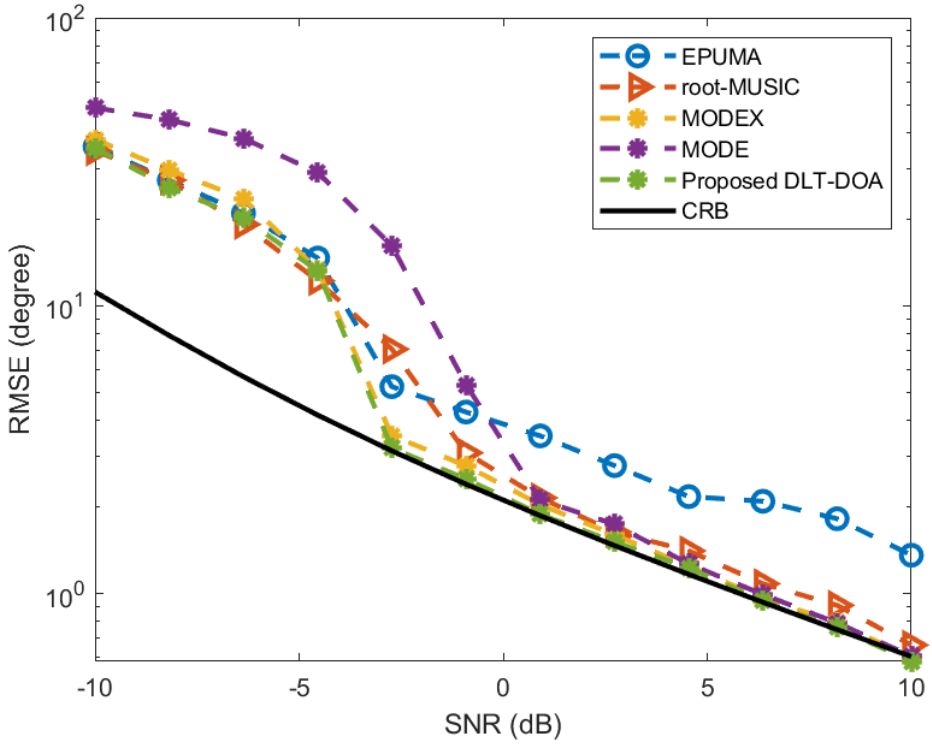

Figure 5.2 SNR-RMSE Performance for M = 4, N = 1, and K = 10

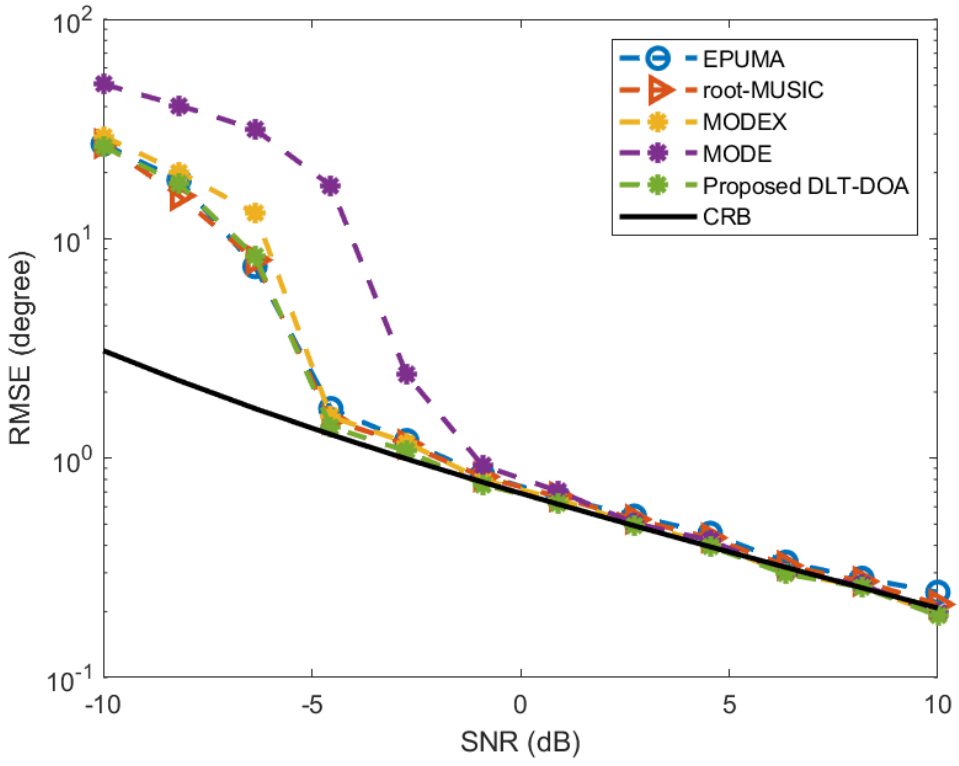

Figure 5.3 SNR-RMSE Performance for M = 8, N= 1, and K = 10

This section presents a scenario with a limited, finite number of snapshot samples for a single-source signal of interest. Figure 5.2 and Figure 5.3 present the RMSE of the DOA estimation against varying SNR input received data matrix ranging from -10 to 10 dB, where the number of snapshot samples is $K = 10$ and the number of sensor array elements $M = 4$ and $M = 8$, respectively. It is also assumed that the number of impinging signals, $N = 1$ is static and does not deviate with time at the instant of data collection on the receiving end. In addition, Table 5.2 presents the RMSE results of all the proposed DOA techniques for comparison.

It is seen in Figure 5.2 that the proposed technique outperforms MODE, root-MUSIC, and EPUMA on average when SNR is < -5 dB. Furthermore, the RMSE of the proposed method retains the CRB when SNR is > 3.5 dB. As SNR increases, the RMSE curves of all techniques are tightly bound towards the CRB, and thus, their estimation performance attains the theoretical CRB lower bound curve. The MODE technique does not perform well due to the small number of antenna array elements and a highly limited number of snapshot samples, even though it utilizes the FBSS method to improve DOA estimation. These poor DOA estimation results can be seen generally throughout the entire SNR range. Furthermore, the proposed technique slightly outperforms EPUMA, MODE, and MODEX by 12%. As SNR increases, the proposed method still outperforms the other methods by an average of 7% in DOA estimation performance gain.

Figure 5.3 presents a similar simulation environment but with a higher number of antenna array elements. Comparing this with Figure 5.2, the performance gained for the proposed method is slightly less compared to the other techniques. In addition, all DOA estimation techniques presented here approach the CRB limit at a much lower SNR due to the increase in antenna element number. It can observe that MODE performs among the compared techniques at low SNR. The proposed approach achieves the best DOA estimation performance when the SNR is high at > 3.5 dB. In addition, the proposed method performs the best at high SNR compared to the other demonstrated DOA estimator as it is much closer to the CRB limit.

Table 5.2 Summary of Simulation Results for Single Signal Source

Scenario	RMSE (Degrees)				
	EPUMA	Root-MUSIC	MODEX	MODE	DLT-DOA
M = 4, SNR = -10 dB	29.9	32.1	36.6	48.5	30.6
M = 4, SNR = 10 dB	1.55	0.66	0.61	0.61	0.60
M = 8, SNR = -10 dB	25.8	24.4	29.8	50.34	26.8
M = 8, SNR = 10 dB	0.23	0.23	0.21	0.66	0.20

5.3.2 Limited Finite Snapshot Sample with Multiple Signal Sources of Interest

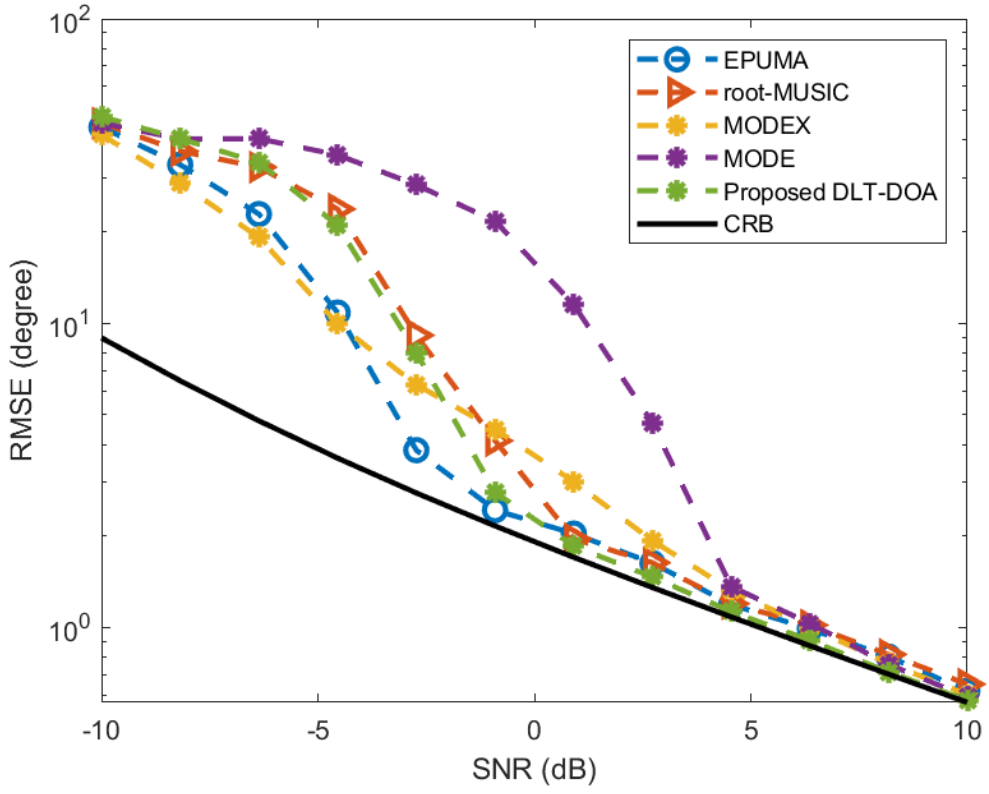

Figure 5.4 SNR-RMSE Performance for M = 8, N = 2, Δθ=10°, and K = 10

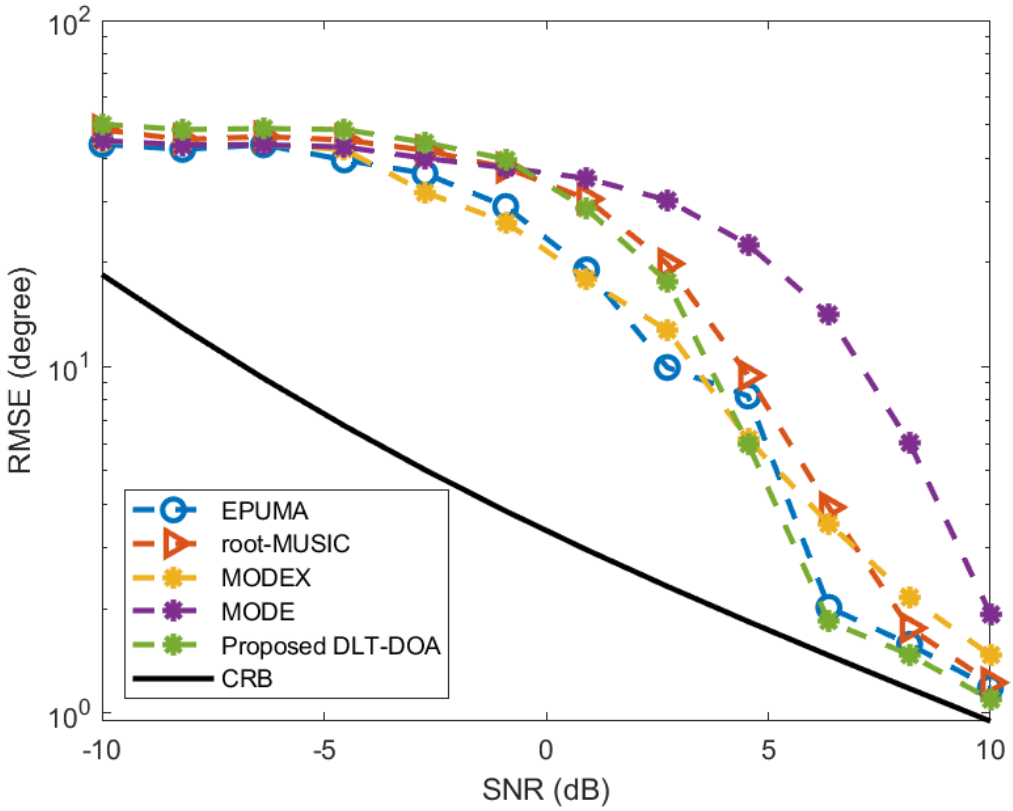

Figure 5.5 SNR-RMSE Performance for M = 8, N = 2, Δθ=5°, and K = 10

In this example, a simulation study is conducted with a limited number of snapshot samples with two signal sources of interest. Figure 5.4 presents a scenario where the signal sources of interest are of an angular separation of 10°. It is clear that the EPUMA technique generally has a better DOA estimation performance – particularly at low SNR of < -5 dB. It is worth highlighting that the MODE technique has a substantial estimation performance reduction compared to the other methods. This estimation deficit is because MODE is highly sensitive to the number of signal sources. One potential reason is the symmetric assumption used in the MODE solver algorithm. This reason is consistent across the wide range of scenarios, especially when comparing the results in Figure 5.2 and Figure 5.3. Nevertheless, the proposed technique performs relatively well across the spectrum of SNR. However, EPUMA and root-MUSIC are still outperforming it due to the spatial smoothing modification with an average DOA estimation performance deficit of 7%. At higher SNR of > 0 dB, the proposed method outperforms all the other techniques by 2.8% and is closely bounded by the theoretical CRB limit.

To highlight the DOA estimation resolution among closely spaced signal sources, Figure 5.5 presents a scenario where the angular separation is 5°. EPUMA performs best in this scenario in low SNR of < 0 dB and can robustly determine the two closely related signals of interest. Furthermore, root-MUSIC here serves the worse, even though it employs the

FBSS modification due to the sensitivity in the virtual array setup for spatial smoothing. This result is followed closely by the proposed method in terms of RMSE performance. When SNR is high at > 0 dB, all techniques approach the CRB limit but do not perform as well as in Figure 5.4 where the signal sources are separated further. Comparing the DOA estimation performance between Figure 5.4 and Figure 5.5, the performance difference on average is 15%. In other words, the estimation performance difference results in a 3%/$\Delta\theta$ based on the simulation results. Table 5.3 presents a summary of the DOA estimators for multiple signal sources for both the lowest and highest SNR.

Table 5.3 Summary of Simulation Results for Multiple Signal Sources

Scenario	**RMSE (Degrees)**				
	EPUMA	Root-MUSIC	MODEX	MODE	DLT-DOA
$\Delta\theta = 10°$, SNR = -10 dB	42.1	44.2	38.2	43.6	46.2
$\Delta\theta = 10°$, SNR = 10 dB	0.62	0.64	0.61	0.62	0.59
$\Delta\theta=5°$, SNR = -10 dB	45.5	48.0	46.7	45.5	50.5
$\Delta\theta=5°$, SNR = 10 dB	1.17	1.31	1.49	2.14	1.13

5.3.3 Single Snapshot Sample with a Single Signal Source of Interest

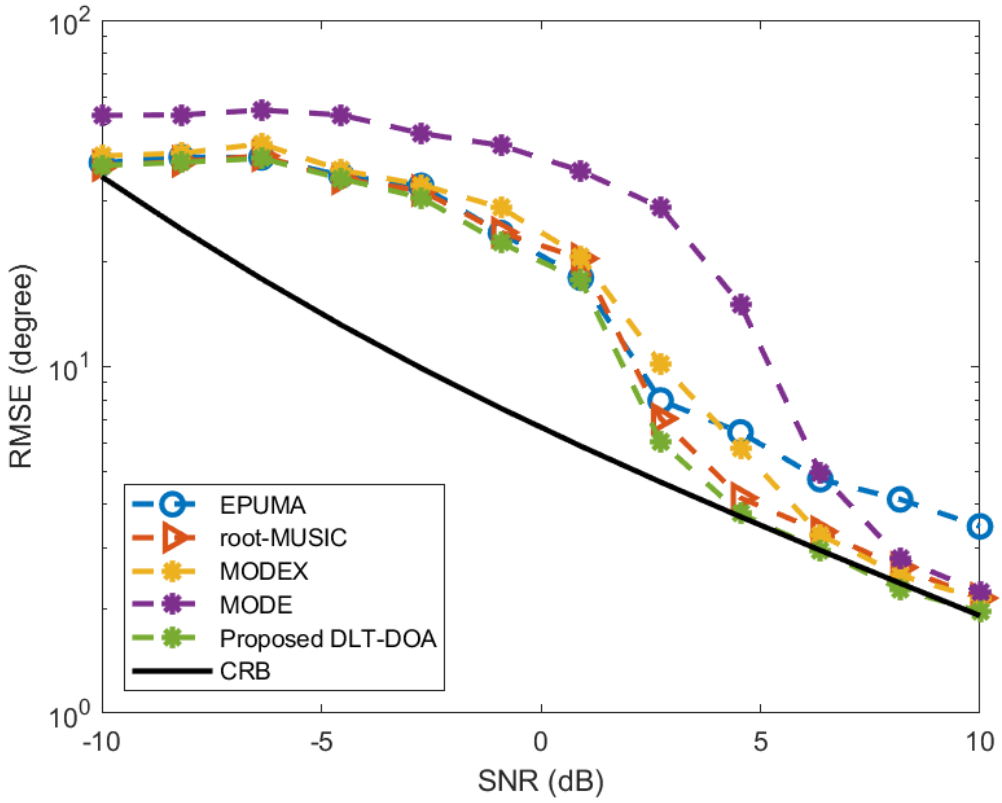

Figure 5.6 SNR-RMSE Performance for M = 4, N = 1, and K = 1

This section conducts a quantitative analysis of the proposed technique where the number of snapshot samples is $K = 1$. This simulation parameter presents a worst-case scenario where only a single snapshot is available at the array sensor as a limitation, where the results are shown in Figure 5.6. All other parameters are the same as in the previous section, which can be referred to in Table 5.1, while Table 5.4 provides the summarized RMSE results of the DOA estimators.

Similarly, the MODE technique performs worse across the wide range of SNR. Comparing the results in Figure 5.5 against a similar simulation environment as in Figure 5.2, the DOA estimation only approaches the CRB limit at a much higher SNR. This result is consistent where the number of snapshots changes the raw performance of all the demonstrated DOA estimators. The proposed technique performs relatively well in a single snapshot scenario compared to EPUMA, root-MUSIC, and MODEX, although the DOA estimation performance difference is negligible at approximately 2%. This phenomenon may be within the margin of error, particularly in low SNR of < 0 dB. The performance difference across the different techniques at high SNR at > 0 dB is something that is worth highlighting. The proposed approach generally performs the best compared to the other methods. This RMSE result is followed closely behind with EPUMA. In general, the

proposed method achieves the best estimation performance across the wide range of SNR with an average DOA estimation performance gain of 8.5% compared to the following best estimator.

The proposed technique performs better than the rest in a single snapshot environment mainly due to the optimized diagonal loading factor technique as demonstrated in (5.9) and its implementation in (5.11). The iterative nature of (5.9) proves that it is an efficient method in determining accurate DOA estimation as compared to a static diagonal loading factor.

Table 5.4 Summary of Simulation Results for Single Snapshot Scenario

Scenario	RMSE (Degrees)				
	EPUMA	Root-MUSIC	MODEX	MODE	DLT-DOA
SNR = -10 dB	39.5	40.5	42.4	53.4	41.1
SNR = 10 dB	3.54	2.18	2.05	2.13	1.92

5.4 Performance Summary for DLT-DOA

This chapter presents a reconstruction of the sample covariance matrix with uniformed linear arrays in the presence of noise. By effectively utilizing a suitable diagonally loaded value to modify the incoming covariance matrix, the need for high snapshots is reduced in a wide range of SNR environments. Using a modified diagonal loading technique to the sample covariance matrix, the proposed method performs best in a scenario with a minimal number of snapshot samples. This allows the utilization of the algorithm in an environment where the sensors are used small and lightweight without costly hardware for real-world implementation. In addition, high power transmission is not required for accurate DOA estimation for a sensor device emitting a signal due to the excellent performance in low SNR scenarios. It allows fast and precise network directivity and localization in an electronic device like a position sensor for transportation, vehicular systems, or motorsports applications to sense location and orientation in a relatively wide range of SNR and sampling numbers.

5.5 A Comparison between CbSS and DLT-DOA

This research introduced two novel DOA algorithms that meet real-world application. Both these methods complement each other, with enhanced accuracy and estimation time, that can adapt to different scenarios. For example, CbSS provides the user with configurability between estimation time and DOA estimation accuracy. At the same time, DLT-DOA offers a fixed and straightforward DOA estimator with fast and accurate DOA estimation.

The table below presents a performance comparison of the two proposed methods. The comparison is based on the same 4-element ULA and simulation parameters conducted in previous chapters. The results are based on an averaged performance across a range of SNR from 0 – 5 dB.

Table 5.5 Features Comparison Between CbSS and DLT-DOA

Features	CbSS, $\delta = 0.01$	CbSS, $\delta = 10$	DLT-DOA
User Configurability	Configurable		Fixed
Single Source, Single Snapshot DOA Estimation Accuracy	98.7%	60.5%	81.2%
Average Single Snapshot Estimation Time (ms)	0.23	0.08	0.12

With reference to Table 5.5, the critical difference between CbSS and DLT-DOA is the option to have configurability, dependent on the application. CbSS allows the algorithm user to prioritise computational time or DOA estimation accuracy. Alternatively, DLT-DOA offers a fixed configuration without a significant and detrimental impact on the DOA estimation accuracy and estimation time which is a trade-off compared to CbSS.

Some key factors must be considered for a user to pick which algorithm to choose. One example would be the cost of implementation. For example, as CbSS is iterative due to the delta parameter, the hardware platform, and thus cost, must be considered as CbSS is relatively more computationally expensive than DLT-DOA. However, CbSS offers the flexibility to configure to any specific scenarios it has to perform. For example, in an HSR environment where computational time is a concern [110] or V2V applications, both base stations and targets are not moving as fast and require higher DOA estimation accuracy [111].

6 Conclusion and Future Work

6.1 Conclusion

The research presented in this thesis was aimed to identify and solve the critical challenge faced by existing DOA estimators that are aligned with the unique demands of real-world scenarios. There are two crucial issues with existing DOA estimators. Firstly, it is due to the lack of estimation accuracy when the snapshot samples are reduced. Secondly, the long computational time due to high complexities and snapshot sample data load is undesirable in a scenario where real-time computations are required.

State-of-the-art DOA estimation algorithms, CbSS and DLT-DOA, were proposed and investigated in this thesis to address the challenges. Based on a quantitative and qualitative analysis of the proposed algorithms, it can be concluded that the proposed techniques have met the requirements for real-time applications, such as in the transportation industry.

A novel CbSS DOA estimator that meets both the requirements of fast computational time and high estimation accuracy was proposed in Chapter 4. The numerical simulation results confirm its effectiveness in multiple environmental scenarios, such as single and multiple signal sources of interest. The benefit of the CbSS method is that the DOA is derived based on defining the root cause of errors that existing DOA estimators have often overlooked. Furthermore, CbSS has been proven effective using a single snapshot data sample, yielding up to 25.5% lower DOA estimation degradation in multiple uncorrelated and coherent signal source environments. Furthermore, the CbSS technique also offers fast computational time by up to 0.08 milliseconds without compromising estimation accuracy. Compared to existing techniques, such as the PR approach and other subspace-based methods, the CbSS technique is more suitable for real-time wireless communication where the environment tends to have low SNR with rapid changes to the DOAs.

An improved and novel DOA estimation method, DLT-DOA, further enhancing the CbSS technique, has also been proposed and presented in Chapter 5. DLT-DOA employs an adaptive diagonal loading technique to further improve DOA estimation accuracy. Similarly, simulation scenarios consist of single and multiple signal sources of interest as well as single snapshot-based DOA estimation. The simulation results proved the effectiveness and were validated against the existing state-of-the-art DOA estimation techniques such as EPUMA and MODEX. In a finite number of snapshots with a single signal source, DLT-DOA performs

9.5% better than EPUMA and MODEX, 2.8% in multiple signal sources and 8.5% in a single snapshot environment in terms of DOA estimation accuracy.

In summary, this thesis has presented two state-of-the-art DOA estimation algorithms suitable for transportation applications that meet the demand for fast computational time and high estimation accuracy: CbSS and DLT-DOA.

6.2 Future Work

The research and DOA estimation algorithms derived from this thesis could be further enhanced in the following aspects:

1. To implement and validate via hardware for proposed DOA algorithms,
2. To extend the proposed algorithms into other antenna array structures,
3. To validate the performance of the proposed algorithms in a dynamic scenario,
4. To experiment and evaluate the proposed DOA estimators in a specific real-world application.

6.2.1 Hardware Implementation for Proposed DOA Algorithms

As the research conducted in this thesis was only based on simulation, hardware implementation for real-world scenarios is required for further validation. One of the critical assumptions that were made in the development of the work of this thesis is that the antenna array is assumed to be a perfect geometry. In reality, the array spacing in an antenna system tends to have deviation due to manufacturing defects and tolerances. The antenna array's misalignment may pose a challenge for accurate DOA estimation, affecting the covariance matrix formulation, which is a crucial data point for DOA algorithms. The calibration error is expected to cause some form of perturbation and may lack estimation accuracy. Hardware implementation and validation can be carried out using a Field Programmable Gate Array (FPGA), such as in [112], or by using modular software-defined radio hardware such as in [113, 114] before being implemented into a complete end-to-end system such as a smart antenna with beamforming such as in [44, 78] [115].

6.2.2 Extension of CbSS and DL-DOA Technique to Other Antenna Array Structures

In this thesis, only the ULA antenna array structure was considered to develop the proposed DOA estimation techniques to ensure simplicity in the development stage.

Furthermore, only the azimuth angle of the impinging signal was considered due to the ULA structure limitation. Nevertheless, the proposed CbSS and diagonal-loading method for DOA estimation could be further extended to cover other antenna array geometry such as a Uniform Circular Array (UCA) or a Uniform Rectangular Array (URA) to validate the robustness in different scenarios such as in [116, 117] which would increase the DOA estimation accuracy for an increased number of signal sources of interest concurrently.

The proposed DOA techniques can be expanded to consider the elevation angle of the signal of interest by extending the antenna array steering matrix. Some examples of DOA estimations with both azimuth and elevation angle derivation in the steering matrix can be found in [52, 118, 119]. For instance, in [120], an L-shaped antenna array structure is first considered. Then, by utilizing a sub-array system, the horizontal elements of the array can be used to determine the azimuth angle. At the same time, the vertical elements along the array can be used to determine the elevation angle for accurate, independent DOA estimation.

6.2.3 Extended Performance Validation of Proposed Techniques into a Dynamic Scenario

The work done in this thesis is solely based on assumptions and simulation work with models based on real-world scenarios. Furthermore, it is assumed to be a static scenario with only an AWGN noise perturbation for a more straightforward estimation performance analysis. The proposed DOA estimation techniques in this thesis could be further tested and developed for scenarios such as in a dynamic system where the signal source of interest is constantly moving with respect to the antenna array. Some dynamic strategies that have been carried out can be referred to in [121]. In addition, real-world scenarios tend to have a variety of noise interference. The estimation performance of the proposed techniques could then be further verified in different real-world scenarios.

6.2.4 Real-world Impact & Potential of the Proposed DOA Estimation Techniques

Many real-world scenarios utilize DOA estimation – particularly as a sub-system of a smart antenna beamforming system. For example, [122] highlights the importance and the challenges required for a suitable smart antenna system for a modern transportation market with real-world implementation, such as enabling smart city networks, closed-circuit television (CCTV) monitoring, and many other public operations and services. Furthermore,

[122] highlighted that the critical challenges faced in the transportation market are high capital and operational expenses. With the help of a suitably designed smart antenna system with beamforming, the number of field equipment can be reduced due to smaller deployment and maintenance costs. Furthermore, wireless interference such as mutual coupling and environmental factors such as noise can be reduced by having a beam steering system such as a good beamformer and DOA estimation algorithm between a wireless transmitter and a receiver that are always pointing to each other with narrow beam and nulls in all other direction. Therefore, the transportation application aspect would be one of many suitable platforms to apply the proposed DOA estimation technique proposed in this thesis.

Bibliography

[1] M. Muhammad, M. Li, Q. Abbasi, C. Goh, and M. A. Imran, "A Covariance Matrix Reconstruction Approach for Single Snapshot Direction of Arrival Estimation," *Sensors,* vol. 22, no. 8, 2022, doi: 10.3390/s22083096.

[2] M. Muhammad, M. Li, Q. H. Abbasi, C. Goh, and M. A. Imran, "An Adaptive Diagonal Loading Technique to Improve Direction of Arrival Estimation Accuracy for Linear Antenna Array Sensors," *IEEE Sensors Journal,* pp. 1-1, 2022, doi: 10.1109/JSEN.2022.3168785.

[3] M. Muhammad, M. Li, Q. H. Abbasi, C. Goh, and M. Imran, "Direction of Arrival Estimation using Root-Transformation Matrix Technique," in *2019 IEEE International Symposium on Antennas and Propagation and USNC-URSI Radio Science Meeting*, 7-12 July 2019, pp. 1369-1370, doi: 10.1109/APUSNCURSINRSM.2019.8889249.

[4] M. Muhammad, M. Li, Q. H. Abbasi, C. Goh, and M. Imran, "Performance Evaluation for Direction of Arrival Estimation Using 4-Element Linear Array," in *2019 13th European Conference on Antennas and Propagation (EuCAP)*, 31 March-5 April 2019 2019, pp. 1-5.

[5] M. Muhammad, M. Li, Q. H. Abbasi, C. Goh, and M. Imran, "Auto-calibration of Linear Array Antenna Positioning for Single Snapshot Direction of Arrival Estimation," in *2020 IEEE International Symposium on Antennas and Propagation and North American Radio Science Meeting*, 5-10 July 2020, pp. 491-492, doi: 10.1109/IEEECONF35879.2020.9330495.

[6] M. Muhammad, M. Li, Q. H. Abbasi, C. Goh, and M. Imran, "Direction of Arrival Estimation Using Hybrid Spatial Cross-Cumulants and Root-MUSIC," in *2020 14th European Conference on Antennas and Propagation (EuCAP)*, 15-20 March 2020, pp. 1-5, doi: 10.23919/EuCAP48036.2020.9135813.

[7] M. Muhammad, M. Li, Q. H. Abbasi, C. Goh, and M. Imran, "A Novel Subspace-Averaging Direction of Arrival Estimation Technique," in *2021 IEEE 6th International Conference on Signal and Image Processing (ICSIP)*, 22-24 Oct. 2021 2021, pp. 744-748, doi: 10.1109/ICSIP52628.2021.9688940.

[8] S. Dai, M. Li, Q. H. Abbasi, and M. A. Imran, "A Fast Blocking Matrix Generating Algorithm for Generalized Sidelobe Canceller Beamformer in High Speed Rail Like

Scenario," *IEEE Sensors Journal,* vol. 21, no. 14, pp. 15775-15783, 2021, doi: 10.1109/JSEN.2020.3002699.

[9] P. Stoica and A. Nehorai, "MUSIC, maximum likelihood, and Cramer-Rao bound," *IEEE Transactions on Acoustics, Speech, and Signal Processing,* vol. 37, no. 5, pp. 720-741, 1989, doi: 10.1109/29.17564.

[10] C. Qian, L. Huang, N. D. Sidiropoulos, and H. C. So, "Enhanced PUMA for Direction-of-Arrival Estimation and Its Performance Analysis," *IEEE Transactions on Signal Processing,* vol. 64, no. 16, pp. 4127-4137, 2016, doi: 10.1109/TSP.2016.2543206.

[11] M. Yang *et al.*, "Machine-Learning-Based Fast Angle-of-Arrival Recognition for Vehicular Communications," *IEEE Transactions on Vehicular Technology,* vol. 70, no. 2, pp. 1592-1605, 2021, doi: 10.1109/TVT.2021.3054757.

[12] Z. Liu, C. Zhang, and P. S. Yu, "Direction-of-Arrival Estimation Based on Deep Neural Networks With Robustness to Array Imperfections," *IEEE Transactions on Antennas and Propagation,* vol. 66, no. 12, pp. 7315-7327, 2018, doi: 10.1109/TAP.2018.2874430.

[13] Y. Mao, Q. Guo, J. Ding, F. Liu, and Y. Yu, "Marginal Likelihood Maximization Based Fast Array Manifold Matrix Learning for Direction of Arrival Estimation," *IEEE Transactions on Signal Processing,* vol. 69, pp. 5512-5522, 2021, doi: 10.1109/TSP.2021.3112922.

[14] M. Xue and C. Zhu, "A Study and Application on Machine Learning of Artificial Intellligence," in *2009 International Joint Conference on Artificial Intelligence*, 25-26 April 2009 2009, pp. 272-274, doi: 10.1109/JCAI.2009.55.

[15] S. Laha, N. Chowdhury, and R. Karmakar, "How Can Machine Learning Impact on Wireless Network and IoT? – A Survey," in *2020 11th International Conference on Computing, Communication and Networking Technologies (ICCCNT)*, 1-3 July 2020 2020, pp. 1-7, doi: 10.1109/ICCCNT49239.2020.9225652.

[16] C. Ko and J. Lee, "Performance of ESPRIT and Root-MUSIC for Angle-of-Arrival(AOA) Estimation," in *2018 IEEE World Symposium on Communication Engineering (WSCE)*, 28-30 Dec. 2018 2018, pp. 49-53, doi: 10.1109/WSCE.2018.8690541.

[17] R. Roy and T. Kailath, "ESPRIT-estimation of signal parameters via rotational invariance techniques," *IEEE Transactions on Acoustics, Speech, and Signal Processing,* vol. 37, no. 7, pp. 984-995, 1989, doi: 10.1109/29.32276.

[18] G. K. Papageorgiou, M. Sellathurai, and Y. C. Eldar, "Deep Networks for Direction-of-Arrival Estimation in Low SNR," *IEEE Transactions on Signal Processing,* vol. 69, pp. 3714-3729, 2021, doi: 10.1109/TSP.2021.3089927.

[19] B. Sun, C. Wu, J. Shi, H. Ruan, and W. Ye, "Direction-of-Arrival Estimation Under Array Sensor Failures with ULA," *IEEE Access,* vol. 8, pp. 26445-26456, 2020, doi: 10.1109/ACCESS.2019.2959274.

[20] K. R, F. H, and M. A. M, "A comprehensive analysis and performance evaluation of different direction of arrival estimation algorithms," in *2012 IEEE Symposium on Computers & Informatics (ISCI)*, 18-20 March 2012 2012, pp. 256-259, doi: 10.1109/ISCI.2012.6222705.

[21] M. Sun, Y. Wang, and J. Pan, "Direction of Arrival Estimation by a Modified Orthogonal Propagator Method With Spline Interpolation," *IEEE Transactions on Vehicular Technology,* vol. 68, no. 11, pp. 11389-11393, 2019, doi: 10.1109/TVT.2019.2944516.

[22] D. M. Vijayan and S. K. Menon, "Direction of arrival estimation in smart antenna for marine communication," in *2016 International Conference on Communication and Signal Processing (ICCSP)*, 6-8 April 2016 2016, pp. 1535-1540, doi: 10.1109/ICCSP.2016.7754416.

[23] Â. M. C. R. Borzino, J. A. Apolinário, and M. L. R. d. Campos, "Robust DOA estimation of heavily noisy gunshot signals," in *2015 IEEE International Conference on Acoustics, Speech and Signal Processing (ICASSP)*, 19-24 April 2015 2015, pp. 449-453, doi: 10.1109/ICASSP.2015.7178009.

[24] C. Uysal and T. Filik, "Contactless respiration rate estimation using MUSIC algorithm," in *2017 10th International Conference on Electrical and Electronics Engineering (ELECO)*, 30 Nov.-2 Dec. 2017 2017, pp. 606-610.

[25] A. Rajani and P. Kora, "Direction of Arrival Estimation by Using Artificial Neural Networks," in *2021 Third International Conference on Intelligent Communication Technologies and Virtual Mobile Networks (ICICV)*, 4-6 Feb. 2021 2021, pp. 1360-1363, doi: 10.1109/ICICV50876.2021.9388514.

[26] M. Yanovsky, A. Gorbenko, and V. Kharchenko, "Adaptive WiFi systems: Principles of design and application support," in *The International Conference on Digital Technologies 2013*, 29-31 May 2013 2013, pp. 203-206, doi: 10.1109/DT.2013.6566312.

[27] M. Seufert, C. Moldovan, V. Burger, and T. HoBfeld, "Applicability and limitations of a simple WiFi hotspot model for cities," in *2017 13th International Conference*

on Network and Service Management (CNSM), 26-30 Nov. 2017 2017, pp. 1-7, doi: 10.23919/CNSM.2017.8255985.

[28] A. Abdelaziz, R. Burton, F. Barickman, J. Martin, J. Weston, and C. E. Koksal, "Enhanced Authentication Based on Angle of Signal Arrivals," *IEEE Transactions on Vehicular Technology,* vol. 68, no. 5, pp. 4602-4614, 2019, doi: 10.1109/TVT.2019.2898898.

[29] A. Fascista, G. Ciccarese, A. Coluccia, and G. Ricci, "Angle of Arrival-Based Cooperative Positioning for Smart Vehicles," *IEEE Transactions on Intelligent Transportation Systems,* vol. 19, no. 9, pp. 2880-2892, 2018, doi: 10.1109/TITS.2017.2769488.

[30] G. Han, L. Wan, L. Shu, and N. Feng, "Two Novel DOA Estimation Approaches for Real-Time Assistant Calibration Systems in Future Vehicle Industrial," *IEEE Systems Journal,* vol. 11, no. 3, pp. 1361-1372, 2017, doi: 10.1109/JSYST.2015.2434822.

[31] C. Xuesong, Y. Xuefeng, and A. P. Yuste, "Direction-of-arrival estimation using single antenna in high-speed-train environments," in *2016 10th European Conference on Antennas and Propagation (EuCAP)*, 10-15 April 2016 2016, pp. 1-4, doi: 10.1109/EuCAP.2016.7481736.

[32] M. Jomoto, N. Kikuma, and K. Sakakibara, "Simultaneous estimation of DOA and angular spread of incident radio waves by DOA-Matrix method with SLS and SAGE algorithms," in *2015 International Symposium on Antennas and Propagation (ISAP)*, 9-12 Nov. 2015 2015, pp. 1-2.

[33] X. Yin, L. Ouyang, and H. Wang, "Performance Comparison of SAGE and MUSIC for Channel Estimation in Direction-Scan Measurements," *IEEE Access,* vol. 4, pp. 1163-1174, 2016, doi: 10.1109/ACCESS.2016.2544341.

[34] J. Webber, S. Tsukamoto, S. Ano, N. Kukutsu, and T. Kumagai, "Direction of arrival estimation apparatus for communication based train control system using ESPAR antenna," in *2015 Third International Conference on Digital Information, Networking, and Wireless Communications (DINWC)*, 3-5 Feb. 2015 2015, pp. 49-54, doi: 10.1109/DINWC.2015.7054216.

[35] R. Qian and M. Sellathurai, "Direction-of-arrival estimation with espar antennas using Bayesian compressive sensing," in *2016 IEEE International Conference on Acoustics, Speech and Signal Processing (ICASSP)*, 20-25 March 2016 2016, pp. 3076-3080, doi: 10.1109/ICASSP.2016.7472243.

[36] M. Plotka, M. Tarkowski, K. Nyka, and L. Kulas, "A novel calibration method for RSS-based DoA estimation using ESPAR antennas," in *2018 22nd International Microwave and Radar Conference (MIKON)*, 14-17 May 2018 2018, pp. 65-68, doi: 10.23919/MIKON.2018.8405316.

[37] Z. Dai, Y. He, V. Tran, N. Trigoni, and A. Markham, "DeepAoANet: Learning Angle of Arrival From Software Defined Radios With Deep Neural Networks," *IEEE Access,* vol. 10, pp. 3164-3176, 2022, doi: 10.1109/ACCESS.2021.3140146.

[38] S. Ravindran and R. Jose, "Direction of Arrival and Channel Estimation using Machine Learning for Multiple Input Multiple Output System," in *2019 International Conference on Communication and Electronics Systems (ICCES)*, 17-19 July 2019 2019, pp. 1327-1330, doi: 10.1109/ICCES45898.2019.9002097.

[39] L. Wu and Z. Huang, "Coherent SVR Learning for Wideband Direction-of-Arrival Estimation," *IEEE Signal Processing Letters,* vol. 26, no. 4, pp. 642-646, 2019, doi: 10.1109/LSP.2019.2901641.

[40] M. Coutino, R. Pribic, and G. Leus, "Direction of arrival estimation based on information geometry," in *2016 IEEE International Conference on Acoustics, Speech and Signal Processing (ICASSP)*, 20-25 March 2016 2016, pp. 3066-3070, doi: 10.1109/ICASSP.2016.7472241.

[41] Y. Dong, C. Dong, W. Liu, M. Liu, and Z. Tang, "Scaling Transform Based Information Geometry Method for DOA Estimation," *IEEE Transactions on Aerospace and Electronic Systems,* vol. 55, no. 6, pp. 3640-3650, 2019, doi: 10.1109/TAES.2019.2910363.

[42] Y. Wen, X. Chen, Y. Wei, Y. Fan, T. Zeng, and Z. Ding, "SAR Parameter Estimation Method for Rectangle Plane Based on Information Geometry," in *2019 IEEE International Conference on Signal, Information and Data Processing (ICSIDP)*, 11-13 Dec. 2019 2019, pp. 1-5, doi: 10.1109/ICSIDP47821.2019.9173226.

[43] M. Scherreik and B. Rigling, "Online Estimation of Radar Emitter Cardinality via Bayesian Nonparametric Clustering," *IEEE Transactions on Aerospace and Electronic Systems,* vol. 57, no. 6, pp. 3791-3800, 2021, doi: 10.1109/TAES.2021.3103582.

[44] M. C. Tan, M. Li, Q. H. Abbasi, and M. A. Imran, "A Wideband Beamforming Antenna Array for 802.11ac and 4.9 GHz in Modern Transportation Market," *IEEE Transactions on Vehicular Technology,* vol. 69, no. 3, pp. 2659-2670, 2020, doi: 10.1109/TVT.2019.2963111.

[45] C. Wu, D. Krishnasamy, and J. Elangage, "Hardware Implementation and RF High-Fidelity Modeling and Simulation of Compressive Sensing Based 2D Angle-of-Arrival Measurement System for 2–18 GHz Radar Electronic Support Measures," *Sensors,* vol. 21, no. 20, 2021, doi: 10.3390/s21206823.

[46] R. Pribić, "Information Distances in Stochastic Resolution Analysis," in *Geometric Science of Information*, Cham, F. Nielsen and F. Barbaresco, Eds., 2017// 2017: Springer International Publishing, pp. 847-855.

[47] D. Zachariah, P. Stoica, and M. Jansson, "Comments on “Enhanced PUMA for Direction-of-Arrival Estimation and Its Performance Analysis”," *IEEE Transactions on Signal Processing,* vol. 65, no. 22, pp. 6113-6114, 2017, doi: 10.1109/TSP.2017.2742982.

[48] M. Trinh-Hoang, M. Viberg, and M. Pesavento, "Partial Relaxation Approach: An Eigenvalue-Based DOA Estimator Framework," *IEEE Transactions on Signal Processing,* vol. 66, no. 23, pp. 6190-6203, 2018, doi: 10.1109/TSP.2018.2875853.

[49] M. Trinh-Hoang, M. Viberg, and M. Pesavento, "CramÉr-rao Bound for DOA Estimators under the Partial Relaxation Framework," in *ICASSP 2019 - 2019 IEEE International Conference on Acoustics, Speech and Signal Processing (ICASSP)*, 12-17 May 2019 2019, pp. 4469-4473, doi: 10.1109/ICASSP.2019.8682980.

[50] Q. Lin, L. Huang, and P. Shuai, "Two-dimensional direction-of-arrival estimation of non-circular signals using one snapshot," in *2016 IEEE International Geoscience and Remote Sensing Symposium (IGARSS)*, 10-15 July 2016 2016, pp. 4290-4293, doi: 10.1109/IGARSS.2016.7730118.

[51] S. M. Prasad, T. Panigrahi, and A. Dubey, "Computationally Efficient Near-Field Source Localization Using Single Snapshot," in *2017 14th IEEE India Council International Conference (INDICON)*, 15-17 Dec. 2017 2017, pp. 1-5, doi: 10.1109/INDICON.2017.8487943.

[52] H. Semira, H. Belkacemi, and N. Doghmane, "Single snapshot projection based method for azimuth/elevation directions of arrival estimation," in *2007 9th International Symposium on Signal Processing and Its Applications*, 12-15 Feb. 2007 2007, pp. 1-4, doi: 10.1109/ISSPA.2007.4555533.

[53] B. Errasti-Alcalá, D. Escot-Bocanegra, D. Poyatos-Martínez, A. Jurado-Lucena, and R. Fernández-Recio, "Joint Direction of Arrival and amplitude estimation using Particle Swarm Optimization and a single snapshot," in *Digests of the 2010 14th Biennial IEEE Conference on Electromagnetic Field Computation*, 9-12 May 2010 2010, pp. 1-1, doi: 10.1109/CEFC.2010.5481660.

[54] P. Li, J. Li, and G. Zhao, "Low Complexity DOA Estimation for Massive UCA with Single Snapshot," *Journal of Systems Engineering and Electronics,* vol. 33, no. 1, pp. 22-27, 2022, doi: 10.23919/JSEE.2022.000003.

[55] L. Lan, M. Rosamilia, A. Aubry, A. D. Maio, and G. Liao, "Single-Snapshot Angle and Incremental Range Estimation for FDA-MIMO Radar," *IEEE Transactions on Aerospace and Electronic Systems,* vol. 57, no. 6, pp. 3705-3718, 2021, doi: 10.1109/TAES.2021.3083591.

[56] R. Wu, M. Wang, and Z. Zhang, "Computationally Efficient DOA and Carrier Estimation for Coherent Signal Using Single Snapshot and Its Time-Delay Replications," *IEEE Transactions on Aerospace and Electronic Systems,* vol. 57, no. 4, pp. 2469-2480, 2021, doi: 10.1109/TAES.2021.3061821.

[57] R. Cao, B. Liu, F. Gao, and X. Zhang, "A Low-Complex One-Snapshot DOA Estimation Algorithm with Massive ULA," *IEEE Communications Letters,* vol. 21, no. 5, pp. 1071-1074, 2017, doi: 10.1109/LCOMM.2017.2652442.

[58] R. T. O. Brien and K. Kiriakidis, "Single-snapshot robust direction finding," *IEEE Transactions on Signal Processing,* vol. 53, no. 6, pp. 1964-1978, 2005, doi: 10.1109/TSP.2005.847828.

[59] A. Elnashar, S. M. Elnoubi, and H. A. El-Mikati, "Further Study on Robust Adaptive Beamforming With Optimum Diagonal Loading," *IEEE Transactions on Antennas and Propagation,* vol. 54, no. 12, pp. 3647-3658, 2006, doi: 10.1109/TAP.2006.886473.

[60] W. Miao, C. Luo, G. Min, Y. Mi, and Z. Yu, "Location-Based Robust Beamforming Design for Cellular-Enabled UAV Communications," *IEEE Internet of Things Journal,* vol. 8, no. 12, pp. 9934-9944, 2021, doi: 10.1109/JIOT.2020.3028853.

[61] D. Zhang, J. Tang, and G. Zheng, "Covariance matrix estimation depending on bias correction of the sample eigenvalues for STAP," in *2017 IEEE Radar Conference (RadarConf)*, 8-12 May 2017 2017, pp. 0304-0307, doi: 10.1109/RADAR.2017.7944217.

[62] F. Vincent and O. Besson, "Steering vector errors and diagonal loading," *Radar, Sonar and Navigation, IEE Proceedings -,* vol. 151, pp. 337-343, 01/10 2005, doi: 10.1049/ip-rsn:20041069.

[63] C. Chen and P. P. Vaidyanathan, "Quadratically Constrained Beamforming Robust Against Direction-of-Arrival Mismatch," *IEEE Transactions on Signal Processing,* vol. 55, no. 8, pp. 4139-4150, 2007, doi: 10.1109/TSP.2007.894402.

[64] X. Wu, W. Zhu, and J. Yan, "A Toeplitz Covariance Matrix Reconstruction Approach for Direction-of-Arrival Estimation," *IEEE Transactions on Vehicular Technology,* vol. 66, no. 9, pp. 8223-8237, 2017, doi: 10.1109/TVT.2017.2695226.

[65] R. L. Haupt, *Antenna arrays: a computational approach* (no. Book, Whole). Hoboken, N.J: Wiley-IEEE Press (in English), 2010.

[66] R. Schmidt, "Multiple emitter location and signal parameter estimation," *IEEE Transactions on Antennas and Propagation,* vol. 34, no. 3, pp. 276-280, 1986, doi: 10.1109/TAP.1986.1143830.

[67] B. D. Rao and K. V. S. Hari, "Performance Analysis Of Root-music/sup *," in *Twenty-Second Asilomar Conference on Signals, Systems and Computers*, 31 Oct.-2 Nov. 1988 1988, vol. 2, pp. 578-582, doi: 10.1109/ACSSC.1988.754608.

[68] B. Yao, W. Zhang, and Q. Wu, "Weighted Subspace Fitting for Two-Dimension DOA Estimation in Massive MIMO Systems," *IEEE Access,* vol. 5, pp. 14020-14027, 2017, doi: 10.1109/ACCESS.2017.2731379.

[69] M. Viberg, B. Ottenten, and T. Kailath, "Direction-of-arrival estimation and detection using weighted subspace fitting," in *Twenty-Third Asilomar Conference on Signals, Systems and Computers, 1989.*, 30 Oct.-1 Nov. 1989 1989, vol. 2, pp. 604-608, doi: 10.1109/ACSSC.1989.1200969.

[70] M. Jansson, A. L. Swindlehurst, and B. Ottersten, "Weighted subspace fitting for general array error models," *IEEE Transactions on Signal Processing,* vol. 46, no. 9, pp. 2484-2498, 1998, doi: 10.1109/78.709536.

[71] B. Boustani, A. Baghdad, A. Sahel, A. Ballouk, and A. Badr, "Performance analysis of direction of arrival estimation under hard condition," in *2018 4th International Conference on Optimization and Applications (ICOA)*, 26-27 April 2018 2018, pp. 1-5, doi: 10.1109/ICOA.2018.8370544.

[72] X. Guanghan, S. D. Silverstein, R. H. Roy, and T. Kailath, "Beamspace ESPRIT," *IEEE Transactions on Signal Processing,* vol. 42, no. 2, pp. 349-356, 1994, doi: 10.1109/78.275607.

[73] G. Xu, S. D. Silverstein, R. H. Roy, and T. Kailath, "Parallel implementation and performance analysis of beamspace ESPRIT," in *[Proceedings] ICASSP 91: 1991 International Conference on Acoustics, Speech, and Signal Processing*, 14-17 April 1991 1991, pp. 1497-1500 vol.2, doi: 10.1109/ICASSP.1991.150731.

[74] C. P. Mathews, M. Haardt, and M. D. Zoltowski, "Implementation and performance analysis of 2D DFT beamspace ESPRIT," in *Conference Record of The Twenty-Ninth*

Asilomar Conference on Signals, Systems and Computers, 30 Oct.-1 Nov. 1995 1995, vol. 1, pp. 726-730 vol.1, doi: 10.1109/ACSSC.1995.540645.

[75] B. Chandna and A. Mahadar, "2D Beamspace ESPRIT with spatial smoothing," in *IEEE Antennas and Propagation Society International Symposium. 1998 Digest. Antennas: Gateways to the Global Network. Held in conjunction with: USNC/URSI National Radio Science Meeting (Cat. No.98CH36*, 21-26 June 1998 1998, vol. 1, pp. 219-222 vol.1, doi: 10.1109/APS.1998.699113.

[76] R. Hamza and K. Buckley, "Multiple cluster beamspace and resolution-enhanced ESPRIT," *IEEE Transactions on Antennas and Propagation,* vol. 42, no. 8, pp. 1041-1052, 1994, doi: 10.1109/8.309995.

[77] T. N. Ferreira, S. L. Netto, and P. S. R. Diniz, "Beamspace covariance-based DoA estimation," in *2008 IEEE 9th Workshop on Signal Processing Advances in Wireless Communications*, 6-9 July 2008 2008, pp. 136-140, doi: 10.1109/SPAWC.2008.4641585.

[78] M. C. Tan, M. Li, Q. H. Abbasi, and M. Imran, "A smart and low-cost enhanced antenna system for industrial wireless broadband communication," in *12th European Conference on Antennas and Propagation (EuCAP 2018)*, 9-13 April 2018 2018, pp. 1-4, doi: 10.1049/cp.2018.1218.

[79] H. Mewes, "Practical comparisons between various high resolution spectral estimation algorithms for radio direction finding," in *1995 Ninth International Conference on Antennas and Propagation, ICAP '95 (Conf. Publ. No. 407)*, 4-7 April 1995 1995, vol. 1, pp. 480-483 vol.1, doi: 10.1049/cp:19950356.

[80] H. Mewes, F. Wolf, and J. L. t. Haseborg, "Experimental investigations on high resolution direction finding algorithms," in *Proceedings of IEEE Antennas and Propagation Society International Symposium and URSI National Radio Science Meeting*, 20-24 June 1994 1994, vol. 3, pp. 1540-1543 vol.3, doi: 10.1109/APS.1994.408204.

[81] H. Feng, "Direction of Arrival Estimation of Coherent Sources for Non-uniform Linear Arrays," in *2013 Third International Conference on Instrumentation, Measurement, Computer, Communication and Control*, 21-23 Sept. 2013 2013, pp. 803-806, doi: 10.1109/IMCCC.2013.179.

[82] J. Jiang, F. Duan, and Y. Li, "Accurate direction-of-arrival estimation for coherent signals," in *2014 10th International Conference on Natural Computation (ICNC)*, 19-21 Aug. 2014 2014, pp. 888-892, doi: 10.1109/ICNC.2014.6975956.

[83] Y. Iwabuchi, H. Li, and K. Ichige, "Direction-of-arrival estimation of coherent sources for ULA based on the relation between array covariance matrix elements," in *2014 6th International Symposium on Communications, Control and Signal Processing (ISCCSP)*, 21-23 May 2014 2014, pp. 648-651, doi: 10.1109/ISCCSP.2014.6877958.

[84] H. Chen *et al.*, "A Low Computational Cost Lightning Mapping Algorithm With a Nonuniform L-Shaped Array: Principle and Verification," *IEEE Transactions on Geoscience and Remote Sensing,* vol. 60, pp. 1-10, 2022, doi: 10.1109/TGRS.2021.3139388.

[85] Z. Liu, J. Wu, S. Yang, and W. Lu, "DOA Estimation Method Based on EMD and MUSIC for Mutual Interference in FMCW Automotive Radars," *IEEE Geoscience and Remote Sensing Letters,* vol. 19, pp. 1-5, 2022, doi: 10.1109/LGRS.2021.3058729.

[86] Veerendra, M. Bakhar, R. M. Vani, and P. V. Hunagund, "Implementation and optimization of modified MUSIC algorithm for high resolution DOA estimation," in *2014 IEEE International Microwave and RF Conference (IMaRC)*, 15-17 Dec. 2014 2014, pp. 190-193, doi: 10.1109/IMaRC.2014.7038985.

[87] P. Gupta and S. P. Kar, "MUSIC and improved MUSIC algorithm to estimate direction of arrival," in *2015 International Conference on Communications and Signal Processing (ICCSP)*, 2-4 April 2015 2015, pp. 0757-0761, doi: 10.1109/ICCSP.2015.7322593.

[88] B. D. Rao and K. V. S. Hari, "Performance analysis of Root-Music," *IEEE Transactions on Acoustics, Speech, and Signal Processing,* vol. 37, no. 12, pp. 1939-1949, 1989, doi: 10.1109/29.45540.

[89] Z. Shan and T. P. Yum, "A conjugate augmented approach to direction-of-arrival estimation," *IEEE Transactions on Signal Processing,* vol. 53, no. 11, pp. 4104-4109, 2005, doi: 10.1109/TSP.2005.857012.

[90] H. Chu-lin and W. De-shi, "The Fourth Order Cumulant-Based MUSIC Algorithm for Harmonic Retrieval in Colored Noise," in *2009 WRI International Conference on Communications and Mobile Computing*, 6-8 Jan. 2009 2009, vol. 2, pp. 564-567, doi: 10.1109/CMC.2009.357.

[91] H. Paaso and M. Hirvonen, "Angular Resolution Improvement by Using Multi-Radar and FBSS MUSIC DoA Estimation Algorithm," in *2019 IEEE Intelligent Vehicles Symposium (IV)*, 9-12 June 2019 2019, pp. 730-735, doi: 10.1109/IVS.2019.8813780.

[92] F. Belloni, A. Richter, and V. Koivunen, "Performance of root-MUSIC algorithm using real-world arrays," in *2006 14th European Signal Processing Conference*, 4-8 Sept. 2006 2006, pp. 1-5.

[93] M. Swartling, B. Sallberg, and N. Grbic, "Direction of arrival estimation for speech sources using fourth order cross cumulants," in *2008 IEEE International Symposium on Circuits and Systems (ISCAS)*, 18-21 May 2008 2008, pp. 1696-1699, doi: 10.1109/ISCAS.2008.4541763.

[94] A. S. Sekmen and Z. Bingul, "Comparison of algorithms for detection of the number of signal sources," in *Proceedings IEEE Southeastcon'99. Technology on the Brink of 2000 (Cat. No.99CH36300)*, 25-28 March 1999 1999, pp. 70-73, doi: 10.1109/SECON.1999.766094.

[95] E. Fishler, M. Grosmann, and H. Messer, "Detection of signals by information theoretic criteria: general asymptotic performance analysis," *IEEE Transactions on Signal Processing,* vol. 50, no. 5, pp. 1027-1036, 2002, doi: 10.1109/78.995060.

[96] M. M. Gunjal and A. A. B. Raj, "Improved Direction of Arrival Estimation Using Modified Music Algorithm," in *2020 5th International Conference on Communication and Electronics Systems (ICCES)*, 10-12 June 2020 2020, pp. 249-254, doi: 10.1109/ICCES48766.2020.9137982.

[97] D. Rajeswaran, "Single Snapshot Direction of Arrival(DoA) Estimation Using Variant Min-Norm Method," in *2018 International Conference on Communication and Signal Processing (ICCSP)*, 3-5 April 2018 2018, pp. 0468-0471, doi: 10.1109/ICCSP.2018.8524327.

[98] C. Degen, "On single snapshot direction-of-arrival estimation," in *2017 IEEE International Conference on Wireless for Space and Extreme Environments (WiSEE)*, 10-12 Oct. 2017 2017, pp. 92-97, doi: 10.1109/WiSEE.2017.8124899.

[99] B. Friedlander, "A self-calibration technique for direction estimation with diversely polarized arrays," in *2013 Asilomar Conference on Signals, Systems and Computers*, 3-6 Nov. 2013 2013, pp. 2145-2149, doi: 10.1109/ACSSC.2013.6810688.

[100] B. Friedlander, "Chapter 1 - Wireless Direction-Finding Fundamentals," in *Classical and Modern Direction-of-Arrival Estimation*, T. E. Tuncer and B. Friedlander Eds. Boston: Academic Press, 2009, pp. 1-51.

[101] A. A. Ababneh, "Density-Based Sensor Selection for RSS Target Localization," *IEEE Sensors Journal,* vol. 18, no. 20, pp. 8532-8540, 2018, doi: 10.1109/JSEN.2018.2866062.

[102] O. Besson and F. Vincent, "Performance analysis of beamformers using generalized loading of the covariance matrix in the presence of random steering vector errors," *IEEE Transactions on Signal Processing,* vol. 53, no. 2, pp. 452-459, 2005, doi: 10.1109/TSP.2004.840777.

[103] R. Everson and S. Roberts, "Inferring the eigenvalues of covariance matrices from limited, noisy data," *IEEE Transactions on Signal Processing,* vol. 48, no. 7, pp. 2083-2091, 2000, doi: 10.1109/78.847792.

[104] B. Zhang, J. Zhou, and J. Li, "Improved Shrinkage Estimators of Covariance Matrices With Toeplitz-Structured Targets in Small Sample Scenarios," *IEEE Access,* vol. 7, pp. 116785-116798, 2019, doi: 10.1109/ACCESS.2019.2936402.

[105] F. Shen, F. Chen, and J. Song, "Robust Adaptive Beamforming Based on Steering Vector Estimation and Covariance Matrix Reconstruction," *IEEE Communications Letters,* vol. 19, no. 9, pp. 1636-1639, 2015, doi: 10.1109/LCOMM.2015.2455503.

[106] J. S. Thompson, P. M. Grant, and B. Mulgrew, "Performance of spatial smoothing algorithms for correlated sources," *IEEE Transactions on Signal Processing,* vol. 44, no. 4, pp. 1040-1046, 1996, doi: 10.1109/78.492567.

[107] A. B. Gershman and P. Stoica, "MODE with extra-roots (MODEX): a new DOA estimation algorithm with an improved threshold performance," in *1999 IEEE International Conference on Acoustics, Speech, and Signal Processing. Proceedings. ICASSP99 (Cat. No.99CH36258)*, 15-19 March 1999 1999, vol. 5, pp. 2833-2836 vol.5, doi: 10.1109/ICASSP.1999.761352.

[108] B. D. Carlson, "Covariance matrix estimation errors and diagonal loading in adaptive arrays," *IEEE Transactions on Aerospace and Electronic Systems,* vol. 24, no. 4, pp. 397-401, 1988, doi: 10.1109/7.7181.

[109] P. Stoica and K. C. Sharman, "Maximum likelihood methods for direction-of-arrival estimation," *IEEE Transactions on Acoustics, Speech, and Signal Processing,* vol. 38, no. 7, pp. 1132-1143, 1990, doi: 10.1109/29.57542.

[110] Y. Zheng, Y. Xiao, Z. Ma, P. D. Diamantoulakis, and G. K. Karagiannidis, "Neural Network-Based Multi-DOA Tracking for High Speed Railway Communication Systems," *IEEE Transactions on Vehicular Technology,* pp. 1-5, 2022, doi: 10.1109/TVT.2022.3188848.

[111] C. Warty, R. W. Yu, and K. ElMahgoub, "Collaborative Warning System for Dense Vehicular Networks Using MUSIC Algorithm DoA," in *2013 Third International Conference on Advances in Computing and Communications*, 29-31 Aug. 2013 2013, pp. 228-232, doi: 10.1109/ICACC.2013.110.

[112] A. A. Hussain, N. Tayem, A. H. Soliman, and R. M. Radaydeh, "FPGA-Based Hardware Implementation of Computationally Efficient Multi-Source DOA Estimation Algorithms," *IEEE Access,* vol. 7, pp. 88845-88858, 2019, doi: 10.1109/ACCESS.2019.2926335.

[113] M. Hua, C. Hsu, W. Liao, C. Yao, T. Yeh, and H. Liu, "Direction-of-arrival estimator using array switching on software defined radio platform," in *2011 IEEE International Symposium on Antennas and Propagation (APSURSI)*, 3-8 July 2011 2011, pp. 2821-2824, doi: 10.1109/APS.2011.5997113.

[114] H. Meng-Chang, H. Cheng-Han, and L. Hsin-Chin, "Implementation of direction-of-arrival estimator on software defined radio platform," in *2012 8th International Symposium on Communication Systems, Networks & Digital Signal Processing (CSNDSP)*, 18-20 July 2012 2012, pp. 1-4, doi: 10.1109/CSNDSP.2012.6292676.

[115] V. Molodtsov, A. Kureev, and E. Khorov, "Experimental Study of Smoothing Modifications of the MUSIC Algorithm for Direction of Arrival Estimation in Indoor Environments," *IEEE Access,* vol. 9, pp. 153767-153774, 2021, doi: 10.1109/ACCESS.2021.3127861.

[116] L. Tsung-Hsien and J. M. Mendel, "Azimuth and elevation direction finding using arbitrary array geometries," *IEEE Transactions on Signal Processing,* vol. 46, no. 7, pp. 2061-2065, 1998, doi: 10.1109/78.700985.

[117] B. Liao, J. Wen, L. Huang, C. Guo, and S. C. Chan, "Direction Finding With Partly Calibrated Uniform Linear Arrays in Nonuniform Noise," *IEEE Sensors Journal,* vol. 16, no. 12, pp. 4882-4890, 2016, doi: 10.1109/JSEN.2016.2550664.

[118] Y. B. Nechaev and I. W. Peshkov, "Evaluation of the influence of directivity factor of directive elements of conformal antenna arrays on the performances of Azimuth-elevation DOA estimation," in *2017 Progress In Electromagnetics Research Symposium - Spring (PIERS)*, 22-25 May 2017 2017, pp. 490-495, doi: 10.1109/PIERS.2017.8261791.

[119] J. Liang, "Joint Azimuth and Elevation Direction Finding Using Cumulant," *IEEE Sensors Journal,* vol. 9, no. 4, pp. 390-398, 2009, doi: 10.1109/JSEN.2009.2014416.

[120] N. Tayem, "Azimuth/Elevation Directional Finding with Automatic Pair Matching," *International Journal of Antennas and Propagation,* vol. 2016, p. 5063450, 2016/12/12 2016, doi: 10.1155/2016/5063450.

[121] J. M. Goldberg, "Joint direction-of-arrival and array-shape tracking for multiple moving targets," *IEEE Journal of Oceanic Engineering,* vol. 23, no. 2, pp. 118-126, 1998, doi: 10.1109/48.664091.

[122] M. C. Tan, M. Li, Q. H. Abbasi, and M. A. Imran, *Antenna design challenges and future directions for modern transportation market* (no. Book, Whole). Cham: Springer (in English), 2021.